

Thermal/Structural Analysis

Calculation 08-06-07

Title: Naval Long Oblique Impact inside TEV

Document Identifier: 000-00C-DNF0-01200-000-00A

Page 1 of 58

08/06/07

BSC

Design Calculation or Analysis Cover Sheet

1. QA: QA

2. Page 1

Complete only applicable items.

3. System Naval Spent Nuclear Fuel (SNF)				4. Document Identifier 000-00C-DNF0-01200-000-00A			
5. Title Naval Long Oblique Impact inside TEV							
6. Group Thermal/Structural Analysis							
7. Document Status Designation <input type="checkbox"/> Preliminary <input checked="" type="checkbox"/> Committed <input type="checkbox"/> Confirmed <input type="checkbox"/> Cancelled/Superseded							
8. Notes/Comments The calculations contained in this document were developed by Bechtel SAIC Company, LLC (BSC) and are intended solely for the use of BSC in its work for the Yucca Mountain Project.							
Attachments						Total Number of Pages	
See Section 5						N/A	
RECORD OF REVISIONS							
9. No.	10. Reason For Revision	11. Total # of Pgs.	12. Last Pg. #	13. Originator (Print/Sign/Date)	14. Checker (Print/Sign/Date)	15. EGS (Print/Sign/Date)	16. Approved/Accepted (Print/Sign/Date)
00A	Initial Issue	58	58	Sripathi Nilkar <i>Sripathi Nilkar</i> 08-03-07	Mohan Durani <i>Mohan Durani</i> Aug 3, 2007	J. Viggato <i>J. Viggato</i> 8/3/07	M.J. Anderson <i>M.J. Anderson</i> 8/3/07



CONTENTS

	Page
1.0 PURPOSE	5
2.0 REFERENCES	6
2.1. PROCEDURES/DIRECTIVES	6
2.2. DESIGN INPUTS.....	6
2.3. DESIGN CONSTRAINTS	9
2.4. DESIGN OUTPUTS.....	9
3.0 ASSUMPTIONS	10
3.1. ASSUMPTIONS REQUIRING VERIFICATION.....	10
3.2. ASSUMPTIONS NOT REQUIRING VERIFICATION.....	11
4.0 METHODOLOGY	15
4.1. QUALITY ASSURANCE.....	15
4.2. USE OF COMPUTER SOFTWARE.....	15
4.3. STRESS ANALYSIS APPROACH	16
5.0 LIST OF ATTACHMENTS	17
6.0 BODY OF CALCULATION	20
6.1. MATERIAL PROPERTIES	20
6.1.1. Calculations for True Measures of Ductility	22
6.1.2. Calculations for Tangent Modulus	23
6.2. CALCULATIONS FOR SNF NAVAL CANISTER WALL THICKNESS.....	25
6.2.1. Calculations for SNF Naval Canister CG Location for LS-DYNA.....	26
6.3. IMPACT VELOCITY	27
6.4. FINITE ELEMENT REPRESENTATION	28
7.0 RESULTS AND CONCLUSIONS	35

FIGURES**Page**

Figure 3-1. Layout of Naval Long on the Emplacement Pallet inside TEV.....	10
Figure 3-2. Effective Plastic Strain (fine mesh, 0.759m drop for limiting case [run 2B])	13
Figure 6-1. Standard FER.....	30
Figure 6-2. Standard FER Impact Area Detail.....	30
Figure 6-3. Standard FER Upper Sleeve Region Cut-Away.....	31
Figure 6-4. Standard FER Lower Sleeve Region Cut-Away	31
Figure 6-5. Refined FER.....	32
Figure 6-6. Refined FER Impact Area Detail	32
Figure 6-7. Refined FER Upper Sleeve Region Cut-Away	33
Figure 6-8. Refined FER Lower Sleeve Region Cut-Away.....	33
Figure 6-9. FER Initial Contact of Lower Sleeve with TEV Rail (Upper Sleeve Slapdown)	34
Figure 6-10. FER Initial Contact of Upper Sleeve with TEV Rail (Lower Sleeve Slapdown)	34
Figure 7-1. OCB Maximum Shear Stress (Pa) Location for Fine Mesh (run 1B).....	40
Figure 7-2. OCB Maximum Shear Stress for Fine Mesh (run 1B)	40
Figure 7-3. OCB Shell-Upper Lid Interface MSS (Pa) Location for Standard Mesh (run 2A).....	41
Figure 7-4. OCB Shell-Upper Lid Interface MSS (Pa) Location for Standard Mesh (run 2A).....	41
Figure 7-5. OCB Through-Wall Maximum Shear Stress for Standard Mesh (run 2A).....	42
Figure 7-6. OCB Through-Wall Maximum Shear Stress for Standard Mesh (run 2A).....	42
Figure 7-7. OCB Through-Wall Averaged Maximum Shear Stress for Standard Mesh (run 2A)	43
Figure 7-8. OCB Through-Wall Averaged Maximum Shear Stress for Standard Mesh (run 2A)	43
Figure 7-9. OCB Shell-Upper Lid Interface MSS (Pa) Location for Fine Mesh (run 2B).....	44
Figure 7-10. OCB Shell-Upper Lid Interface MSS (Pa) Location for Fine Mesh (run 2B).....	44
Figure 7-11. OCB Through-Wall Maximum Shear Stress for Fine Mesh (run 2B).....	45
Figure 7-12. OCB Through-Wall Averaged Maximum Shear Stress for Fine Mesh (run 2B)	45
Figure 7-13. OCB Shell-Lower Lid Interface MSS (Pa) Location for Fine Mesh (run 3B).....	46
Figure 7-14. OCB Shell-Lower Lid Interface MSS (Pa) Location for Fine Mesh (run 3B).....	46
Figure 7-15. OCB Through-Wall Maximum Shear Stress for Fine Mesh (run 3B).....	47
Figure 7-16. OCB Through-Wall Averaged Maximum Shear Stress for Fine Mesh (run 3B)	47
Figure 7-17. OCB Shell-Upper Lid Interface MSS (Pa) Location for Fine Mesh (run 4).....	48
Figure 7-18. OCB Shell-Upper Lid Interface MSS (Pa) Location for Fine Mesh (run 4).....	48
Figure 7-19. OCB Through-Wall Maximum Shear Stress for Fine Mesh (run 4).....	49
Figure 7-20. OCB Through-Wall Averaged Maximum Shear Stress for Fine Mesh (run 4)	49
Figure 7-21. OCB Shell-Upper Lid Interface MSS (Pa) Location for Fine Mesh (run 5).....	50
Figure 7-22. OCB Shell-Upper Lid Interface MSS (Pa) Location for Fine Mesh (run 5).....	50
Figure 7-23. OCB Through-Wall Maximum Shear Stress for Fine Mesh (run 5).....	51
Figure 7-24. OCB Through-Wall Averaged Maximum Shear Stress for Fine Mesh (run 5)	51
Figure 7-25. Maximum Shear Stress (Pa) Location for Fine Mesh (run 6).....	52
Figure 7-26. Max. Shear Stress (Pa) Location (vertically along OCB Lid) for Fine Mesh (run 6).....	52
Figure 7-27. OCB (Vertical) Maximum Shear Stress for Fine Mesh (run 6).....	53
Figure 7-28. OCB (Vertical-Averaged) Maximum Shear Stress for Fine Mesh (run 6)	53
Figure 7-29. MSS (Pa) Location (horizontally along OCB Lid) for Fine Mesh (run 6)	54
Figure 7-30. OCB (Horizontal) Maximum Shear Stress for Fine Mesh (run 6).....	54
Figure 7-31. OCB (Horizontal-Averaged) Maximum Shear Stress for Fine Mesh (run 6).....	55
Figure 7-32. OCB Shell-Lower Lid Interface MSS (Pa) Location for Fine Mesh (run 6)	55
Figure 7-33. OCB Through-Wall Maximum Shear Stress for Fine Mesh (run 6).....	56
Figure 7-34. OCB Through-Wall Averaged Maximum Shear Stress for Fine Mesh (run 6)	56
Figure 7-35. OCB Shell-Lower Lid Interface MSS (Pa) Location for Fine Mesh (run 7)	57
Figure 7-36. OCB Shell-Lower Lid Interface MSS (Pa) Location for Fine Mesh (run 7)	57
Figure 7-37. OCB Through-Wall Maximum Shear Stress for Fine Mesh (run 7).....	58
Figure 7-38. OCB Through-Wall Averaged Maximum Shear Stress for Fine Mesh (run 7)	58

TABLES

	Page
Table 5-1. List of Electronic Files in Attachment	17
Table 6-1. Tangent Moduli at RT	24
Table 7-1. Weight Verification	35
Table 7-2. Mesh Verification.....	35
Table 7-3. Maximum Stress Intensity	37

1.0 PURPOSE

The purpose and objective of this calculation is to determine the structural response of the Naval Spent Nuclear Fuel (SNF) Long Waste Package (WP) to oblique drop events inside the Transport Emplacement Vehicle (hereinafter termed TEV) (Reference 2.2.22, Section 4.3.5). The information regarding the WP and TEV used in this calculation is based on sketches and drawings in References 2.2.19 to 2.2.21, and 2.2.31.

The scope of this document is limited to reporting the calculation and results of analysis of the response of the Naval SNF Long WP to oblique drop events. The results are reported in terms of maximum shear stress and bounds on primary stress intensities in the outer corrosion barrier (hereinafter termed OCB) of the WP.

2.0 REFERENCES

2.1. PROCEDURES/DIRECTIVES

- 2.1.1 EG-PRO-3DP-G04B-00037, Rev. 09. *Calculations and Analyses*. Las Vegas, Nevada: Bechtel SAIC Company. ACC: [ENG.20070717.0004](#).
- 2.1.2 BSC (Bechtel SAIC Company) 2006. *Quality Management Directive*. QA-DIR-10, Rev. 1. Las Vegas, Nevada: Bechtel SAIC Company. ACC: [DOC.20070330.0001](#).
- 2.1.3 IT-PRO-0011, Rev. 5, Software Management. Las Vegas, Nevada: Bechtel SAIC Company. ACC: [DOC.20070521.0001](#).
- 2.1.4 ORD (Office of Repository Development) 2007. *Repository Project Management Automation Plan*. 000-PLN-MGR0-00200-000-00E. Las Vegas, Nevada: Bechtel SAIC Company. ACC: [ENG.20070326.0019](#).

2.2. DESIGN INPUTS

- 2.2.1 Not Used.
- 2.2.2 DOE 2003. *Validation Test Report for LS-DYNA Version 970.3858 D MPP. 10300-VTR-970.3858 D MPP. 10300-00*. Las Vegas, Nevada: US Department of Energy, Office of Repository Development. ACC: [MOL.20031218.0337](#).
- 2.2.3 ASM 1980. *Properties and Selection: Stainless Steels, Tool Materials and Special-Purpose Metals*. Volume 3 of *Metals Handbook*. 9th Edition. Benjamin, D., ed. Metals Park, Ohio: American Society for Metals. TIC: 209801. ISBN: 0-87170-009-3
- 2.2.4 LS-DYNA V.970.3858 D MPP. HP Itanium2, HP-UX 11.22.10300-970.3858 D MPP-00.
- 2.2.5 ASME (American Society of Mechanical Engineers) 2001. *2001 ASME Boiler and Pressure Vessel Code (includes 2002 addenda)*. New York, New York: American Society of Mechanical Engineers. TIC: 251425.
- 2.2.6 ASTM (American Society of Testing and Materials) G 1-90 (Reapproved 1999). 1999. *Standard Practice for Preparing, Cleaning, and Evaluating Corrosion Test Specimens*. West Conshohocken, Pennsylvania: American Society for Testing and Materials. TIC: 238771.
- 2.2.7 Avallone, E.A. and Baumeister, T., III, eds. 1987. *Marks' Standard Handbook for Mechanical Engineers*. 9th Edition. New York, New York: McGraw-Hill. TIC: 206891. ISBN: 0-07-004127-X

- 2.2.8 Boyer, H.E., ed. 2000. *Atlas of Stress-Strain Curves*. Metals Park, Ohio: ASM International. TIC: 248901. ISBN: 0-87170-240-1
- 2.2.9 Dieter, G.E. 1976. *Mechanical Metallurgy*. 2nd Edition. Materials Science and Engineering Series. New York, New York: McGraw-Hill Book Company. TIC: 247879. ISBN: 0-07-016891-1
- 2.2.10 Halliday, D.; Resnick, R.; and Merrill, J. 1988. *Fundamentals of Physics*. 3rd Edition Extended. New York, New York: John Wiley & Sons. TIC: 234765. ISBN: 0-471-81995-6
- 2.2.11 Not Used.
- 2.2.12 BSC 2004. *Stress Intensity Classification: Waste Package Outer Corrosion Barrier Stresses due to Horizontal Drop Event*. [000-00C-MGR0-01600-000-00A](#). Las Vegas, Nevada: Bechtel SAIC Company. ACC: [ENG.20041122.0001](#)
- 2.2.13 Livermore Software Technology Corporation. 2003. *LS-DYNA Keyword User's Manual*. Version 970. Two volumes. Livermore, California: Livermore Software Technology Corporation. TIC: 254203.
- 2.2.14 [LL020603612251.015](#). Slow Strain Rate Test Generated Stress Corrosion Cracking Data. Submittal date: 08/27/2002.
- 2.2.15 Meriam, J.L. and Kraige, L.G. 1987. *Statics*. Volume 1 of *Engineering Mechanics*. 2nd Edition. Pages. 441, 443. New York, New York: John Wiley & Sons. TIC: 241293.
- 2.2.16 Naples, E.M. 1999. Thermal, Shielding, and Structural Information on the Naval Spent Nuclear Fuel (SNF) Canister. Letter from E.M. Naples (Department of the Navy) to D.C. Haught (DOE/YMSCO), August 6, 1999, with enclosures. ACC: [MOL.19991001.0133](#).
- 2.2.17 Nicholas, T. 1980. *Dynamic Tensile Testing of Structural Materials Using A Split Hopkinson Bar Apparatus*. AFWAL-TR-80-4053. Wright-Patterson Air Force Base, Ohio: Air Force Wright Aeronautical Laboratories. TIC: 249469.
- 2.2.18 Mecham, D.C., ed. 2004. *Waste Package Component Design Methodology Report*. 000-30R-WIS0-00100-000-002. Las Vegas, Nevada: Bechtel SAIC Company. ACC: [ENG.20040713.0003](#).
- 2.2.19 BSC (Bechtel SAIC Company) 2007. *Naval Long Waste Package Sketch*. 000-MWK-DNF0-00301-000-00B. Las Vegas, Nevada: Bechtel SAIC Company. ACC: ENG.20070227.0001.

-
- 2.2.20 BSC (Bechtel SAIC Company) 2007. *Naval Long Waste Package Sketch*. 000-MWK-DNF0-00302-000-00B. Las Vegas, Nevada: Bechtel SAIC Company. ACC: ENG.20070227.0002.
- 2.2.21 BSC (Bechtel SAIC Company) 2007. *Naval Long Waste Package Sketch*. 000-MWK-DNF0-00303-000-00B. Las Vegas, Nevada: Bechtel SAIC Company. ACC: ENG.20070227.0003.
- 2.2.22 BSC (Bechtel SAIC Company) 2007. *Provisional Event Sequence Definitions for Waste Packages (DC#51120)*. 000-30R-WIS0-00900-000-000. Las Vegas, Nevada: Bechtel SAIC Company. ACC: [ENG.20070307.0014](#)
- 2.2.23 BSC (Bechtel SAIC Company) 2006. *Basis of Design for the TAD Canister-Based Repository Design Concept*. 000-3DR-MGR0-00300-000-000. Las Vegas, Nevada: Bechtel SAIC Company. ACC: [ENG.20061023.0002](#).
- 2.2.24 DOE (U.S. Department of Energy) 2007. *High-Level Radioactive Waste and U.S. Department of Energy and Naval Spent Nuclear Fuel to the Monitored Geologic Repository*. Volume 1 of *Integrated Interface Control Document*. DOE/RW-0511, Rev. 3. Washington, D.C.: U.S. Department of Energy, Office of Civilian Radioactive Waste Management. ACC: DOC.[20070125.0002](#)
- 2.2.25 BSC (Bechtel SAIC Company) 2005. *Q-List*. 000-30R-MGR0-00500-000-003. Las Vegas, Nevada: Bechtel SAIC Company. ACC: [ENG.20050929.0008](#).
- 2.2.26 Not Used
- 2.2.27 Not Used
- 2.2.28 Roark, R.J. and Young, W.C. 1975. *Formulas for Stress and Strain*. 5th Edition. New York, New York: McGraw-Hill. TIC: [240746](#). ISBN: 0-07-053031-9
- 2.2.29 BSC (Bechtel SAIC Company) 2005. *IED Waste Package Processes, Ground Motion Time Histories, and Testing and Materials [Sheet 1 of 1]*. 800-IED-WIS0-00501-000-00A. Las Vegas, Nevada: Bechtel SAIC Company. ACC: [ENG.20050406.0004](#).
- 2.2.30 BSC (Bechtel SAIC Company) 2006. *Naval Long Waste Package With Emplacement Pallet Drop (DC #49771)*. 000-00C-DNF0-00100-000-00B. Las Vegas, Nevada: Bechtel SAIC Company. ACC: [ENG.20061120.0012](#)
- 2.2.31 BSC (Bechtel SAIC Company) 2007. *Emplacement and Retrieval Transport and Emplacement Vehicle Mechanical Equipment Envelope (DC #51221)*. 800-MJ0-HE00-00101-000-00A. Las Vegas, Nevada: Bechtel SAIC Company. ACC: [ENG.20070312.0016](#)

2.3. DESIGN CONSTRAINTS

None

2.4. DESIGN OUTPUTS

This calculation is performed to support information in the License Application and the Naval Waste Package Design Report (000-00C-DNF0-00800-000-00B).

3.0 ASSUMPTIONS

In the course of developing this document, the following assumptions are made regarding the WP structural calculations

3.1. ASSUMPTIONS REQUIRING VERIFICATION

3.1.1 The dimensions, masses and materials of the WP and TEV used in the development of this calculation, corresponding to the drawings and sketches of References 2.2.19 to 2.2.21, and 2.2.31, are assumed to be the same as the final definitive design. The rationale for this assumption is that the design of References 2.2.19 to 2.2.21, and 2.2.31 is created for the License Application (LA). This assumption is used in Section 6.4 and will require verification at completion of the final definitive design.

3.1.2 The drop height, drop orientation and Support Shelf (hereinafter termed as TEV Rail Ledge) dimensions including assumed fillet radius of one inch used in the development of this calculation, correspond to that listed in Figure 3-1, which is based on Reference 2.2.31. The rationale for this assumption is that the design of Reference 2.2.31 is created for the License Application (LA). This assumption is used in Section 6.4 and will require verification at completion of the final definitive design.

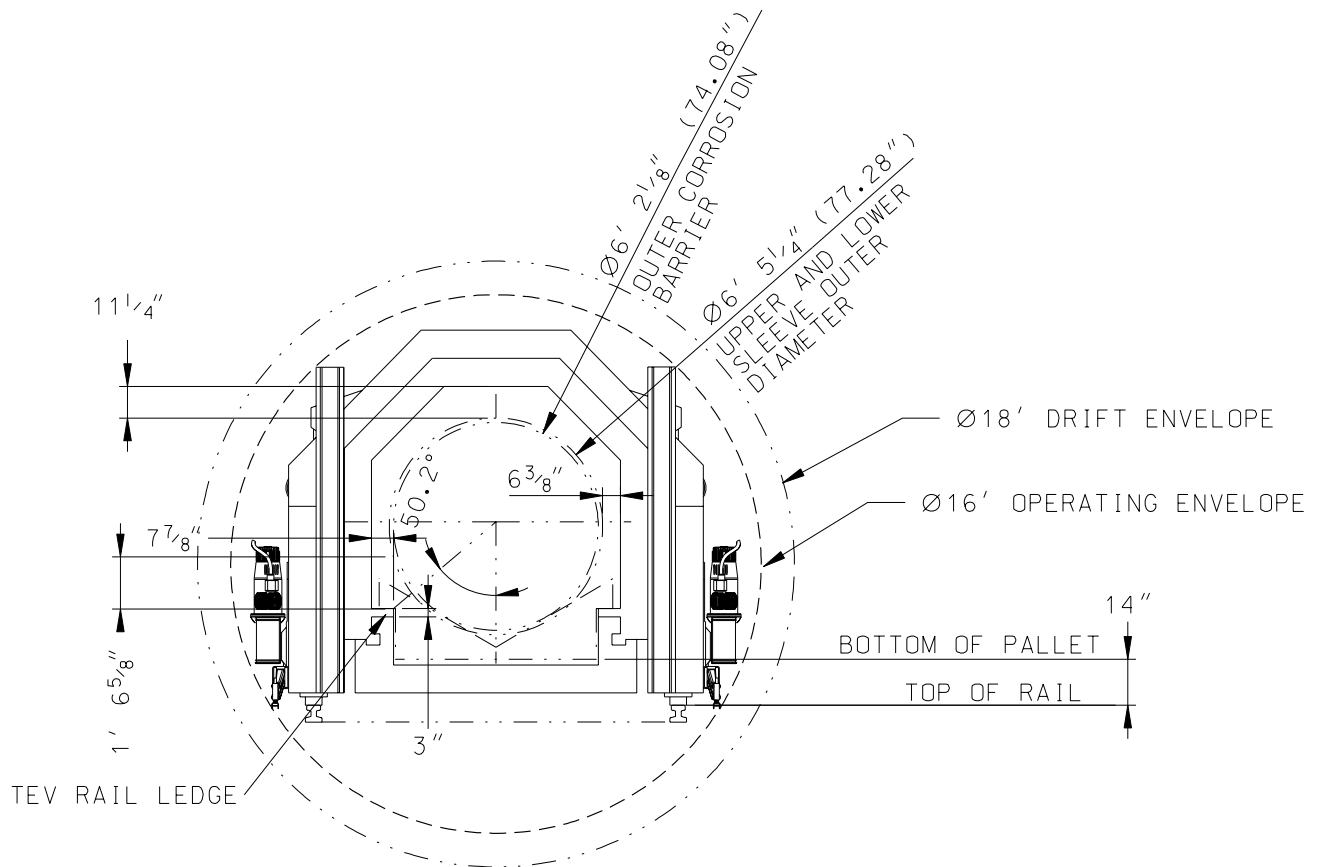


Figure 3-1. Layout of Naval Long on the Emplacement Pallet inside TEV

3.2. ASSUMPTIONS NOT REQUIRING VERIFICATION

3.2.1 The room temperature (RT) (20 °C [68 °F]) Poisson's ratio of ASME SB-575 [UNS N06022] hereinafter termed Alloy 22, is not published in traditional sources (e.g., the ASTM, ASME and ASM standards, codes and metal property data). Therefore, the RT Poisson's ratio of ASME SB-443 [UNS N06625], hereinafter termed Alloy 625, is assumed for Alloy 22. The chemical compositions of Alloy 22 and Alloy 625 are similar since they are both 600 series nickel-base alloys (Reference 2.2.5, Section II, Part B, SB-575, Table 1 and Reference 2.2.3, p 143, respectively). Therefore, the difference in their Poisson's ratio is expected to be small. The rationale for this expectation is that the Reference 2.2.3 pages 141, 143 and 145 indicate small differences in RT Poisson's ratio values for the 600 Series nickel-base alloy family:

$$\text{Alloy 600 [UNS N06600]} = 0.290$$

$$\text{Alloy 625 [UNS N06625]} = 0.278$$

$$\text{Alloy 690 [UNS N06690]} = 0.289$$

The impact on stress results of small differences in Poisson's ration is anticipated to be negligible. The rationale for this anticipation is that the Reference 2.2.28 Table 30 stress formulas for cylindrical shells indicate insensitivity to Poisson's ratio. For the loading case of uniform radial shear loads (Case 8), the key breaching stress, the maximum hoop circumferential membrane stress, is proportional to Poisson's ratio, ν , through the term $(1-\nu^2)^{1/4}$. Using the lowest and the highest values of the three 600 Series nickel-base alloys ν values, 0.278 and 0.290, the difference in maximum hoop circumferential membrane stress values, all things being equal except ν , is a negligible 0.2%. Therefore, this study of parametric variations provides verification of this assumption per Reference 2.1.1 page 4 ("*Verification may include ... studies of parametric variations*") and further verification of this assumption is not required. This assumption is used in Section 6.1 and is consistent with Section 5.2.8.2 of Reference 2.2.18.

3.2.2 The RT uniform strain (engineering strain corresponding to engineering tensile strength) of ASME SA 240 [UNS S31603] hereinafter termed 316L stainless steel [SS] is not listed in traditional sources. Therefore, it is assumed that the RT uniform engineering strain is 60% of the RT minimum specified elongation. The rationale for this assumption is based on measurements of RT engineering stress-strain curves for "as received" 316L material at moderate strain rate (8 sec^{-1}) (Reference 2.2.8, page 305). Therefore this assumption does not require verification. This assumption is used in Section 6.1.1 and corresponds to Section 5.2.6.2. of Reference 2.2.18.

3.2.3 The RT Poisson's ratio of 316L SS is not published in traditional sources. Therefore, the RT Poisson's ratio of ASME SA-240 [UNS S31600 with modified N & C] hereinafter termed 316 SS is assumed for 316L SS. The chemical compositions of 316L SS and 316 SS are similar (Reference 2.2.5, Section II, Part A, SA240, Table 1) because they are both 300 Series (austenitic) stainless steels. Therefore, the difference in their Poisson's ratio is expected to be small. The rationale for this expectation, is that Reference 2.2.3 page 755

Figure 15 indicates small differences in RT Poisson's ratio values for the 300 Series SS family:

Type 304 SS [UNS S30400] = 0.290

Type 316 SS [UNS S31600] = 0.298

Type 310 SS [UNS S31000] = 0.308

The impact on stress results of small differences in Poisson's ratio is anticipated to be negligible. The rationale for this anticipation is that Reference 2.2.28 Table 30 stress formulas for cylindrical shells indicate insensitivity to Poisson's ratio. For the loading case of uniform radial shear loads (Case 8), the key breaching stress, the maximum hoop circumferential membrane stress, is proportional to Poisson's ratio, ν , through the term $(1-\nu^2)^{1/4}$. Using the lowest and highest values of the three 300 Series SS ν values, 0.290 and 0.308, the difference in maximum hoop circumferential membrane stress values, all things being equal except ν , is a negligible 0.3%. Therefore, this study of parametric variations provides verification of this assumption per Reference 2.1.1 Page 4 ("*Verification may include . . . studies of parametric variations*") and further verification of this assumption is not required. This assumption is used in Section 6.1 and is consistent with Section 5.2.8.2 of Reference 2.2.18.

3.2.4 The Poisson's ratio and density at elevated temperatures are not published in traditional sources for Alloy 22, 316 SS and 316L. The RT Poisson's ratio and density are assumed for these materials. The impact of using RT Poisson's ratio and density is anticipated to be small. The rationale for this assumption is that the temperature sensitivities of these material properties are expected to be small and small variations will have negligible effect on the calculation's stress results. Assumptions 3.2.1 and 3.2.3 provide parametric studies in this calculation that verify this for Poisson's Ratio. The change in density will be downward as the material expands, inversely related to the volumetric expansion term $(1+\Delta T\alpha)^3$, where ΔT is the temperature increase above RT and α is the relative (to RT) coefficient of thermal expansion. Using $\Delta T = 280\text{ }^\circ\text{C}$ and a clearly upper bound value of $10^{-6}\text{ }(^{\circ}\text{C})^{-1}$ for the materials' α values from $20\text{ }^\circ\text{C}$ to $300\text{ }^\circ\text{C}$, leads to a density change of less than 0.1%. The total mass will remain unchanged, so the effect of density change on stress is unclear, however even in the unlikely event that the resulting stress effect is a magnitude greater than the density change, it will be negligible. These studies of variations in Poisson's ratio and density provides verification of this assumption per Reference 2.1.1 page 4 ("*Verification may include . . . studies of parametric variations*"). Further verification of this assumption is not required. This assumption is used in Section 6.1 and is consistent with Section 5.2.8.6 of Reference 2.2.18.

3.2.5 Not Used.

3.2.6 The RT uniform strain of Alloy 22 and 316 SS is not listed in traditional sources. Therefore, it is assumed that the RT uniform strain is 90% of the RT minimum specified elongation for both materials. The rationale for this assumption is based on measurement of RT engineering stress-strain curves for the materials (Reference 2.2.8, page 304 and Reference 2.2.14, S02234_001, Mechanical Deformation, file: "LL020603612251.015,

Instron Data yr 2002”). The use of Reference 2.2.14 was approved as the appropriate data for the intended use in an Information Exchange Document (Reference 2.2.29). Therefore this assumption does not require verification. This assumption is used in Section 6.1.1 and corresponds to paragraph 5.2.6.3 of Reference 2.2.18.

- 3.2.7 Strain-rate dependent material properties are not published in traditional sources for Alloy 22, 316 SS, and 316L SS. The material properties obtained under static loading conditions are assumed for these materials. The rationale for this assumption is that results presented in this calculation do not significantly change at the peak strain rates reached during the oblique drop (peak effective strain rate [maximum slope of the curve] = $(0.1925 - 0.03498) / (0.13682 - 0.12606) \text{ sec}^{-1} = 0.15752 / 0.01076 \{ (m/m) / \text{sec}^{-1} \} = 14.639 \text{ sec}^{-1}$, see Figure 3-2). The presented element is characterized by the highest effective plastic strain in the OCB of the fine mesh finite element representation (FER) at the end of the RT simulation. For this value of strain rate, Reference 2.2.17 (Figures 27 and 30, pp. 42 and 45) indicates only a moderate strengthening of the materials. Therefore this assumption does not require verification. This assumption is used in Section 6.1 and corresponds to paragraph 5.2.5 in Reference 2.2.18.

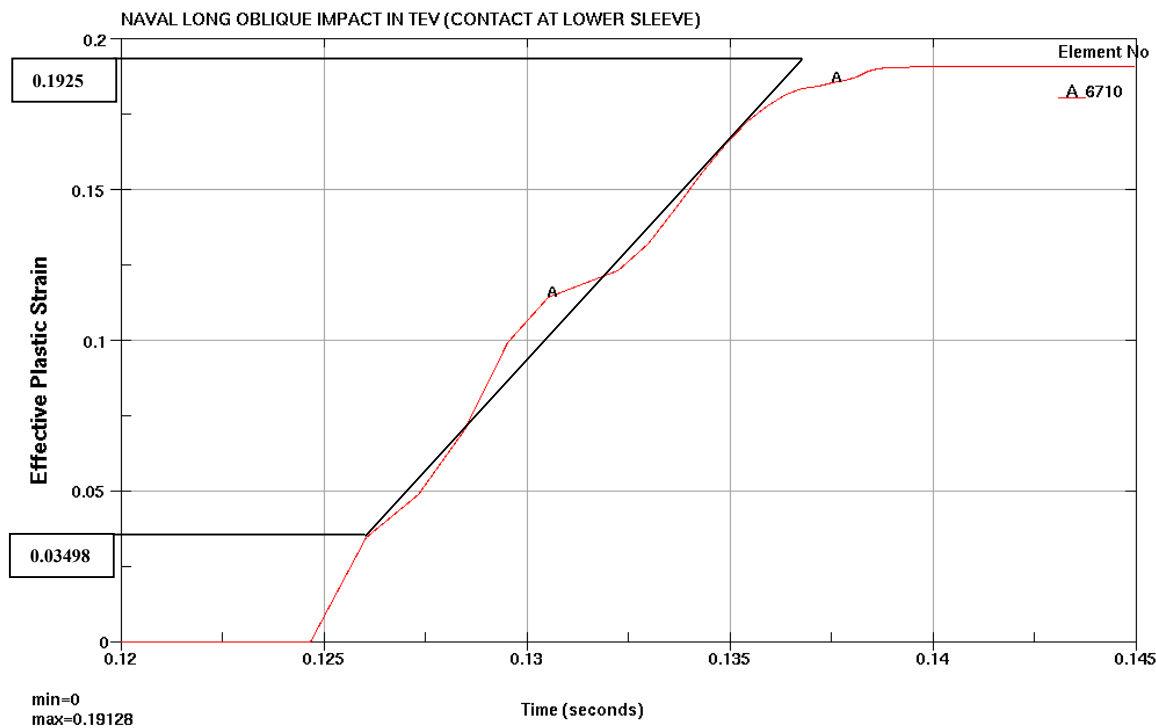


Figure 3-2. Effective Plastic Strain (fine mesh, 0.759m drop for limiting case [run 2B])

- 3.2.8 The exact mass and geometry of the loaded Naval SNF canister is simplified for the purpose of this calculation. The maximum recordable weight, 49,320 kilogram (*kg*) (54.25 tons), Reference 2.2.24, Figure C-17, Note 3, is assumed to be distributed in a thick-walled (9.1 inch [*in*]) hollow cylinder with a 15 *in* top plug, 3.5 *in* bottom lid (Reference 2.2.16, Enclosure 3B, Drawing 6251E52) and properties of 316L SS (Reference 2.2.16, Enclosure 3,

page 4). Note that this information is not available in References 2.2.23, and 2.2.24. Hence this information obtained from Reference 2.2.16 is suitable for use in this calculation. The increased side wall thickness is back calculated from the targeted weight and the top and bottom plugs are modeled using the actual dimensions (nominal thickness and diameter). The increased canister stiffness because of the increased side wall thickness is offset by the ignored SNF stiffness. The geometry of the Naval SNF canister is thus simplified for the purpose of this calculation. Since the overall thickness of the side wall of the Naval SNF canister is increased to compensate for the weight of the SNF that has not been modeled in the FER, the SNF weight is effectively smeared uniformly along the side wall of the Naval SNF canister. Therefore the overall weight of the Naval SNF canister is maintained and the weight distribution is reasonably representative. Therefore, this assumption does not require verification. This assumption is used in Sections 6.2 and 6.4.

3.2.9 The loaded Naval SNF canister FER is comprised of 316L SS. The rationale for this assumption is that the canister will be fabricated primarily from Type 316L SS material (Reference 2.2.24, Figure C-17, Note 1). Therefore, this assumption does not require verification. This assumption is used in Section 6.1.

3.2.10 The friction coefficients for contacts occurring between the materials used in this calculation are not published in traditional sources. It is therefore, assumed that the dynamic (sliding) friction coefficient is 0.4 for all contacts. The rationale for this assumption is that this friction coefficient represents a reasonable lower bound value for most metal-on-metal dry contact surfaces involving steel and nickel (see Reference 2.2.15, p. 441 and Reference 2.2.7, Table 3.2.1, page 3-26), nickel being the dominant component in Alloy 22 (Reference 2.2.5, Section II, Part B, SB-575, Table 1). For this drop event, minute relative motion between contact surfaces exists, and the choice of dynamic friction coefficient will have insignificant effect on the results. Therefore this assumption does not require verification. This assumption is used in Section 6.4 and corresponds to paragraph 5.2.14.1 of Reference 2.2.18.

3.2.11 The variation of functional friction coefficient between the static and dynamic values as a function of relative velocity between the contact surfaces is not published in traditional sources for the materials used in this calculation. Therefore, the effect of relative velocity of the surfaces in contact is not included in this calculation by assuming that the functional friction coefficient and static friction coefficient, both are equal to the dynamic friction coefficient. This will provide a constant lower bound frictional coefficient. A sensitivity study was conducted in Reference 2.2.30 that indicates the lower bound friction coefficient value of 0.4 used is high enough to create lock-up of the critical contact surfaces and therefore the impact of this assumption presented in this calculation is negligible. The impact of this assumption on results presented in this document is anticipated to be negligible. The rationale for this assumption is that it provides bounding results by minimizing the impact energy dissipation by friction. Therefore, this assumption does not require verification. This assumption is used in Section 6.4 and corresponds to paragraph 5.2.14.2 of Reference 2.2.18.

4.0 METHODOLOGY

4.1. QUALITY ASSURANCE

This calculation is prepared in accordance with EG-PRO-3DP-G04B-00037 (Reference 2.1.1). Naval SNF Long WP is classified as a safety category item (important to safety and important to waste isolation) according to the *Q-List* (Reference 2.2.25, page A-9). The TEV is classified as a safety category item (important to safety and important to waste isolation) according to the *Basis of Design for the TAD Canister-Based Repository Concept* (Reference 2.2.23, Section 14.1.2). Therefore this calculation is subject to the requirements of the *Quality Management Directive* (Reference 2.1.2, Sections 2.1.C.1.1.a.i and 17.E.) and final the version is designated as QA: QA.

Event sequences were taken from *Provisional Event Sequence Definitions for Waste Packages (DC#51120)* (Reference 2.2.22, Section 4.3.5) and not from *Basis of Design for the TAD Canister-Based Repository Concept* (Reference 2.2.23, Section 12.2.3.1) because the BOD has not been updated for the new operations in the various facilities at Yucca Mountain Project.

4.2. USE OF COMPUTER SOFTWARE

The qualified finite element analysis computer code used for this calculation is Livermore Software Technology Corporation (LSTC) LS-DYNA (V970.3858 D MPP-00, Reference 2.2.4). This program was obtained from Software Configuration Management in accordance with IT-PRO-0011, *Software Management* (Reference 2.1.3), and is identified by the Software Tracking Number 10300-970.3858 D MPP-00. LS-DYNA V970.3858 D MPP-00 (hereinafter referred to as LS-DYNA) is a commercially available finite element analysis code and is appropriate for structural analysis of the WP as performed in this calculation. The calculation using the LS-DYNA software was executed on the Hewlett-Packard (HP) Itanium2 (IA64) series UNIX workstations equipped with Operating System HP-UX 11.22, identified with Yucca Mountain Project (YMP) tag number 501711 located in Las Vegas, NV. The LS-DYNA evaluation performed for this calculation is fully within the range of the validation performed for the LS-DYNA (Reference 2.2.4). Access to the code was granted by the Software Configuration Management in accordance with the appropriate procedures. LS-DYNA was used with the help of *Keyword User's Manual* (Reference 2.2.13)

The pre-processor TrueGrid V2.3.0 (Software Tracking Number 610418-2.2.0-00, hereinafter termed as TrueGrid), is used in this calculation solely for the purpose of meshing geometric representations of the WP. The suitability and adequacy of this mesh is based on visual examination, engineering judgment, and the results of mesh verification in Section 7 (Table 7-2). TrueGrid is considered Level 2 Software per IT-PRO-0011, *Software Management* (Reference 2.1.3, Attachment 12), as stated in Section 1.2 of this procedure. Modeling and mesh generation using TrueGrid were executed on the Hewlett-Packard (HP) "OPUS" computer (YMP tag number 151664) running operating system HP-UX 11.00. The suitability and adequacy of generated mesh is verified by visual inspection.

LS-PREPOST V1.0 (LSTC), hereinafter referred to as LS-PREPOST, is the post-processor used only for visual display and graphical representation of results. LS-PREPOST was executed on the

Hewlett-Packard (HP) "OPUS" computer (YMP tag number 151664) running operating system HP-UX 11.00. The suitability and adequacy of displayed results is verified by engineering judgment and visual inspection.

The input and output files are listed in Section 5, and Table 5-1 of this document. They are located in Attachment I, the compact disc (CD) to this document. The input files are identified by ".k" and ".inc" file extensions for LS-DYNA and ".tg" for TrueGrid V2.3. The output files (d3hsp) from LS-DYNA are also provided in Attachment I.

Microsoft Excel 2003 (Version 11.8120.8122) SP2, which is a component of Microsoft Office 2003, is used for performing calculations in Sections 6.2 and 7.0. Usage of Microsoft Office in this calculation constitutes Level 2 software usage, as defined in IT-PRO-0011 (Reference 2.1.3). Microsoft Office 2003 is listed in the current Level 2 usage Controlled Software Report, as well as the *Repository Project Management Automation Plan* (Reference 2.1.4, Table 6-1).

Microsoft Excel 2003 (Version 11.8120.8122) SP2 was executed on a PC running the Microsoft Windows XP Professional 5.1.2600 Service Pack 2 operating system. The calculations are confirmed by hand calculations.

The other computations within this document are hand calculations.

4.3. STRESS ANALYSIS APPROACH

The finite-element representation (FER) of the WP is created and solved for the oblique drop events using True Grid V2.3 and LS-DYNA. The OCB stress results are reviewed to determine the maximum response location, magnitude, and expected failure location. The results of this calculation are presented in terms of maximum shear stress and bounds on primary stress intensities. The governing OCB stress response is compared to project structural acceptance criteria.

The design information regarding the WP used in the FER is based on the proposed/potential designs presented by the drawings and sketches of References 2.2.19 to 2.2.21, and 2.2.31 (see Assumptions 3.1.1 and 3.1.2).

The Naval Long canister overall dimensions are consistent with the maximum values provided on page 2 of Enclosure 3 in Reference 2.2.16. The weight of the Naval Long canister is based on the maximum recordable weight (Reference 2.2.24, Figure C-17, Note 3). The details of the Naval Long canister and contents are simplified per Assumption 3.2.8.

The inner vessel cavity dimensions, end details of the inner vessel, OCB and sleeves used in this calculation are based from References 2.2.20 and 2.2.21.

5.0 LIST OF ATTACHMENTS

Attachment I (1 CD): Table 5-1 gives the list of files in Attachment I used in this calculation. The input files are identified by “.k” and “.inc” file extensions for LS-DYNA and “.tg” for TrueGrid V2.3. The output files (d3hsp) from LS-DYNA are also provided. The file sizes on the CD may vary with operating system.

Table 5-1. List of Electronic Files in Attachment

Volume in drive C has no label.

Volume Serial Number is 9487-F5C8

Directory of C:\CD_OI

```
07/31/2007 06:11 PM <DIR> .
07/31/2007 06:11 PM <DIR> ..
07/29/2007 12:34 PM <DIR> Run1A
07/29/2007 12:59 PM <DIR> Run1B
07/29/2007 12:28 PM <DIR> Run2A
07/29/2007 12:22 PM <DIR> Run2B
07/29/2007 12:44 PM <DIR> Run3A
07/29/2007 12:52 PM <DIR> Run3B
07/29/2007 12:57 PM <DIR> Run4
07/29/2007 12:57 PM <DIR> Run5
07/31/2007 09:33 AM <DIR> Run6
07/31/2007 09:33 AM <DIR> Run7
07/31/2007 06:11 PM      17,408 Runs_Table.xls
      1 File(s)      17,408 bytes
```

Directory of C:\CD_OI\Run1A

```
07/29/2007 12:34 PM <DIR> .
07/29/2007 12:34 PM <DIR> ..
07/18/2007 01:15 PM      8,601,037 d3hsp.Z
07/29/2007 12:31 PM    22,749,987 NLOIIT_Std_Msh_2_End.inc
07/19/2007 04:53 PM      54,272 NLOIIT_Std_Msh_2_End.k
07/19/2007 06:54 PM     108,985 NLOIIT_Std_Msh_2_End.tg
      4 File(s)    31,514,281 bytes
```

Directory of C:\CD_OI\Run1B

```
07/29/2007 12:59 PM <DIR> .
07/29/2007 12:59 PM <DIR> ..
07/18/2007 10:29 AM    11,630,747 d3hsp.Z
07/29/2007 12:56 PM    30,358,074 NLOIIT_Fine_Msh_2_End.inc
```

07/19/2007 06:40 PM 54,784 NLOIIT_Fine_Msh_2_End.k
07/19/2007 05:06 PM 112,837 NLOIIT_Fine_Msh_2_End.tg
4 File(s) 42,156,442 bytes

Directory of C:\CD_OI\Run2A

07/29/2007 12:28 PM <DIR> .
07/29/2007 12:28 PM <DIR> ..
07/12/2007 03:10 PM 9,344,259 d3hsp.Z
07/12/2007 03:10 PM 22,311,534 NLOIIT_Std_Msh_1_End_LS.inc
07/19/2007 06:19 PM 7,848 NLOIIT_Std_Msh_1_End_LS.k
07/19/2007 06:23 PM 109,121 NLOIIT_Std_Msh_1_End_LS.tg
4 File(s) 31,772,762 bytes

Directory of C:\CD_OI\Run2B

07/29/2007 12:22 PM <DIR> .
07/29/2007 12:22 PM <DIR> ..
07/12/2007 03:10 PM 12,699,071 d3hsp.Z
07/28/2007 10:50 AM 59,319,296 NLOIIT_Fine_Msh_1_End_LS.inc
07/28/2007 10:47 AM 50,688 NLOIIT_Fine_Msh_1_End_LS.k
07/19/2007 06:25 PM 112,975 NLOIIT_Fine_Msh_1_End_LS.tg
4 File(s) 72,182,030 bytes

Directory of C:\CD_OI\Run3A

07/29/2007 12:44 PM <DIR> .
07/29/2007 12:44 PM <DIR> ..
07/12/2007 03:10 PM 9,560,073 d3hsp.Z
07/29/2007 12:37 PM 22,747,545 NLOIIT_Std_Msh_1_End_US.inc
07/19/2007 06:50 PM 7,855 NLOIIT_Std_Msh_1_End_US.k
07/19/2007 06:54 PM 109,061 NLOIIT_Std_Msh_1_End_US.tg
4 File(s) 32,424,534 bytes

Directory of C:\CD_OI\Run3B

07/29/2007 12:52 PM <DIR> .
07/29/2007 12:52 PM <DIR> ..
07/12/2007 03:10 PM 12,598,513 d3hsp.Z
07/29/2007 12:49 PM 30,355,676 NLOIIT_Fine_Msh_1_End_US.inc
07/19/2007 06:51 PM 7,849 NLOIIT_Fine_Msh_1_End_US.k
07/12/2007 03:10 PM 108,648 NLOIIT_Fine_Msh_1_End_US.tg
4 File(s) 43,070,686 bytes

Directory of C:\CD_OI\Run4

```
07/29/2007 12:57 PM <DIR> .
07/29/2007 12:57 PM <DIR> ..
07/26/2007 01:56 PM 12,180,081 d3hsp.Z
07/26/2007 01:56 PM 29,779,344 NLOIIT_Fine_Msh_1_End_LS.inc
07/29/2007 12:20 PM 7,819 NLOIIT_Fine_Msh_1_End_LS.k
07/19/2007 06:25 PM 112,975 NLOIIT_Fine_Msh_1_End_LS.tg
4 File(s) 42,080,219 bytes
```

Directory of C:\CD_OI\Run5

```
07/29/2007 12:57 PM <DIR> .
07/29/2007 12:57 PM <DIR> ..
07/26/2007 09:05 AM 11,718,297 d3hsp.Z
07/26/2007 01:57 PM 29,779,344 NLOIIT_Fine_Msh_1_End_LS.inc
07/29/2007 12:22 PM 7,954 NLOIIT_Fine_Msh_1_End_LS.k
07/19/2007 06:25 PM 112,975 NLOIIT_Fine_Msh_1_End_LS.tg
4 File(s) 41,618,570 bytes
```

Directory of C:\CD_OI\Run6

```
07/31/2007 09:33 AM <DIR> .
07/31/2007 09:33 AM <DIR> ..
07/31/2007 09:30 AM 11,349,927 d3hsp.Z
07/29/2007 12:49 PM 30,180,627 NLOIIT_Fine_Msh_1_End_US.inc
07/30/2007 04:57 PM 51,200 NLOIIT_Fine_Msh_1_End_US.k
07/29/2007 12:14 PM 112,854 NLOIIT_Fine_Msh_1_End_US.tg
4 File(s) 41,694,608 bytes
```

Directory of C:\CD_OI\Run7

```
07/31/2007 09:33 AM <DIR> .
07/31/2007 09:33 AM <DIR> ..
07/31/2007 09:29 AM 11,400,228 d3hsp.Z
07/29/2007 12:49 PM 30,355,676 NLOIIT_Fine_Msh_1_End_US.inc
07/30/2007 04:56 PM 7,957 NLOIIT_Fine_Msh_1_End_US.k
07/12/2007 03:10 PM 108,648 NLOIIT_Fine_Msh_1_End_US.tg
4 File(s) 41,872,509 bytes
```

Total Files Listed:

41 File(s) 420,404,049 bytes

32 Dir(s) 28,414,402,560 bytes free

6.0 BODY OF CALCULATION

6.1 MATERIAL PROPERTIES

Material properties used in this calculation are listed in this section. Some of the temperature-dependent and rate-dependent material properties are not available for Alloy 22, 316 SS, and 316L SS materials. For all materials, RT Poisson's ratio and density were used (see Assumption 3.2.4), and all properties were obtained under static loading conditions (see Assumption 3.2.7).

Alloy 22 ASME SB-575 [UNS N06022]

(OCB, OCB top and bottom lids, top and bottom sleeves):

- (From Reference 2.2.5, Section II, Part B, SB-575 Section 7.1)
Density = 8690 kg/m^3 (0.314 lb/in^3) (at RT)
- (From Reference 2.2.5, Section II, Part D, Table Y-1)
Yield strength = 310 MPa (45.0 ksi) (at RT)
- (From Reference 2.2.5, Section II, Part D, Table U)
Tensile strength = 689 MPa (100 ksi) (at RT)
- (From Reference 2.2.5, Section II, Part B, SB-575 Table 4)
Elongation = 0.45 (at RT)
- From Reference 2.2.3, p. 143; Assumption 3.2.1
Poisson's ratio = 0.278 (at RT)
- (From Reference 2.2.11, p. 14, Table "Average Dynamic Modulus of Elasticity")
(This is the best available data and suitable for use in the calculation)
Modulus of elasticity = 206 GPa ($29.9 * 10^6 \text{ psi}$) (at RT)

316 SS ASME SA-240 [UNS S31600 with modified N & C]

(Inner Vessel, Inner Vessel top and bottom lids, spread ring, TEV Rail Ledge):

- (From Reference 2.2.6, Table X1.1, p. 7)
Density = 7980 kg/m^3 (0.288 lb/in^3) (at RT)
- (From Reference 2.2.5, Section II, Part D, Table Y-1)
Yield strength = 207 MPa (30.0 ksi) (at RT)
- (From Reference 2.2.5, Section II, Part D, Table U)
Tensile strength = 517 MPa (75.0 ksi) (at RT)
- (From Reference 2.2.5, Section II, Part A, SA-240, Table 2)

Elongation = 0.40 (at RT)

- (From Reference 2.2.3, Figure 15, p. 755)
Poisson's ratio = 0.30 (at RT)
- (From Reference 2.2.5, Section II, Part D, Table TM-1)
Modulus of elasticity = 195 *GPa* ($28.3 \cdot 10^6$ *psi*) (at RT)

316L SS ASME SA-240 [UNS S31603]

(Naval SNF canister)

Assumption 3.2.9

- (From Reference 2.2.6, Table X1.1, p. 7)
Density = 7980 kg/m^3 (0.288 lb/in^3) (at RT)
- (From Reference 2.2.5, Section II, Part D, Table Y-1)
Yield strength = 172 *MPa* (25.0 *ksi*) (at RT)
- (From Reference 2.2.5, Section II, Part D, Table U)
Tensile strength = 483 *MPa* (70.0 *ksi*) (at RT)
- (From Reference 2.2.5, Section II, Part A, SA-240, Table 2)
Elongation = 0.40 (at RT)
- From Reference 2.2.3, Figure 15, p. 755
Poisson's ratio = 0.30 (at RT)
- (From Reference 2.2.5, Section II, Part D, Table TM-1)
Modulus of elasticity = 195 *GPa* ($28.3 \cdot 10^6$ *psi*) (at RT)

Assumption 3.2.3

6.1.1. Calculations for True Measures of Ductility

The material properties in Section 6.1 refer to engineering stress and strain definitions (Reference 2.2.9, Chapter 9):

$$s = \frac{P}{A_0} \text{ and } e = \frac{L - L_0}{L_0}$$

Where P stands for the force applied during a static tensile test, L is the deformed-specimen length, and L_0 and A_0 are original length and cross-sectional area of the specimen, respectively. It is generally accepted that the engineering stress-strain curve does not give a true indication of the deformation characteristics of a material during the plastic deformation since it is based entirely on the original dimensions of the specimen. Therefore, the LS-DYNA finite element code requires input in terms of true stress and true strain definitions:

$$\sigma = \frac{P}{A} \text{ and } \varepsilon = \ln\left(\frac{L}{L_0}\right)$$

The relationships between the true stress and true strain definitions and engineering stress and engineering strain definitions can be readily derived based on constancy of volume ($A_0 \cdot L_0 = A \cdot L$) and strain homogeneity during plastic deformation:

$$\sigma = s \cdot (1 + e) \quad \text{Equation 6.1.1a}$$

$$\varepsilon = \ln(1 + e) \quad \text{Equation 6.1.1b}$$

These expressions are applicable only in the hardening region of stress-strain curve that is limited by the onset of necking.

The following parameters are used in the subsequent calculations:

$s_y \approx \sigma_y$ = yield strength

s_u = engineering tensile strength

σ_u = true tensile strength

$e_y \approx \varepsilon_y$ = strain corresponding to yield strength

e_u = engineering strain corresponding to engineering tensile strength
(uniform strain)

ε_u = true strain corresponding to true tensile strength
(true uniform strain)

In absence of the uniform strain data in available literature, it needs to be estimated based on stress-strain curves and elongation (strain corresponding to rupture of the tensile specimen). For Alloy 22

and 316 SS, the minimum elongation for uniform strain is reduced by 10% (see Assumption 3.2.6). For 316L SS, the minimum elongation for uniform strain is reduced by 40% (see Assumption 3.2.2).

For **Alloy 22** the true measures of ductility are:

$$e_u = 0.9 \cdot \text{elongation} = 0.9 \cdot 0.45 = 0.41 \text{ (at RT)}$$

$$\varepsilon_u = \ln(1 + e_u) = \ln(1 + 0.41) = 0.34 \text{ (at RT)} \quad \text{(using Equation 6.1.1b)}$$

$$\sigma_u = s_u \cdot (1 + e_u) = 689 \cdot (1 + 0.41) = 971 \text{ MPa (at RT)} \quad \text{(using Equation 6.1.1a)}$$

For **316 SS** the true measures of ductility are:

$$e_u = 0.9 \cdot \text{elongation} = 0.9 \cdot 0.40 = 0.36 \text{ (at RT)}$$

$$\varepsilon_u = \ln(1 + e_u) = \ln(1 + 0.36) = 0.31 \text{ (at RT)} \quad \text{(using Equation 6.1.1b)}$$

$$\sigma_u = s_u \cdot (1 + e_u) = 517 \cdot (1 + 0.36) = 703 \text{ MPa (at RT)} \quad \text{(using Equation 6.1.1a)}$$

For **316L SS** the true measures of ductility are:

$$e_u = 0.6 \cdot \text{elongation} = 0.6 \cdot 0.40 = 0.24 \text{ (at all temperatures)}$$

$$\varepsilon_u = \ln(1 + e_u) = \ln(1 + 0.24) = 0.22 \text{ (at all temperatures)}$$

Using Equation 6.1.1a:

$$\sigma_u = s_u \cdot (1 + e_u) = 483 \cdot (1 + 0.24) = 599 \text{ MPa (at RT)}$$

6.1.2. Calculations for Tangent Modulus

The results of this simulation are required to include elastic and plastic deformations for Alloy 22, 316 SS, and 316L SS. When the materials are driven into the plastic range, the slope of the stress-strain curve continuously changes. A simplification for this curve is used to incorporate plasticity into the FER. A standard approximation commonly used in engineering is to use a straight line that connects the yield point and the ultimate tensile strength point of the material (bilinear elastoplastic representation). The parameters used in the subsequent calculations in addition to those defined in Section 6.1.1 are modulus of elasticity (E) and tangent (hardening) modulus (E_1), the two slopes of this bilinear true stress – true strain curve. The tangent (hardening) modulus represents the slope of the stress-strain curve in the plastic region.

In the case of Alloy 22, the strain corresponding to the yield strength is:

$$\varepsilon_y = \sigma_y / E = 310 \cdot 10^6 / 206 \cdot 10^9 = 1.50 \cdot 10^{-3} \text{ (at RT)} \quad \text{(see Section 6.1)}$$

Hence, the tangent modulus is:

$$E_1 = (\sigma_u - \sigma_y) / (\varepsilon_u - \varepsilon_y) = (0.971 - 0.310) / (0.34 - 1.50 \cdot 10^{-3}) = 1.9527 \text{ GPa (at RT)}$$

(see Section 6.1, and 6.1.1)

The values of tangent moduli used in this calculation are presented in Table 6-1 as follows:

Table 6-1. Tangent Moduli at RT

Material	Tangent Modulus (GPa)	Tangent Modulus (psi)
Alloy 22	1.95	$0.283 \cdot 10^6$
316 SS	1.60	$0.232 \cdot 10^6$
316L SS	1.95	$0.283 \cdot 10^6$

6.2. CALCULATIONS FOR SNF NAVAL CANISTER WALL THICKNESS

Total length of canister	$= 210.63 \text{ in}$ $= (210.63)/(12*3.281) \text{ m}$ $= 5.3497 \text{ m}$
Top lid (plug) thickness	$= 15 \text{ in}$ $= (15)/(12*3.281) \text{ m}$ $= 0.381 \text{ m}$
Bottom lid thickness	$= 3.5 \text{ in}$ $= (3.5)/(12*3.281) \text{ m}$ $= 0.0889 \text{ m}$
Canister outer diameter	$= 66.12 \text{ in}$ $= (66.12)/(12*3.281) \text{ m}$ $= 1.6794 \text{ m}$
Canister shell length (between lids)	$= (210.63) - (15 + 3.5) \text{ in}$ $= 192.13 \text{ in}$ $= (192.13)/(12*3.281) \text{ m}$ $= 4.8798 \text{ m}$
Canister weight	$= 49.32 \text{ Tonne (Metric)}$ $= 49,320 \text{ kg (matches closely with LS-DYNA calculated weight of 49,254 kg as given in Table 7-1, part # 90)}$ $= (49,320*2.2046) \text{ lb}$ $= 108,731 \text{ lb}$ $= (108,731/2000) \text{ Ton (Eng.)}$ $= 54.37 \text{ Ton (Eng.)}$
Canister material (316L SS) density	$= 7980 \text{ kg/m}^3$
Top lid (plug) weight (including surrounding shell)	$= (\pi/4)*(dia^2)*(length)*density$ $= (\pi/4)*(1.6794^2)*(0.381)*(7980) \text{ kg}$ $= 6,735 \text{ kg}$ $= (6,735*2.2046) \text{ lb}$ $= 14,848 \text{ lb}$
Bottom lid weight (including surrounding shell)	$= (\pi/4)*(dia^2)*(length)*density$ $= (\pi/4)*(1.6794^2)*(0.0889)*(7980) \text{ kg}$ $= 1572 \text{ kg}$ $= (1572*2.2046) \text{ lb}$ $= 3465 \text{ lb}$

$$\begin{aligned}
 \text{Shell weight (between lids)} &= (\text{total wt.}) - \text{wt. of (top lid \& shell+ bottom lid \& shell)} \\
 &= (49,320) - (6735 + 1572) \text{ kg} \\
 &= 41,013 \text{ kg} \\
 &= (41,013 * 2.2046) \text{ lb} \\
 &= 90,417 \text{ lb}
 \end{aligned}$$

$$\begin{aligned}
 \text{Shell ID calculation} &= (\pi/4) * (\text{OD}^2 - \text{ID}^2) * (\text{shell length}) * (\text{density}) \\
 \text{(see Assumption 3.2.11)} &= (\pi/4) * (1.6794^2 - \text{ID}^2) * (4.8798) * (7980) \text{ kg} \\
 &= 41,013 \text{ kg}
 \end{aligned}$$

$$\begin{aligned}
 (1.6794^2 - \text{ID}^2) &= \{(41,013) / (7980 * 4.8798) * (\pi)\} * (4) \\
 &= 1.341
 \end{aligned}$$

$$\begin{aligned}
 \text{Shell ID} &= (1.6794^2 - 1.341)^{0.5} \text{ m} \\
 &= 1.2163 \text{ m}
 \end{aligned}$$

$$\begin{aligned}
 \text{Shell wall thickness (adjusted)} &= (\text{OD} - \text{ID}) / 2 \\
 &= (1.6794 - 1.2163) / 2 \text{ m} \\
 &= 0.2315 \text{ m} \\
 &= (0.2315 * 3.281 * 12) \text{ in} \\
 &= 9.1165 \text{ in}
 \end{aligned}$$

6.2.1. Calculations for SNF Naval Canister CG Location for LS-DYNA

CG location of the SNF canister:

$$\begin{aligned}
 \text{Canister material (316L SS) density} &= 7980 \text{ kg/m}^3 \\
 &= \{(7980 * 6.24283) / (100 * 12^3)\} \text{ lb/in}^3 \\
 &= 0.288 \text{ lb/in}^3
 \end{aligned}$$

$$\begin{aligned}
 \text{Top lid (plug) weight} &= (\pi/4) * (\text{canister OD}^2 * \text{thickness}) * \text{density} \\
 &= (\pi/4) * (66.12^2 * 15) * 0.288 \text{ lb} \\
 &= 14,848.67 \text{ lb}
 \end{aligned}$$

$$\begin{aligned}
 \text{Bottom lid weight} &= (\pi/4) * (\text{canister OD}^2 * \text{thickness}) * \text{density} \\
 &= (\pi/4) * (66.12^2 * 3.5) * 0.288 \text{ lb} \\
 &= 3,464.69 \text{ lb}
 \end{aligned}$$

$$\begin{aligned}
 \text{Canister shell weight} &= (\pi/4) * \{(\text{canister OD}^2 - \text{canister ID}^2) * \text{length}\} * \text{density} \\
 \text{(length between top \& bottom lids)} &= (\pi/4) * \{66.12^2 - (66.12 - 2 * 9.12)^2\} * 192.13 * 0.288 \\
 &= 90,430.60 \text{ lb}
 \end{aligned}$$

CG location (moments taken about the bottom face of the canister)

$$\begin{aligned}
 &= [\{14,848.67 * (210.63-15/2)\} + (3,464.69 * 3.5/2) + \{90,430.60 * (192.13/2 + 3.5)\}] \\
 &\quad / [(14,848.67 + 3,464.69 + 90,430.60)] \\
 &= (3,016,210.34 + 6,063.21 + 9,003,722.7) / (108,743.96) \\
 &= 110.59 \text{ in}
 \end{aligned}$$

Required CG location

(distance from the bottom of the external surface of the loaded canister)

between (bounding dimensions) = 103 in and 123 in (Reference 2.2.24, Figure C-17)

$$\text{Therefore: } 103 \text{ in} < 110.59 \text{ in} < 123 \text{ in}$$

Meets the requirements per Reference 2.2.24

6.3. IMPACT VELOCITY

To reduce the computer execution time while preserving all features of the problem relevant to the structural calculation, the WP is set in an oblique position just before impact and given an appropriate vertical velocity to simulate the velocity at the time of the impact (oblique free drop). This impact velocity is calculated considering that the WP has been lifted in a horizontal position to a height of 2.49 ft (0.759 m), (Reference 2.2.31).

Use of Newton's equation of motion determines the maximum impact velocity used for input into the LS-DYNA finite element (FE) simulation (Reference 2.2.10, Equation 15, p. 20):

$$V^2 = V_o^2 + 2gh$$

where,

V_o = initial velocity

V = final velocity

g = acceleration due to gravity

h = vertical drop height.

For this calculation:

$V_o = 0.0 \text{ m/s}$ (WP initially at rest)

$g = 9.81 \text{ m/s}^2$ (acceleration due to gravity)

$h = 0.759 \text{ m}$.(drop height)

Substituting these values into Newton's equation of motion, the result provides the final velocity of the falling WP immediately before impacting the unyielding surfaces:

$$V = \{ (V_o^2 + 2gh) \}^{1/2}$$

$$\{ 0^2 + 2(9.81)(0.759) \}^{1/2} = 3.859 \text{ m/s for a } 0.759 \text{ m drop height.}$$

6.4. FINITE ELEMENT REPRESENTATION

A full 3-D finite-element representation (FER) is created in TrueGrid V2.3 for this calculation. Figures 6-1 through 6-4 depict details of the “Standard FER”, Figures 6-5 through 6-8 depict details of the “Refined FER”, Figure 6-9 depicts details of the “FER of Initial Contact of Lower Sleeve with the TEV rail ledge and subsequent upper sleeve slapdown”, and Figure 6-10 depicts details of the FER of Initial Contact of Upper Sleeve with the TEV rail ledge and subsequent lower sleeve slapdown”.

The internal components of the WP are simplified in order to reduce the computer run time. The Naval SNF canister conforms to the dimensions given in Reference 2.2.24, Figure C-17. The shield plug at the top and the lid at the bottom of the Naval SNF canister have been modeled per dimensional details given in the referenced document. Since the details of the spent nuclear fuel inside the Naval SNF canister are not available, the details have not been modeled in the FER directly. The side wall thickness of the Naval SNF canister is increased to account for the weight of the spent nuclear fuel (Assumption 3.2.8). Since the side wall thickness of the canister is uniform, the weight of spent nuclear fuel is thus uniformly distributed, (smeared) along the Naval SNF canister side wall. The TEV rail ledge of 316 SS material is used to represent the target surface.

The orientation of the WP and its contents for the different impact scenarios on the TEV rail ledge was based on Reference 2.2.31. Also, the WP inner vessel outer surface is in contact with the OCB shell in the area where the sleeves contact the TEV rail ledge. This “no-gap” orientation is simulated to create the highest stresses in the OCB.

A static and dynamic friction coefficient of 0.4 was applied between all the parts of the WP (see Assumptions 3.2.10 and 3.2.11).

The mesh of the Standard FER is appropriately generated and refined in the contact regions according to standard engineering practice. The Standard FER was then further refined in the impact region to verify its stability in terms of mesh refinement. The mesh refinement of the outer corrosion barrier for the Standard FER is almost identical in both the lower and upper regions at their highest stressed locations (shell and lid interface of the OCB) and the stress magnitudes were similar. The volume and stress for the outer corrosion barrier elements of highest stress in the shell-lid interface region were compared for the Standard and Refined FER’s according to the method described in Reference 2.2.18, Section 6.2.3.

The travel distance of the WP to the impact point on the TEV rail ledge was reduced to a minimum before impact and the WP is given an initial velocity equal to 3.859 *m/s* for the 0.759 *m* drop height (see Section 6.3).

Transient dynamic analysis was performed on the FER using LS-DYNA.

WP FER's were created and analyzed at room temperature for the following cases and mesh configurations:

Run 1A:	standard mesh, 0.759 m drop @ RT, initial contact at both sleeves; $V = 3.859$ m/s
Run 1B:	refined mesh, 0.759 m drop @ RT, initial contact at both sleeves; $V = 3.859$ m/s
Run 2A:	standard mesh, 0.759 m drop @ RT, initial contact at lower sleeve; $V = 3.859$ m/s
Run 2B:	refined mesh, 0.759 m drop @ RT, initial contact at lower sleeve; $V = 3.859$ m/s
Run 3A:	standard mesh, 0.759 m drop @ RT, initial contact at upper sleeve; $V = 3.859$ m/s
Run 3B:	refined mesh, 0.759 m drop @ RT, initial contact at upper sleeve; $V = 3.859$ m/s
Run 4:	refined mesh, 0.759 m drop @ RT, initial contact at lower sleeve; $V = 7$ m/s
Run 5:	refined mesh, 0.759 m drop @ RT, initial contact at lower sleeve; $V = 10$ m/s
Run 6:	refined mesh (lower sleeve lower weld removed to simulate weld failure), 0.759 m drop @ RT, initial contact at upper sleeve; $V = 10$ m/s
Run 7:	refined mesh, 0.759 m drop @ RT, initial contact at upper sleeve; $V = 10$ m/s

Notes:

1. Runs 4, 5, 6, and 7 were made at higher velocities to determine approximately the limiting failure velocity for ASME failure criterion. The element wall-averaged stress intensity for runs 4, 5, and 7 is the highest at the OCB lid and shell interface, which is the assumed failure (or OCB breach) location. For run 6, the element wall-averaged stress intensity is the highest at the OCB lid horizontal wall section at the point of contact with the lower sleeve (see Figures 7-29 through 7-31). Peak stresses in the weld have not been investigated in detail, as Appendix A of Revision 00A (Reference 2.2.30) indicates that the failure of the upper sleeve welds will not affect the stress response in the wall of the OCB.
2. Runs 6 and 7 were terminated at 80 ms well after the peak stresses were reached and the stresses stabilized to a relatively low level compared to the peak stresses.

NAVAL LONG OBLIQUE IMPACT INSIDE TEV (CONTACT AT BOTH SLEEVES)

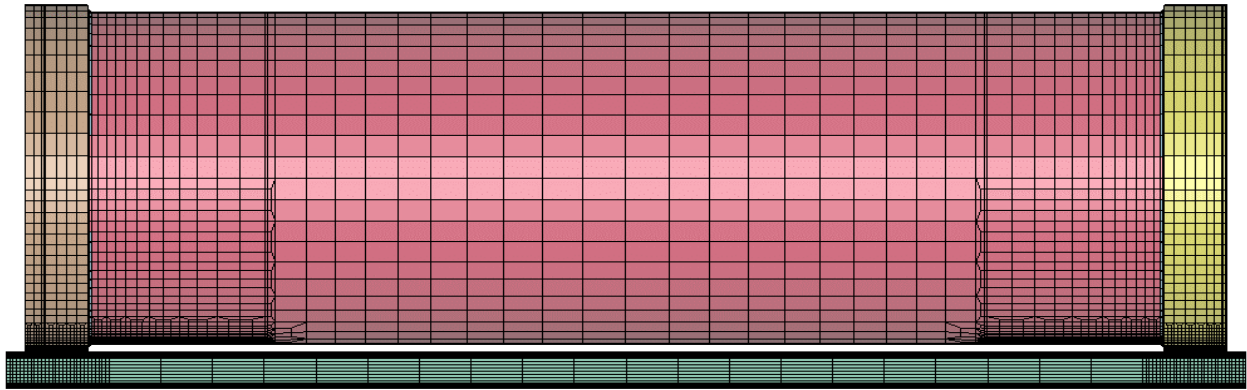


Figure 6-1. Standard FER

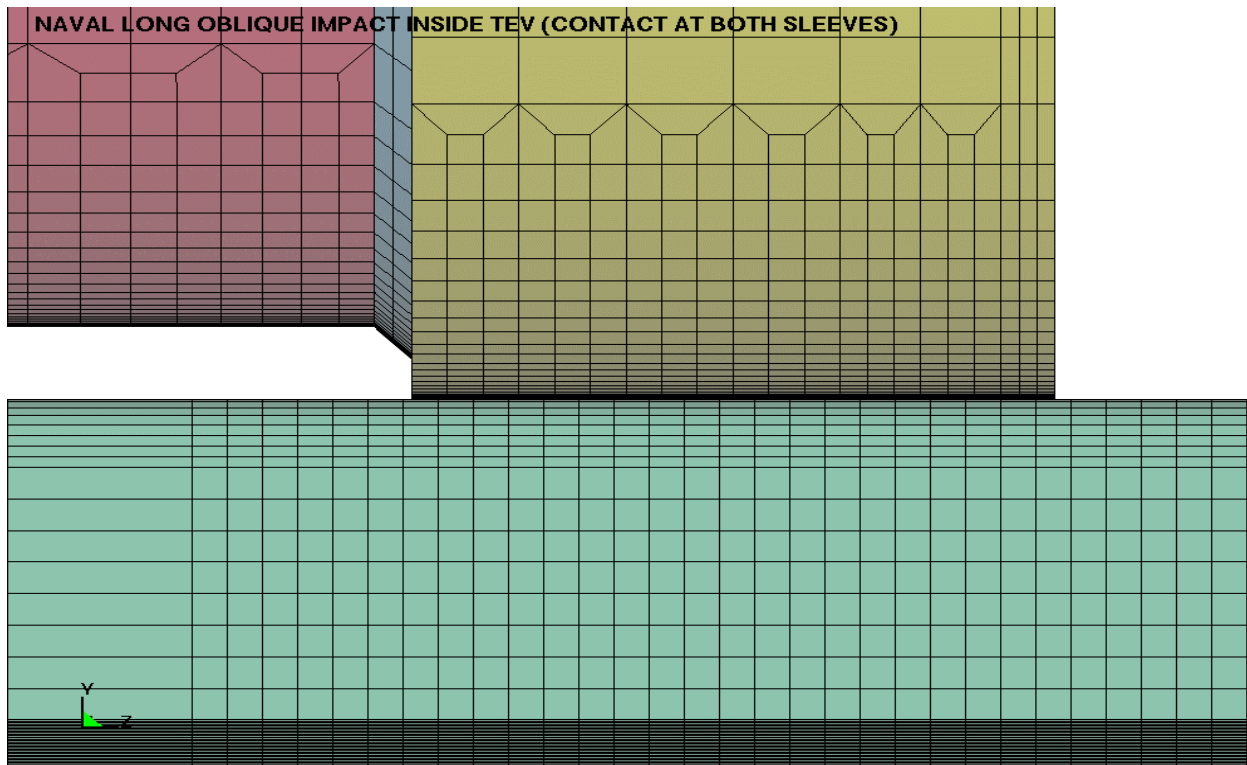


Figure 6-2. Standard FER Impact Area Detail

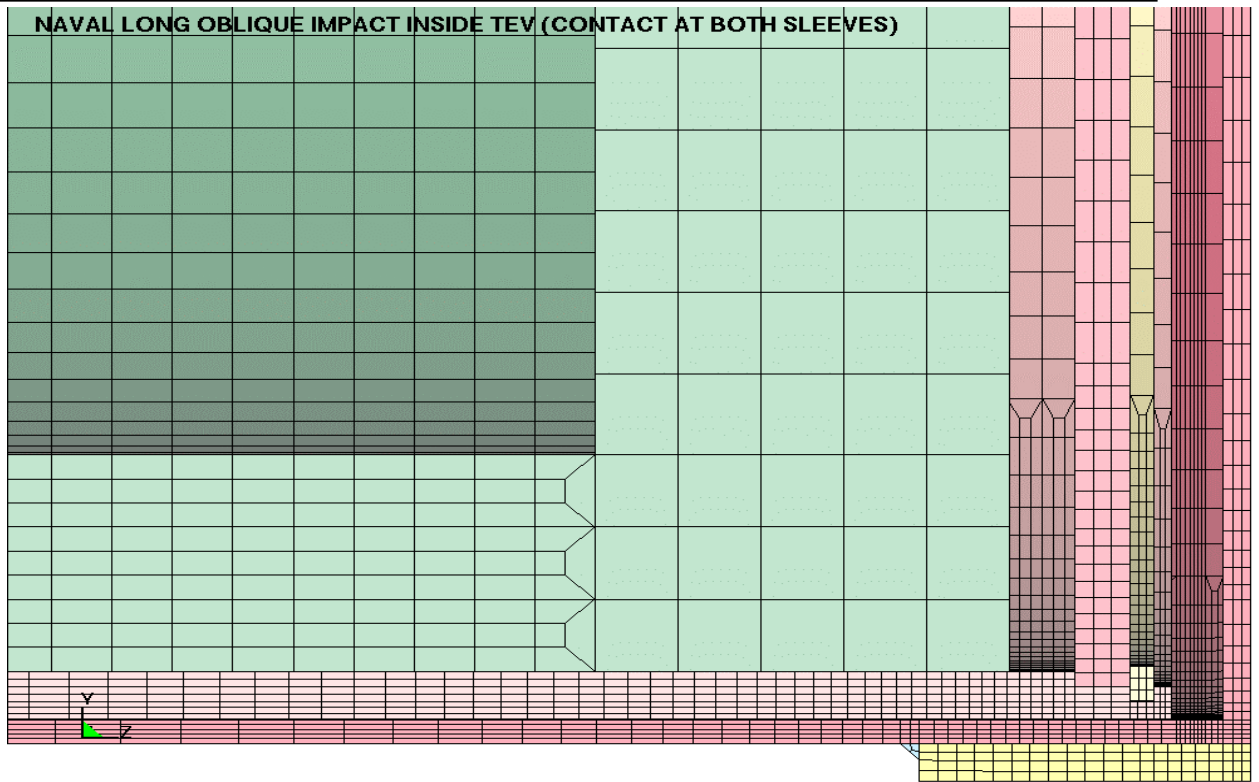


Figure 6-3. Standard FER Upper Sleeve Region Cut-Away

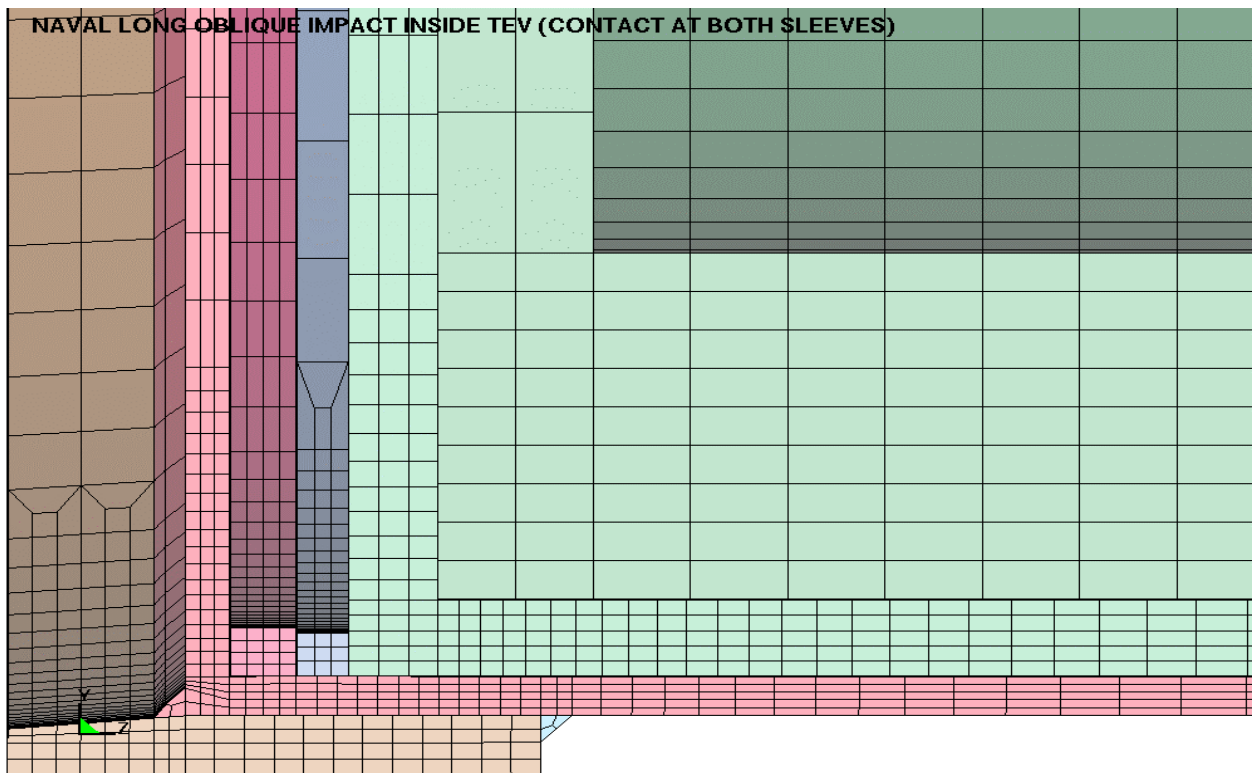


Figure 6-4. Standard FER Lower Sleeve Region Cut-Away

NAVAL LONG OBLIQUE IMPACT INSIDE TEV (CONTACT AT BOTH SLEEVES)

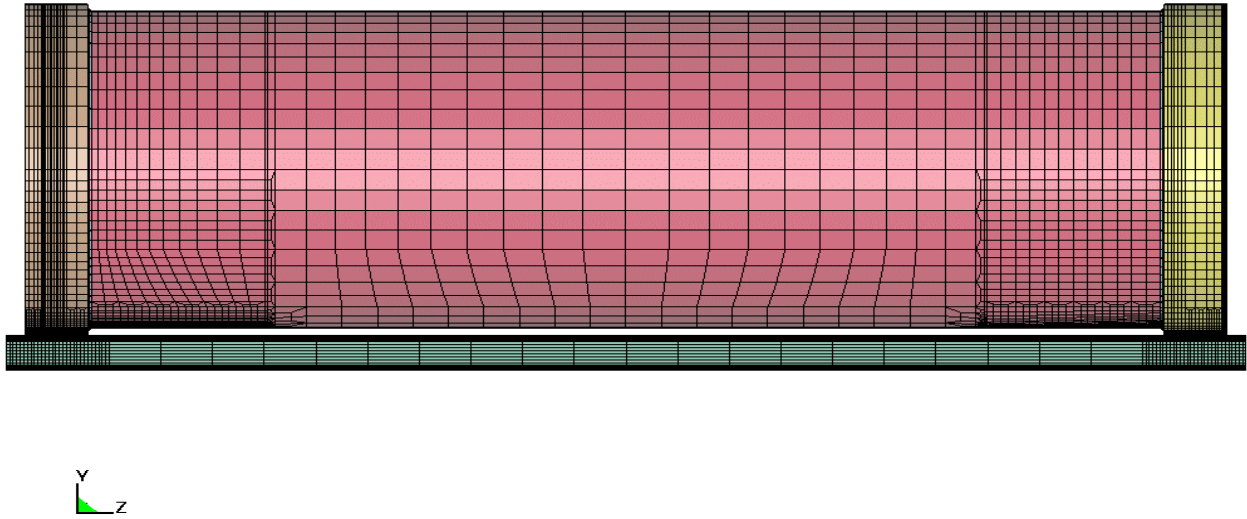


Figure 6-5. Refined FER

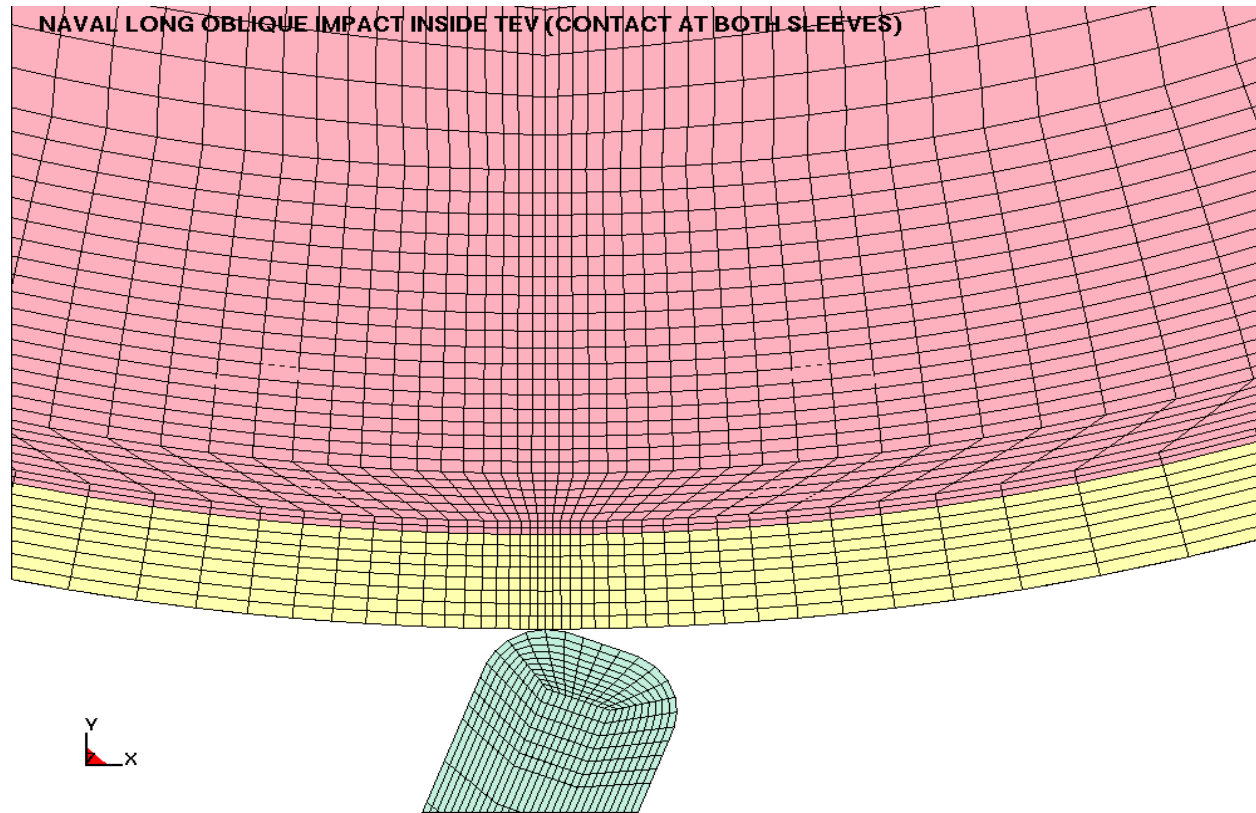


Figure 6-6. Refined FER Impact Area Detail

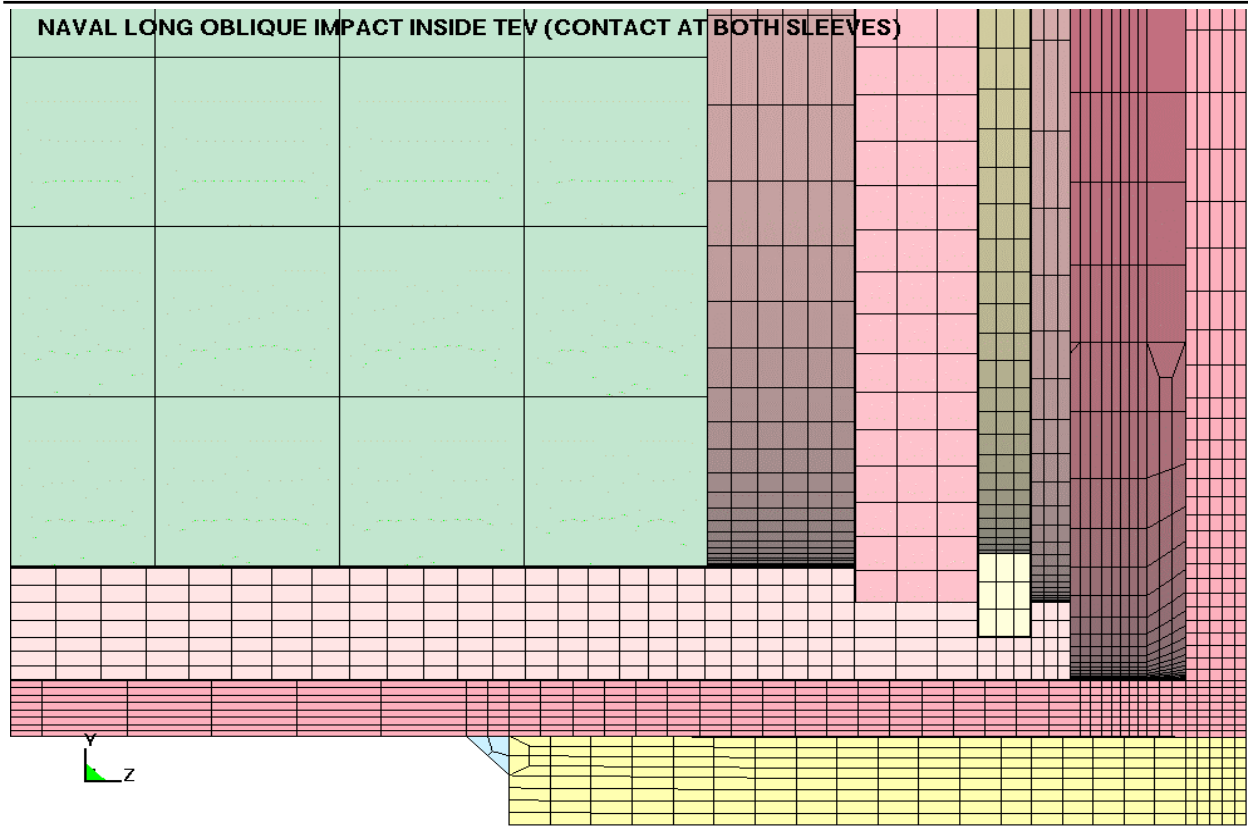


Figure 6-7. Refined FER Upper Sleeve Region Cut-Away

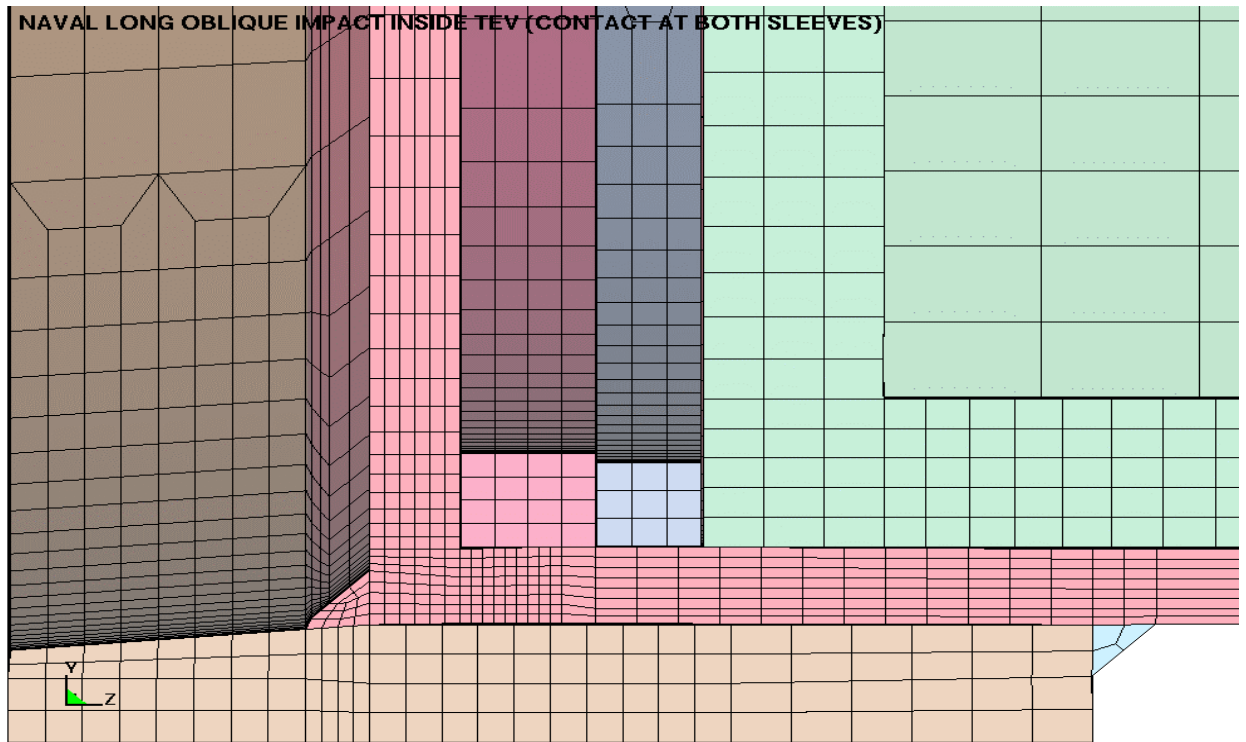


Figure 6-8. Refined FER Lower Sleeve Region Cut-Away

NAVAL LONG OBLIQUE IMPACT IN TEV (INITIAL CONTACT AT LOWER SLEEVE)

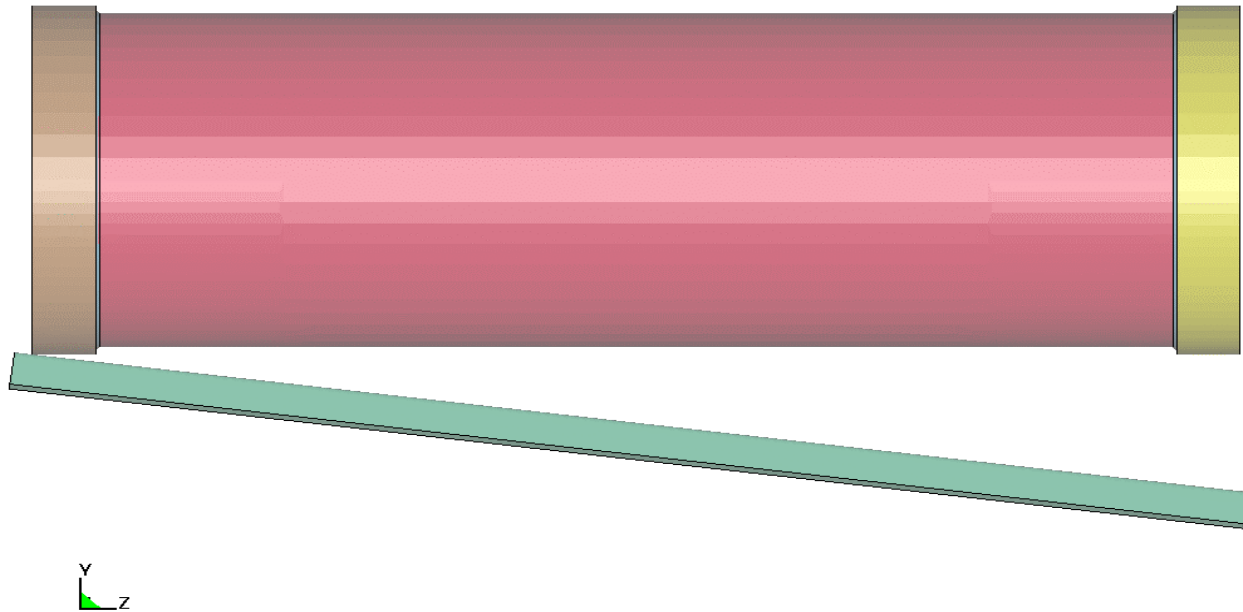


Figure 6-9. FER Initial Contact of Lower Sleeve with TEV Rail (Upper Sleeve Slapdown)

NAVAL LONG OBLIQUE IMPACT IN TEV (INITIAL CONTACT AT UPPER SLEEVE)

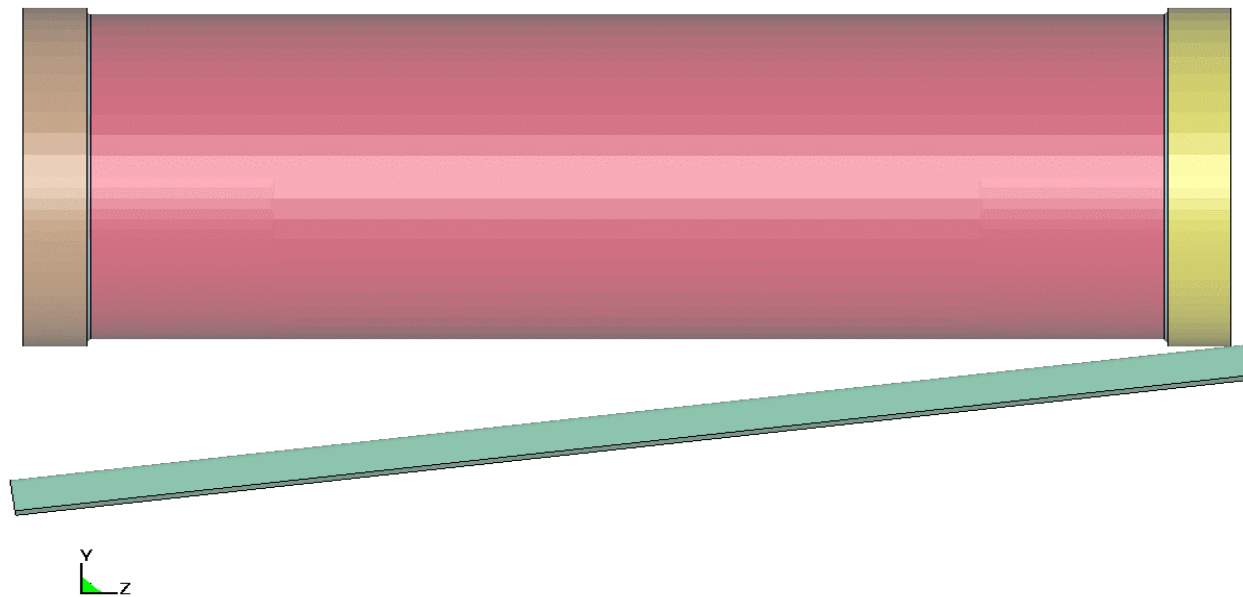


Figure 6-10. FER Initial Contact of Upper Sleeve with TEV Rail (Lower Sleeve Slapdown)

7.0 RESULTS AND CONCLUSIONS

Attachment I (CD) includes the input files and result (output) files that show execution of the successful simulations. The stresses are recorded every 0.0002 seconds at times near the peak response to ensure that all stress peaks have been captured.

The d3hsp result file for run 2B (Attachment I), lists the Refined FER RT masses calculated by LS-DYNA. The appropriate portion of the file is reproduced in Table 7-1 below. As seen, the mass of the FER WP equals 74,199 kg. This includes the mass of the TEV rail ledge (target block). The mass of the target TEV rail ledge is 716 kg., resulting in the net mass of the WP to be 73,483 kg. According to Reference 2.2.19, the mass of the WP is 73,500 kg. The discrepancy between the two masses is 0.023% $\{((73,500-73,483)*100)/73,483\}$, which is a negligible amount.

Table 7-1. Weight Verification

```

*****
Summary of mass
part id = 1 mass= 0.85239063E+04
part id = 2 mass= 0.16309357E+02
part id = 4 mass= 0.64254472E+03
part id = 5 mass= 0.61775378E+03
part id = 6 mass= 0.58568908E+02
part id = 7 mass= 0.37472207E+02
part id = 8 mass= 0.31195552E+04
part id = 9 mass= 0.35131035E+02
part id = 11 mass= 0.95044368E+03
part id = 13 mass= 0.71600560E+03 ***** TEV Rail Ledge
part id = 18 mass= 0.10226793E+05
part id = 90 mass= 0.49254354E+05 ***** Naval Canister

t o t a l m a s s = 0.74198838E+05
*****
    
```

Figures 7-1 to 7-38 show the location, contours, peak and wall averaged maximum shear stress from the LS-DYNA output at the time of maximum OCB stress response for different runs. High stresses are found at the lower sleeve lower weld, OCB lower lid shell interface and OCB upper lid shell interface in the vicinity of the contact area of the sleeves with the TEV rail ledge.

For the mesh refinement check, the limiting case event of initial contact of the lower sleeve with the TEV rail ledge is modeled using the standard (coarse) and fine mesh. Table 7-2 shows the mesh refinement verification results. As discussed in Section 6.4, the elements in the lower and upper lid to OCB shell interface in the vicinity of the contact area of the sleeves with the TEV rail ledge were used for the mesh refinement evaluation because the outer corrosion barrier was most highly stressed in these regions.

Table 7-2. Mesh Verification

	Standard Mesh		Refined Mesh		% Change
Outer Corrosion Barrier	EL#	$V = 6.6763E-07 \text{ m}^3$	EL#	$V = 1.9271E-07 \text{ m}^3$	246
	3988	$\tau_{\max} = 3.5652E+08 \text{ Pa}$ (see Figures 7-3 and 7-5)	6710	$\tau_{\max} = 3.7569E+08 \text{ Pa}$ (see Figures 7-9 and 7-11)	5.1

For the standard mesh, element # 3988 was chosen relative to element # 18797 because the through-wall average maximum stress was higher even though the maximum stress value for element # 18797 was higher by 18 MPa (see Figures 7-3 to 7-8). The percent change in stress is at least one order of magnitude less than the percent change in volume of the element. Thus, the standard mesh is deemed acceptable per Reference 2.2.18 (Section 6.2.3).

The results obtained from LS-DYNA are reported in terms of maximum shear stress. Since the maximum stress intensities are desired, the results needed to be converted. The maximum shear stress (see Reference 2.2.9, Chapter 3) is defined as one half of the difference between maximum and minimum principal stress. Stress intensity (see Reference 2.2.5, Section III, Division 1, Appendix XIII, XIII-1123(a)) is defined as the difference between maximum and minimum principal stress. Therefore, the results obtained from LS-DYNA are multiplied by two, to obtain the corresponding stress intensities.

The maximum stresses are found by carefully examining each time step of LS-DYNA computation, which outputs the element with the highest magnitude of stress, at each step, for each defined part. Table 7-3 shows the maximum stresses in the OCB at RT for a 0.759 m drop events. Table 7-3 also lists the ratios of maximum stress intensity to true tensile strength. It must be noted that wherever the element with maximum shear stress greater than 340 MPa (causing maximum stress intensity limit of 0.7 to be surpassed) did not have a through-wall thickness, an element closest to it with the highest stress and possible through-wall thickness in the assumed failure (or OCB breach) location was chosen. For example, in the limiting case run 2B, element # 37921 exhibited the highest shear stress of 377.02 MPa but did not have the proper through-wall thickness. Hence, the closest element # 6710 that exhibited maximum shear stress value of 375.69 MPa and had the through-wall thickness was chosen (see figures 7-9 and 7-10).

Table 7-3. Maximum Stress Intensity

Run #	Mesh Density	Figure #	Element # OCB	Time Step (seconds)	MSS (MPa) (OCB)	SI (MPa) (OCB)	$\frac{SI}{\sigma_u}$
1A	Standard	None	18797	0.0140	309.92	619.84	0.638
1B	Fine	7-2	121581	0.0164	338.04	676.08	0.696
2A	Standard (wall average)	7-7	3988	0.1391	325.09	650.18	0.670
2B	Fine (wall average)	7-12	6710	0.1399	328.102	656.20	0.676
3A	Standard (wall average)	None	65483	0.1356	310.2	620.40	0.639
3B	Fine (wall average)	7-16	128235	0.1347	312.55	625.10	0.644
4	Fine (wall average)	7-20	6728	0.0877	393.53	787.06	0.811
5	Fine (wall average)	7-24	6710	0.0656	416.33	832.66	0.858
6	Fine (wall average)	7-34	63034	0.0665	301.03	602.06	0.620
7	Fine (wall average)	7-38	128235	0.0630	446.03	892.06	0.919

Note:

MSS: Maximum Shear Stress

SI: Stress Intensity

 σ_u True Tensile Strength of Alloy 22 at RT = 971 MPa

High stress intensities were observed in the lower sleeve lower weld in the vicinity of the contact area of the lower sleeve with the TEV rail ledge. However, Appendix A of Reference 2.2.30 indicates that the failure of the upper sleeve welds will not affect the stress response in the wall of the OCB. Hence, weld stresses have not been investigated in detail in this calculation. In some OCB wall sections, SI/σ_u ratios are higher than 0.7. To verify that these maximum stress intensities do not cause a failure, a more detailed investigation into the source of the stress was required. Reference 2.2.12 provides this detailed investigation for the horizontal drop event. It concludes that the local primary stress intensity (P_L) should be used for the failure assessment of the outer corrosion barrier in the region of its juncture with the sleeve. The bending stresses contribute to the secondary stress intensity (Q) and need not be taken into account.

The allowable total primary stress intensity (P_L+P_b) limit in Reference 2.2.18 (Section 6.2.4) is $0.9S_u$, which for the non-linear LS-DYNA simulations, translates to $0.9\sigma_u$ (see Reference 2.2.5, Section III, Division 1, Appendix F, F-1322.3(b)). Based on the above considerations, the bending stresses in the OCB in the region of its juncture with the sleeve contribute to Q and $P_b = 0$. Therefore, the allowable maximum P_L stress intensity is $0.9\sigma_u$.

Rigorously performed, this calculation requires: Identification of stress component (signed σ_x , σ_y , σ_z , τ_{xy} , τ_{yz} , τ_{zx}) fields across the wall of the outer corrosion barrier, averaging of the stress component fields to create wall-averaged stress components, translate these wall-averaged stresses to principle stress directions and then calculate the difference between the maximum (S_1) and minimum (S_3) principle stress direction values. This calculation results in a P_L value, provided that the P_L values exceeding 1.1 times the P_m limit do not extend for greater than $\sqrt{R \cdot t}$, where R is the midsurface radius and t is the thickness of the OCB (see Reference 2.2.5, Section III, Division 1, Appendix XIII, XIII-1123(j)).

To simplify the calculation, the wall-average of the element total stress intensity values through the outer corrosion barrier (at the highest stressed element's circumferential location) is used to define P_L . This is a conservative representation of P_L because it ignores changing principle stress planes through the wall and includes (by the total stress intensity values being unsigned) the secondary (wall-bending) and the peak stress contributions. The through wall averaged maximum shear stress curves are shown in Figures 7-7, 7-8, 7-12, and 7-16 respectively.

The allowable P_m stress limit in Reference 2.2.18 (Section 6.2.4) is $0.7S_u$, which for the non-linear LS-DYNA simulations, translates to $0.7\sigma_u$ (see Reference 2.2.5, Section III, Division 1, Appendix F, F-1322.3(b)). Therefore, the P_L values that exceed 1.1 times $0.7\sigma_u = 0.77\sigma_u$ cannot extend for greater than $\sqrt{R \cdot t}$. Since none of the SI values in Table 7-3 exceeds $0.77\sigma_u$ for runs 1A, 1B, 2A, 2B, 3A and 3B, the SI values can be considered (local) P_L values and the $P_L + P_b$ limit is met.

For runs 1A, and 1B, (maximum free drop events), the project tiered acceptance criteria of peak stress $\sigma_{int} < 0.7\sigma_u$ is met at the OCB top and bottom lids respectively in the vicinity of the contact area of the sleeves with the TEV rail ledge (see Figures 7-1 and 7-2 for run 1B). For runs 2A, 2B, 3A, and 3B (maximum free drop events), the project tiered acceptance criteria of wall-averaged $\sigma_{int} < 0.77\sigma_u$ is met at the assumed failure (or breach) location of the OCB lid and shell interface

(see Figures 7-3 through 7-16). For runs 4, 5, and 7 (impact velocities of 7 m/s, 10 m/s, and 10 m/s respectively), the project tiered acceptance criteria of wall-averaged $\sigma_{int} < 0.77 \sigma_u$ mentioned in Reference 2.2.18 (Section 6.2.4) is not met at the assumed failure (or breach) location of the OCB lid and shell interface. For run 6 (impact velocity of 10 m/s with lower sleeve lower weld removed to simulate weld failure during the lower sleeve slakedown), the project tiered acceptance criteria of wall-averaged $\sigma_{int} < 0.77 \sigma_u$ is met at the assumed failure (or breach) location of the OCB lid and shell interface (see Figures 7-32 through 7-34). However, the element wall-averaged stress intensity at the OCB lid horizontal wall section at the point of contact with the lower sleeve (see Figures 7-29 through 7-31) does not meet the project tiered acceptance criteria. As mentioned in Section 6.4, runs 4 through 7 were made to determine approximately the limiting failure velocity for ASME failure criterion.

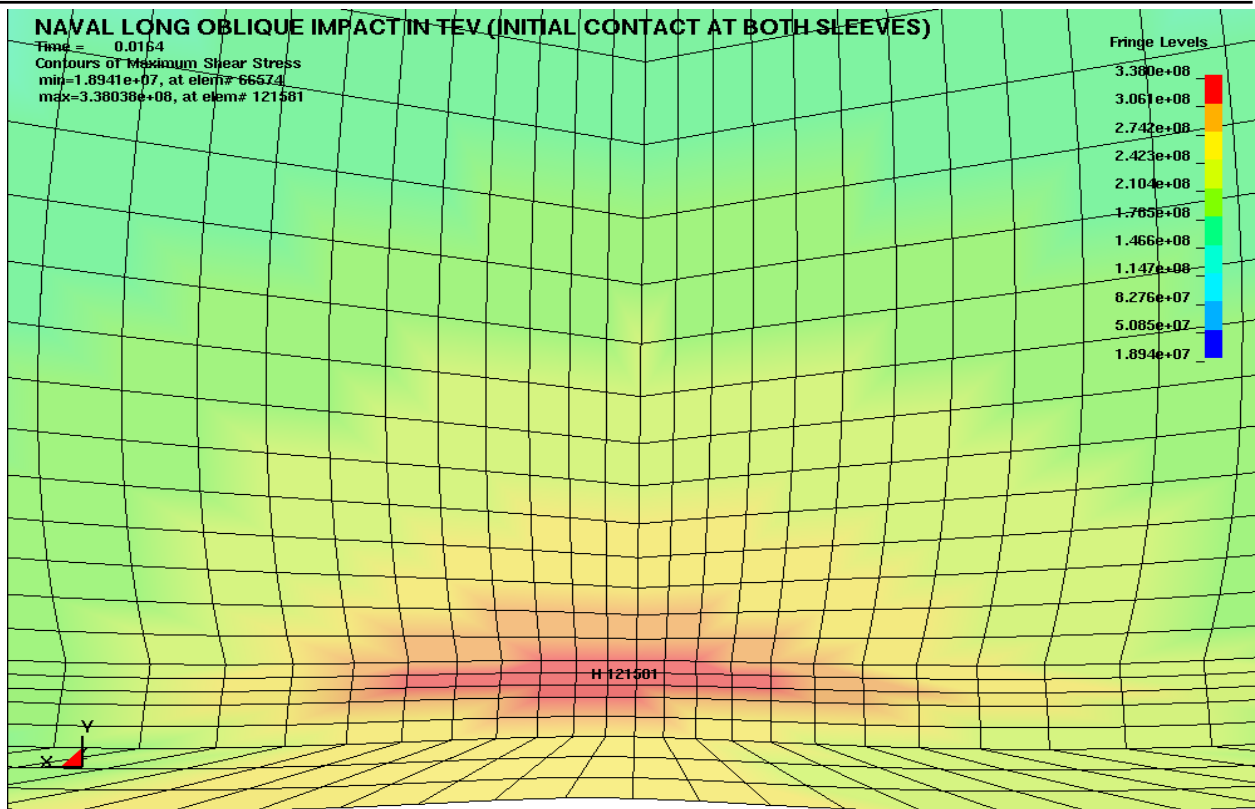


Figure 7-1. OCB Maximum Shear Stress (Pa) Location for Fine Mesh (run 1B)

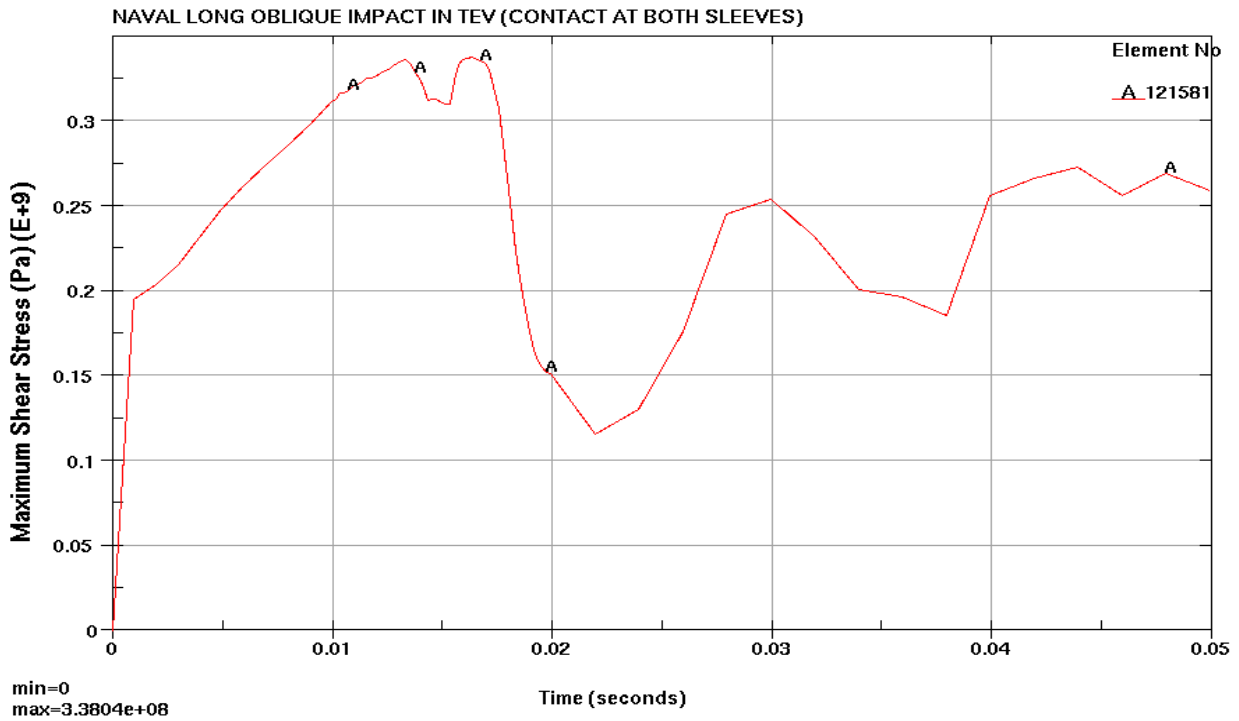


Figure 7-2. OCB Maximum Shear Stress for Fine Mesh (run 1B)

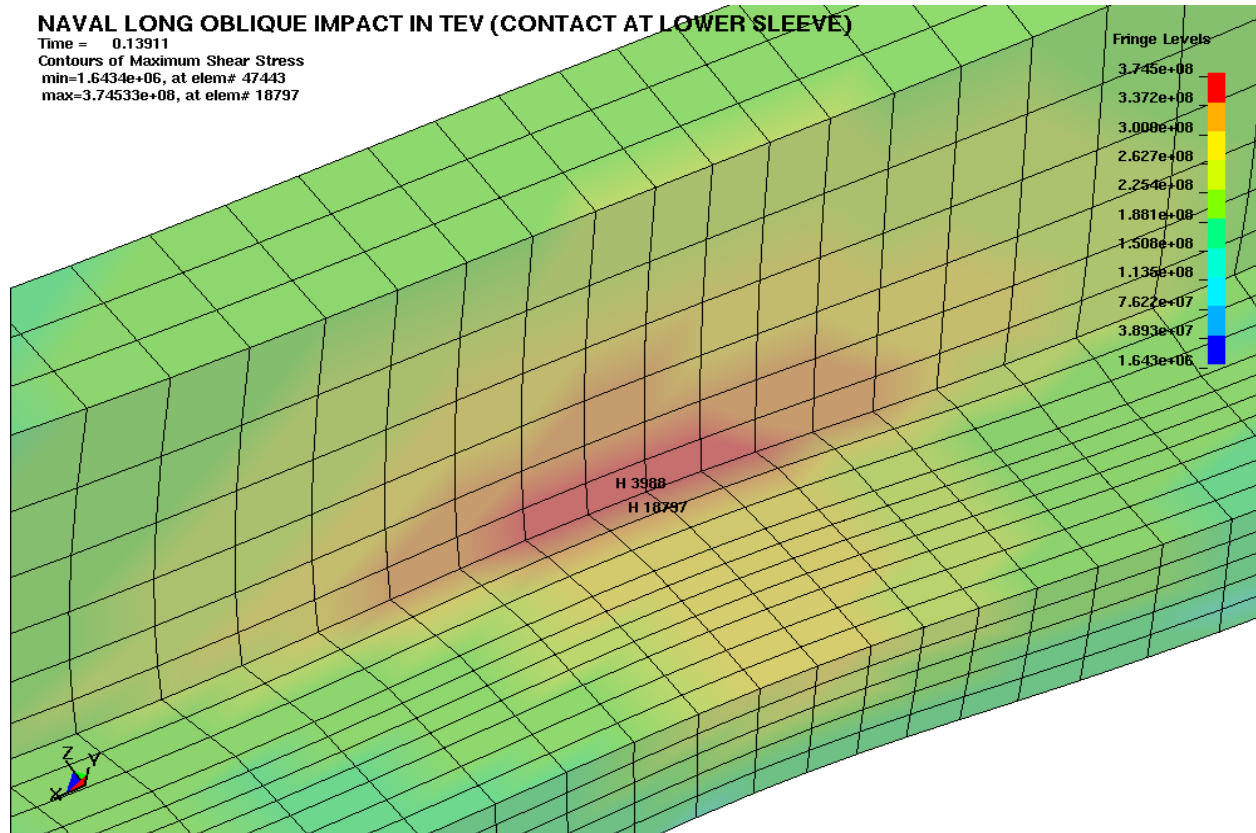


Figure 7-3. OCB Shell-Upper Lid Interface MSS (Pa) Location for Standard Mesh (run 2A)

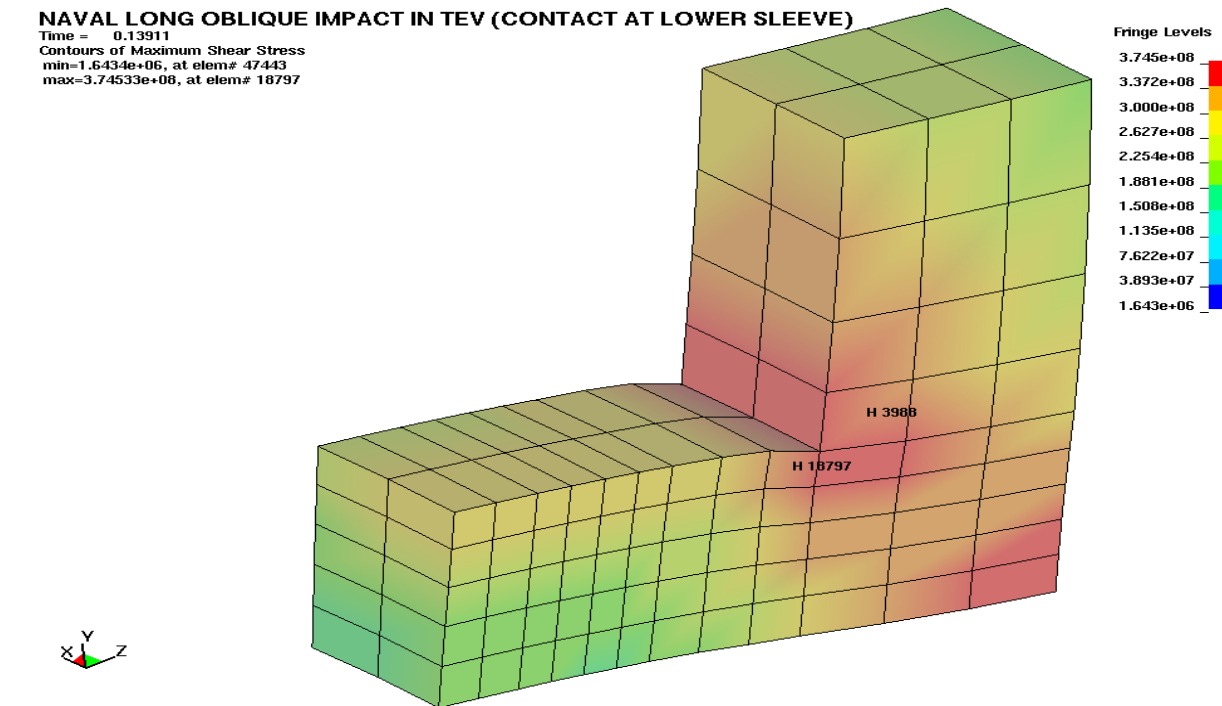


Figure 7-4. OCB Shell-Upper Lid Interface MSS (Pa) Location for Standard Mesh (run 2A)

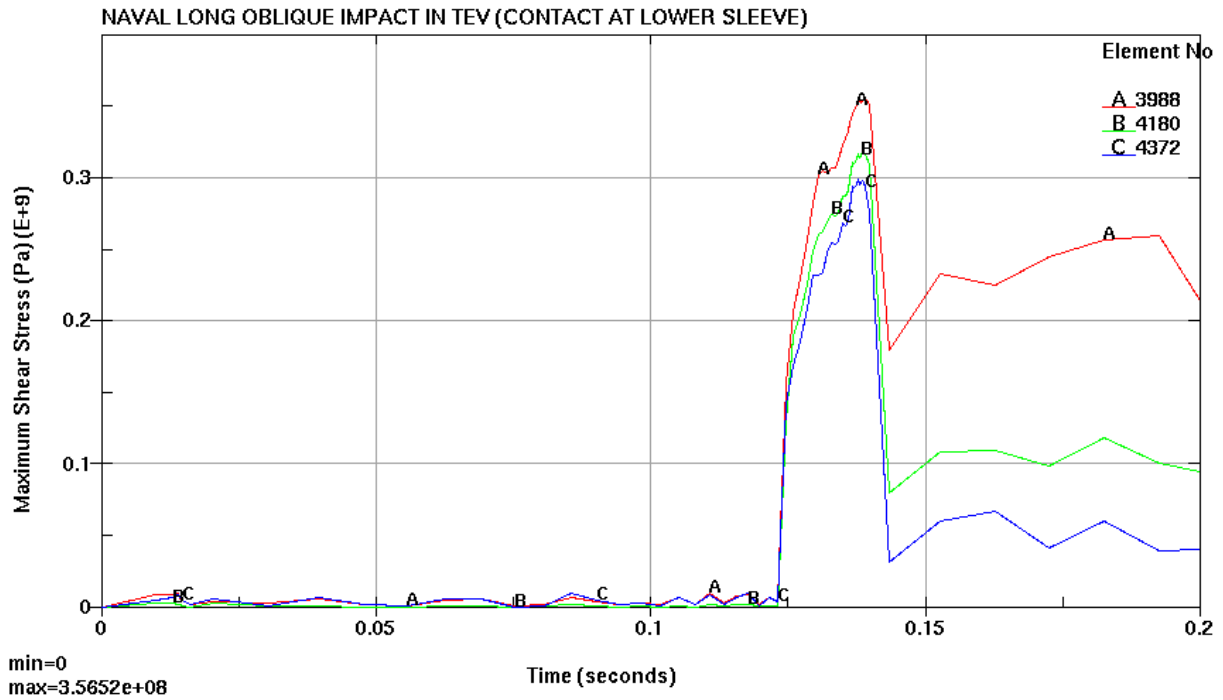


Figure 7-5. OCB Through-Wall Maximum Shear Stress for Standard Mesh (run 2A)

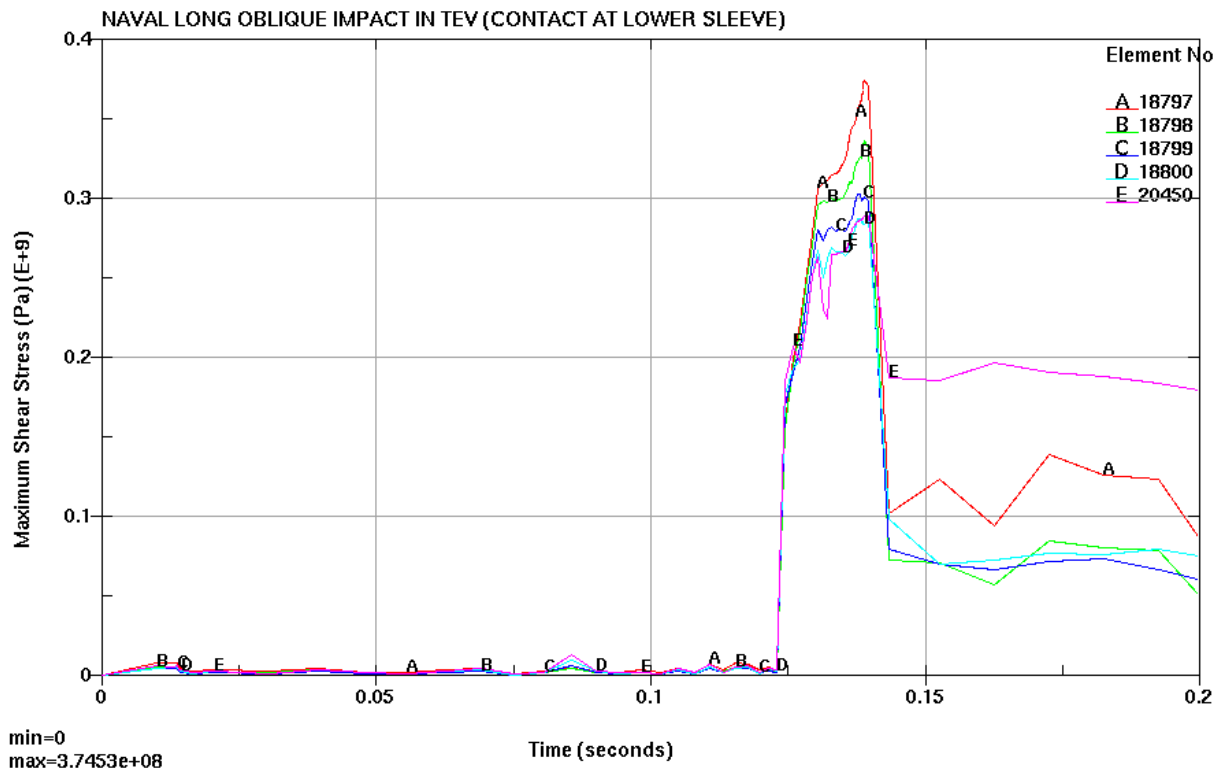


Figure 7-6. OCB Through-Wall Maximum Shear Stress for Standard Mesh (run 2A)

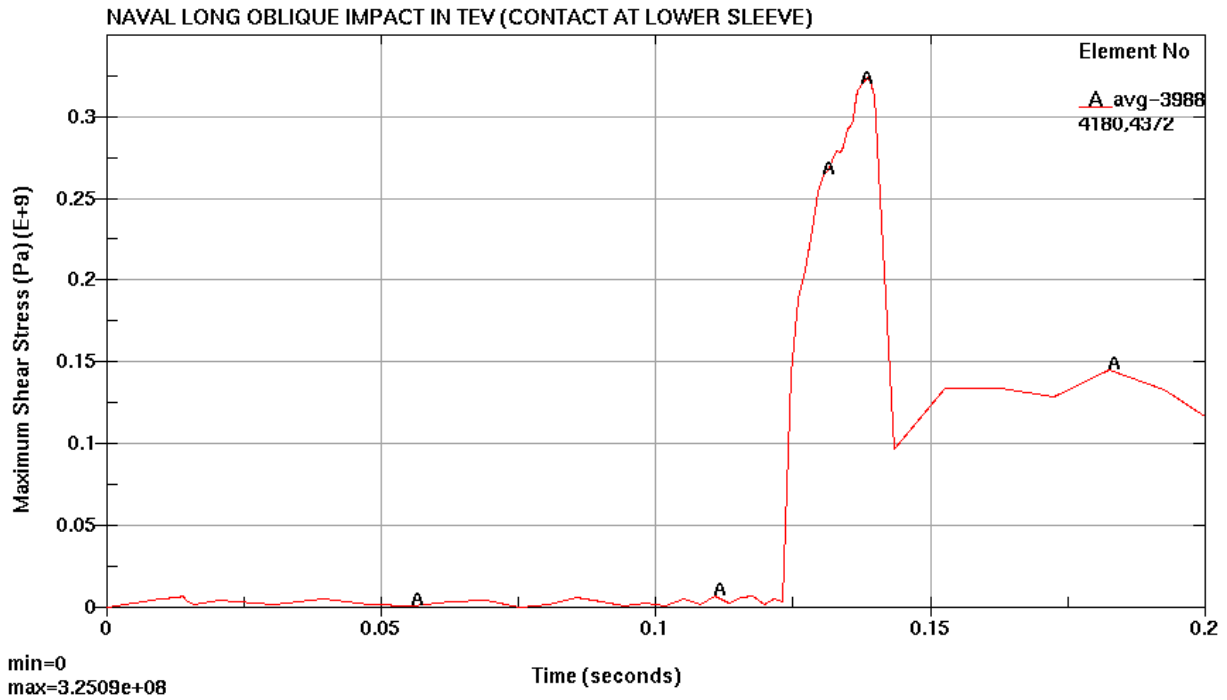


Figure 7-7. OCB Through-Wall Averaged Maximum Shear Stress for Standard Mesh (run 2A)

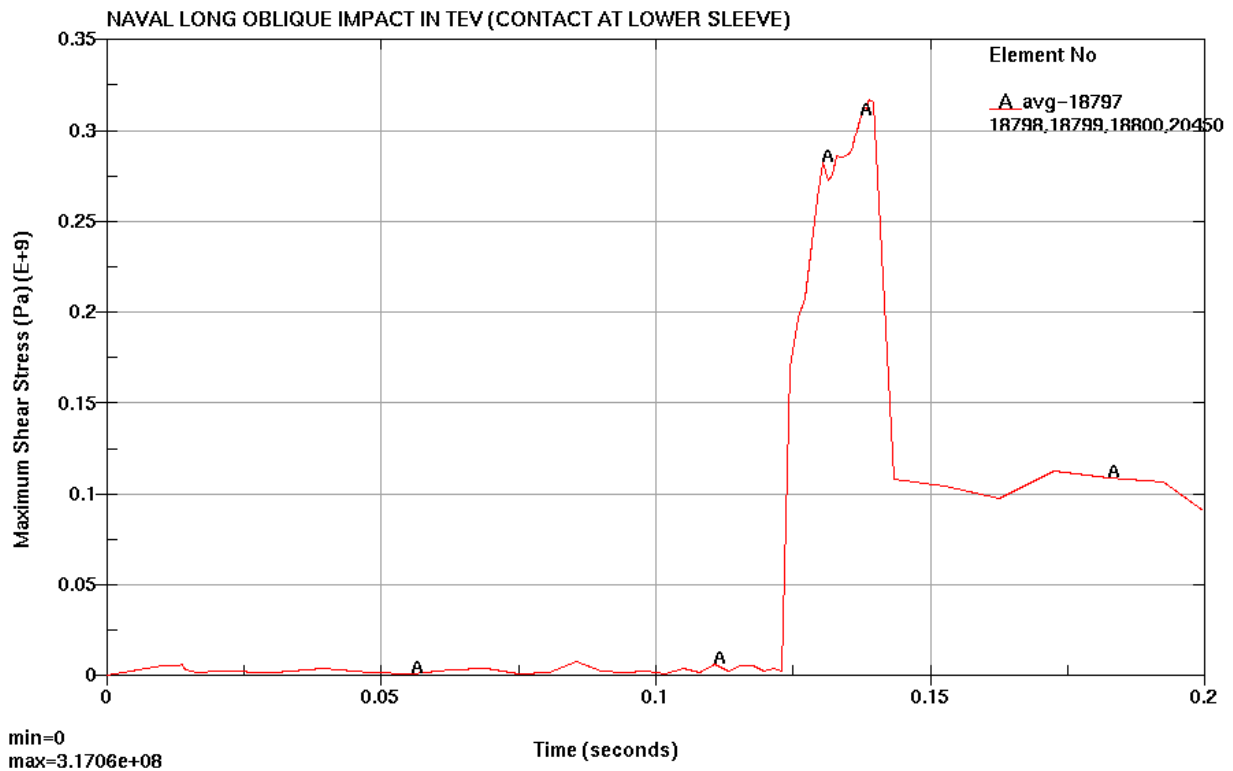


Figure 7-8. OCB Through-Wall Averaged Maximum Shear Stress for Standard Mesh (run 2A)

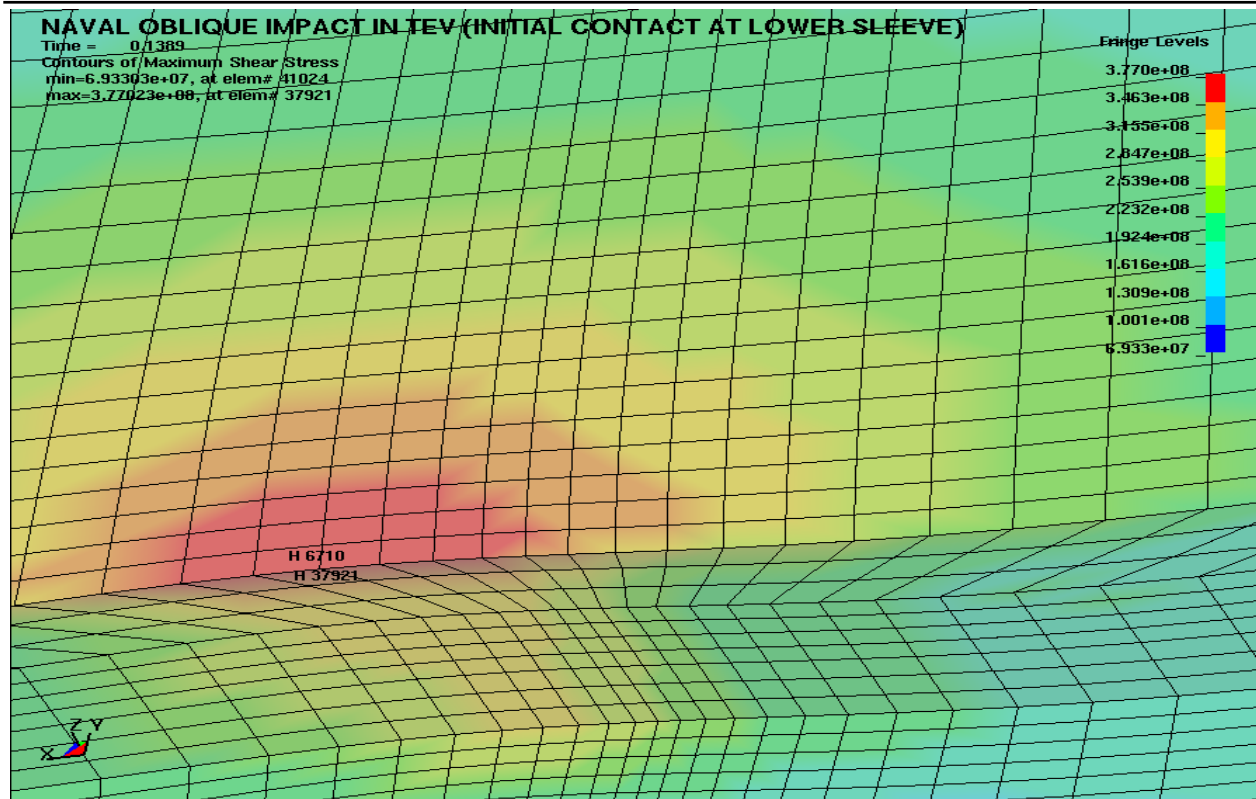


Figure 7-9. OCB Shell-Upper Lid Interface MSS (Pa) Location for Fine Mesh (run 2B)

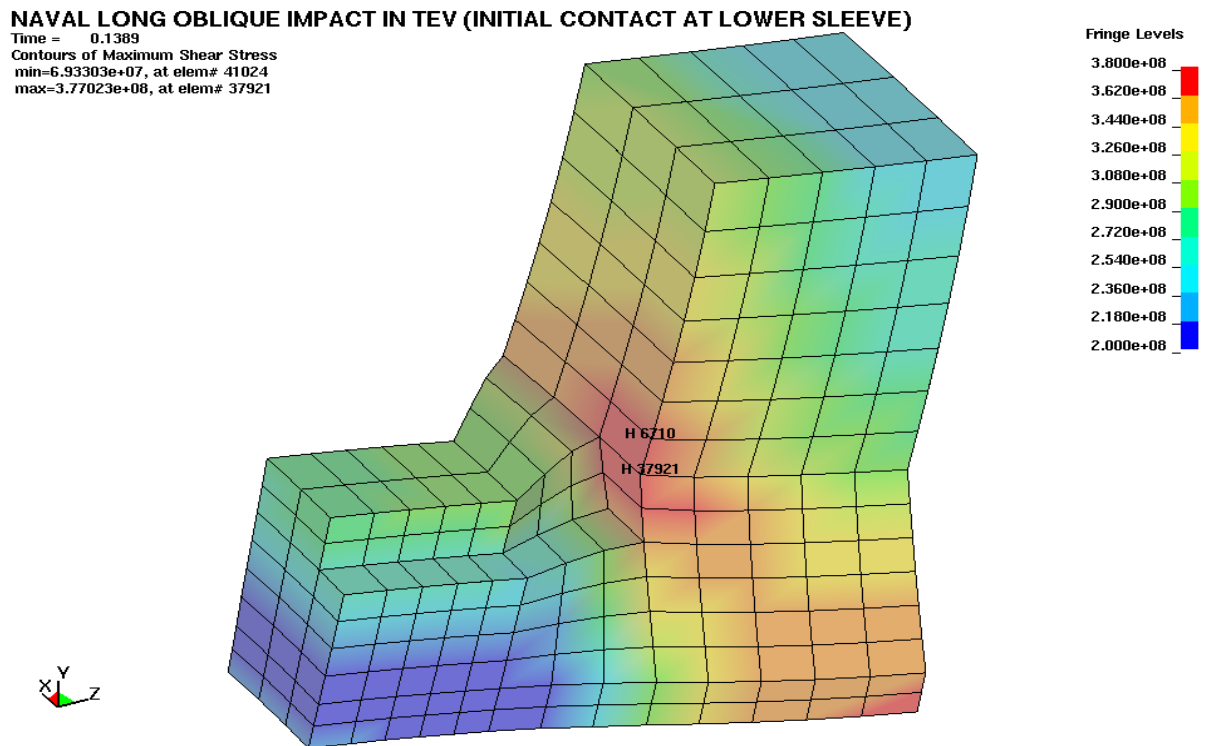


Figure 7-10. OCB Shell-Upper Lid Interface MSS (Pa) Location for Fine Mesh (run 2B)

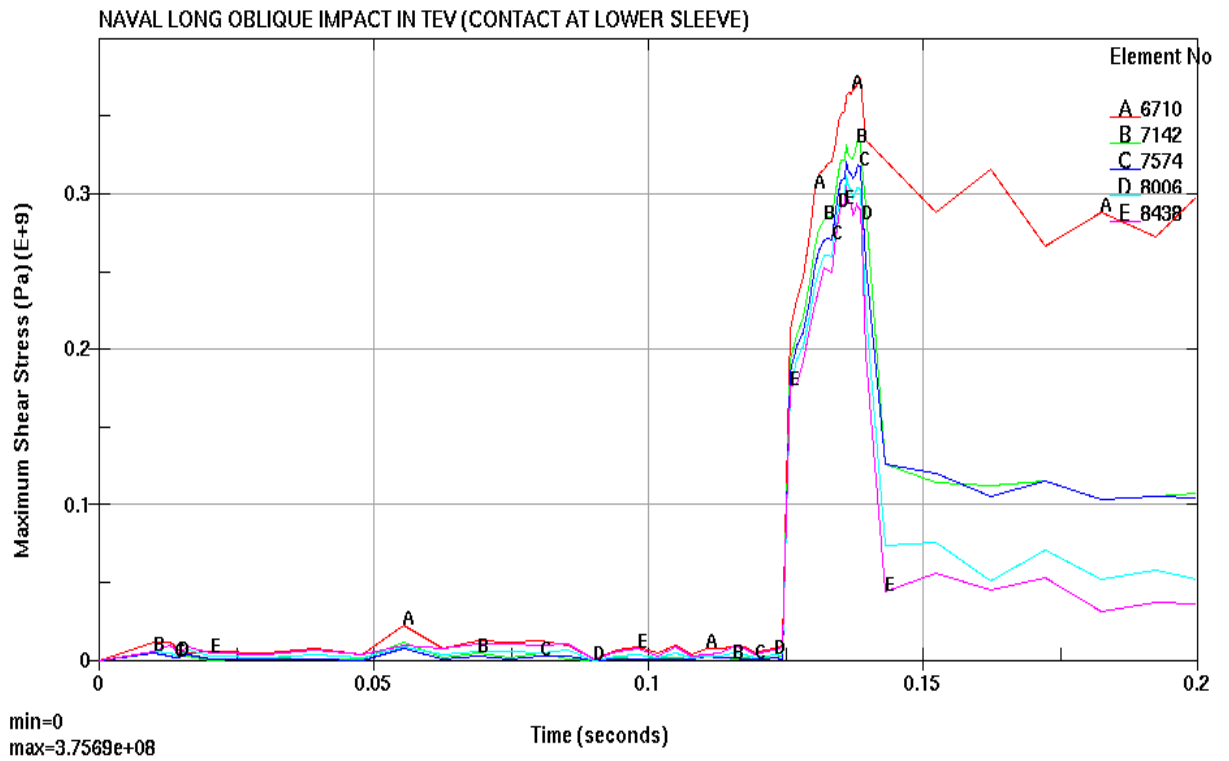


Figure 7-11. OCB Through-Wall Maximum Shear Stress for Fine Mesh (run 2B)

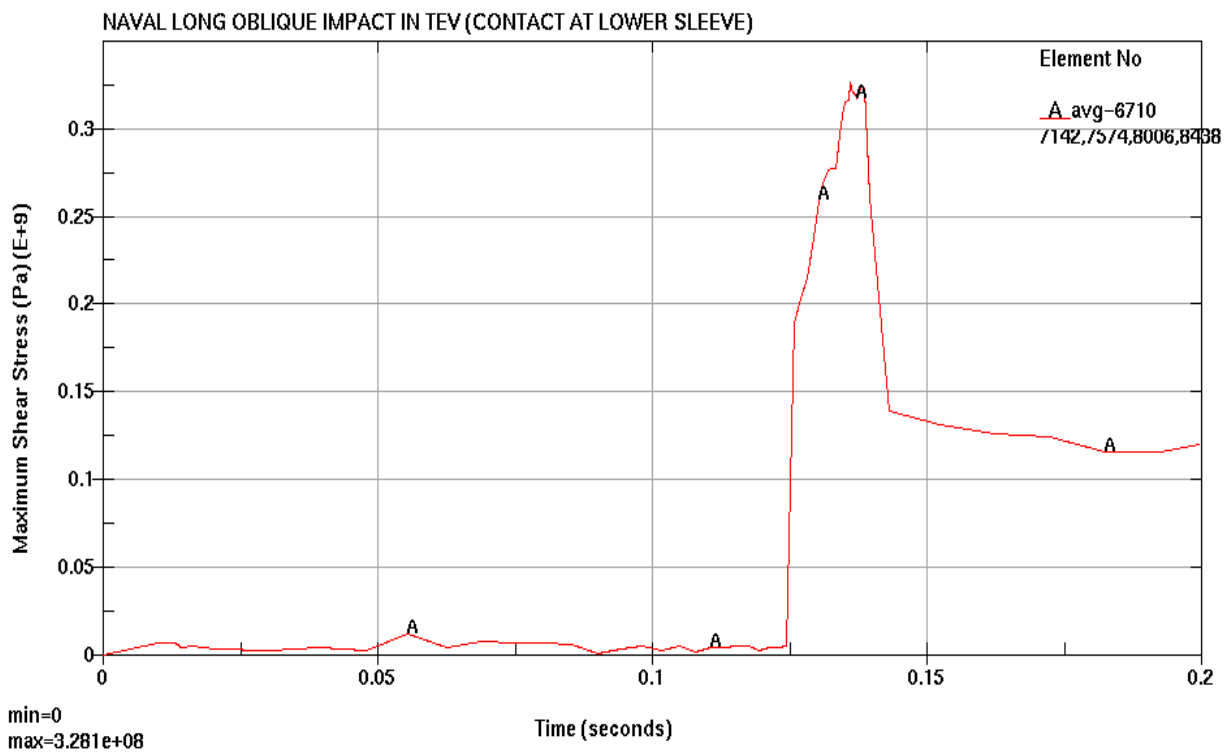


Figure 7-12. OCB Through-Wall Averaged Maximum Shear Stress for Fine Mesh (run 2B)

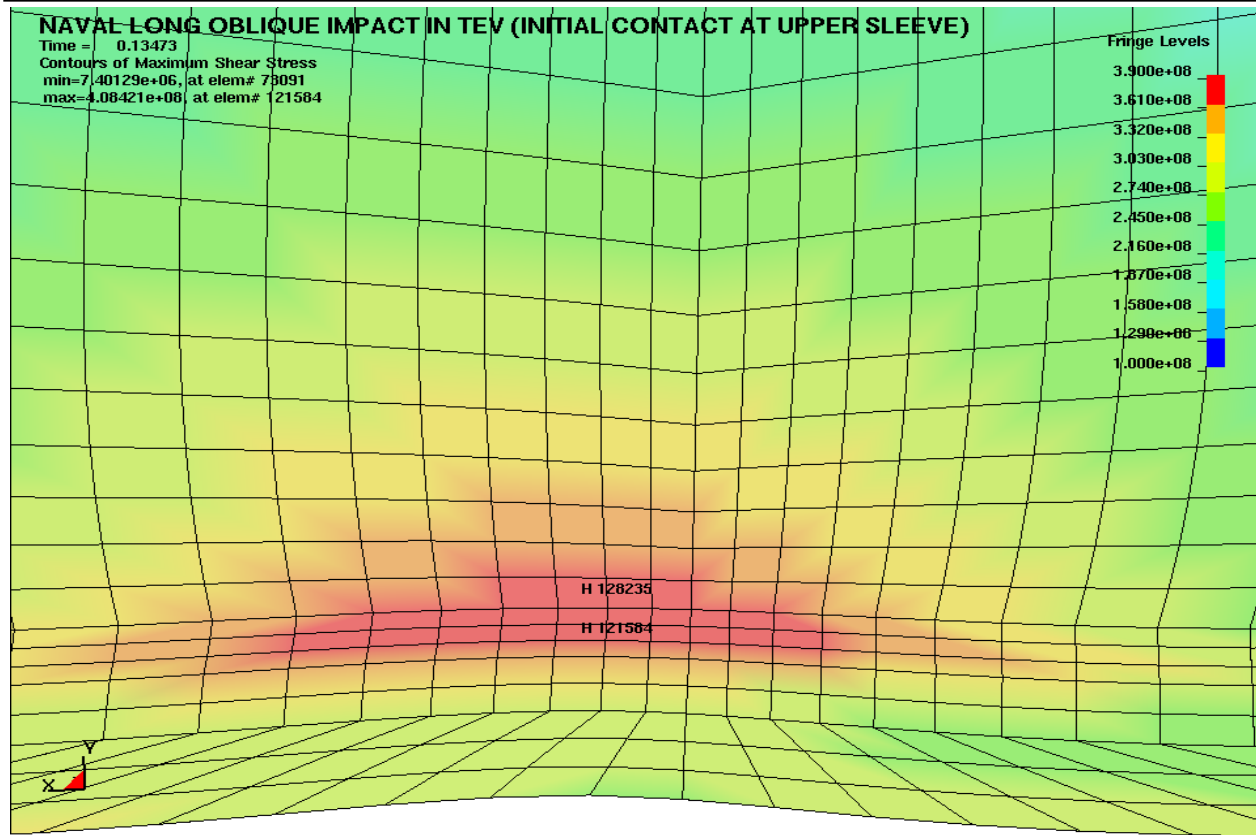


Figure 7-13. OCB Shell-Lower Lid Interface MSS (Pa) Location for Fine Mesh (run 3B)

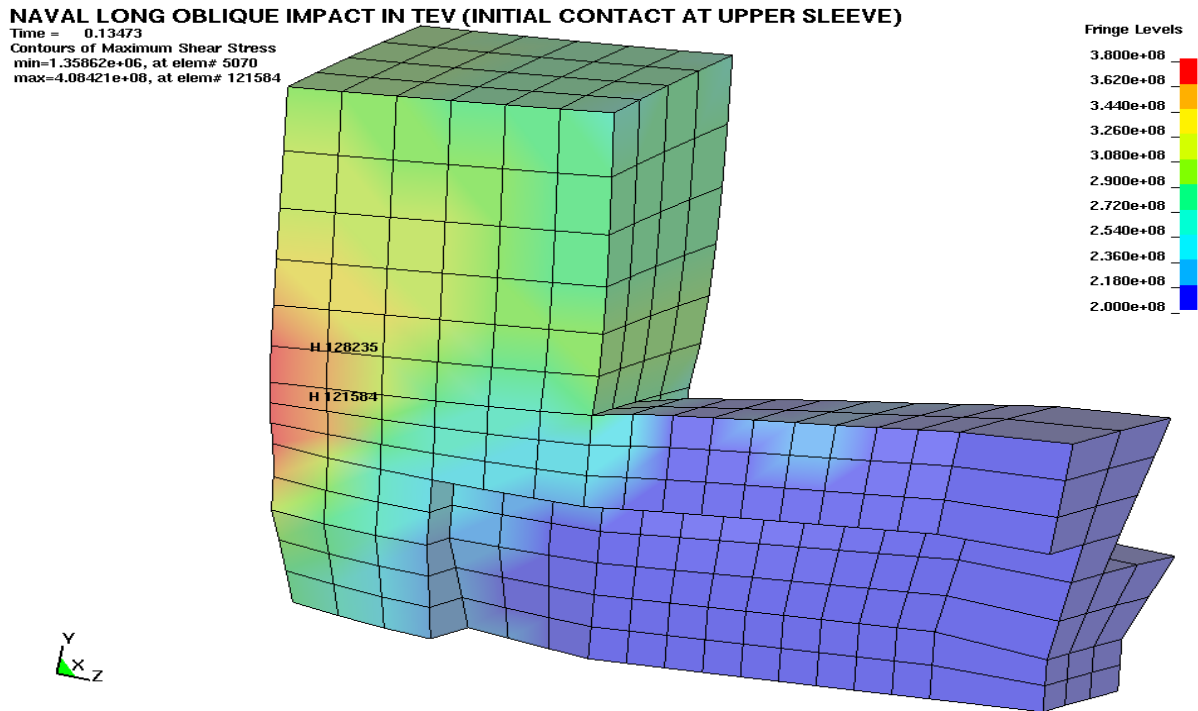


Figure 7-14. OCB Shell-Lower Lid Interface MSS (Pa) Location for Fine Mesh (run 3B)

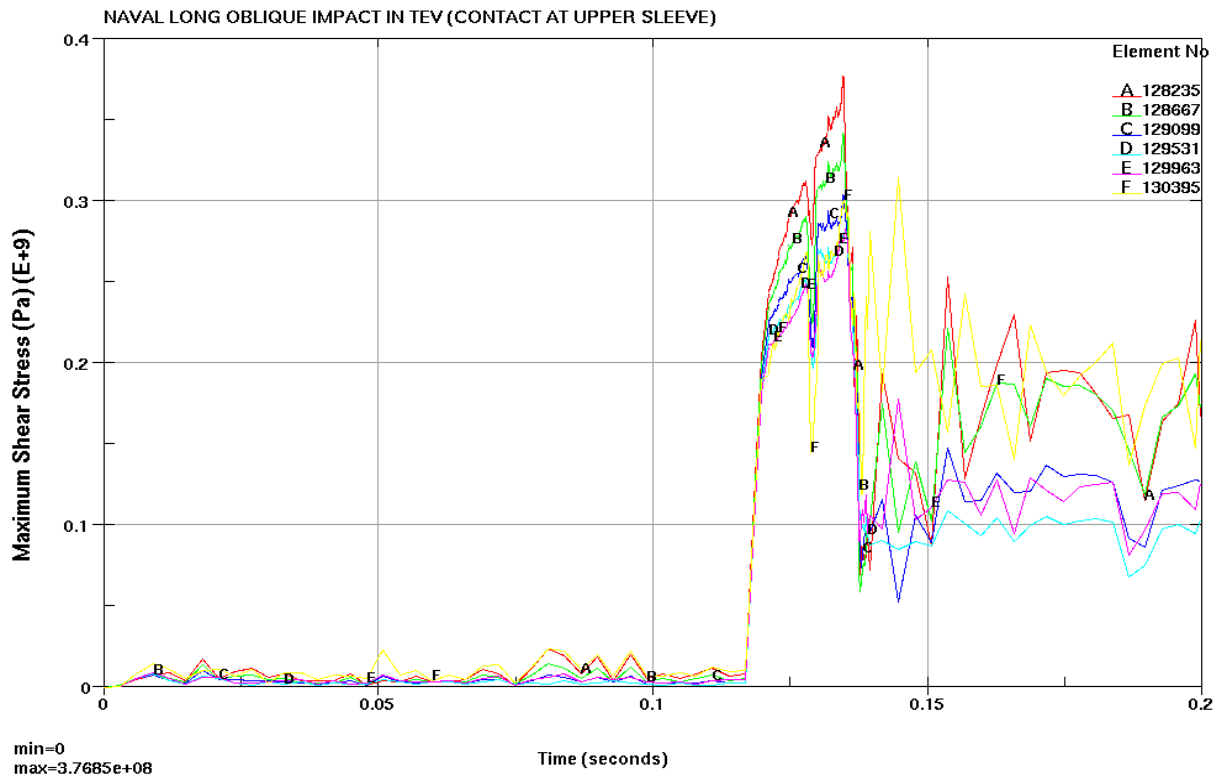


Figure 7-15. OCB Through-Wall Maximum Shear Stress for Fine Mesh (run 3B)

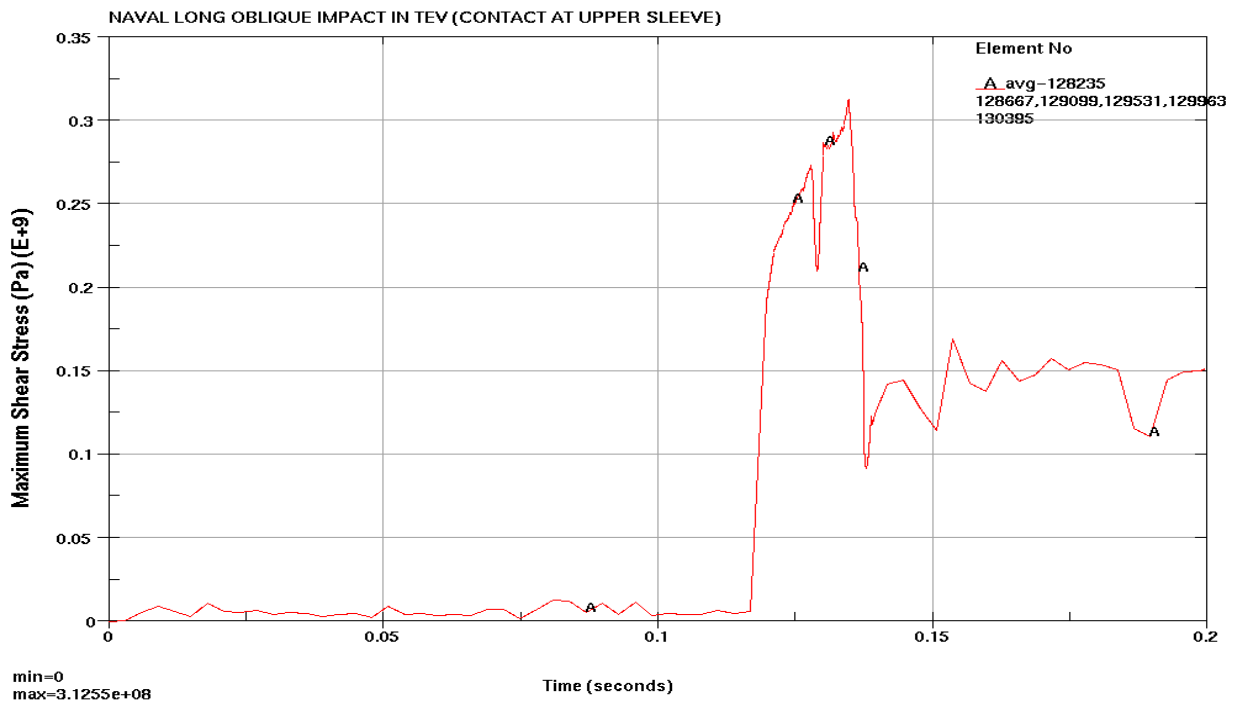


Figure 7-16. OCB Through-Wall Averaged Maximum Shear Stress for Fine Mesh (run 3B)

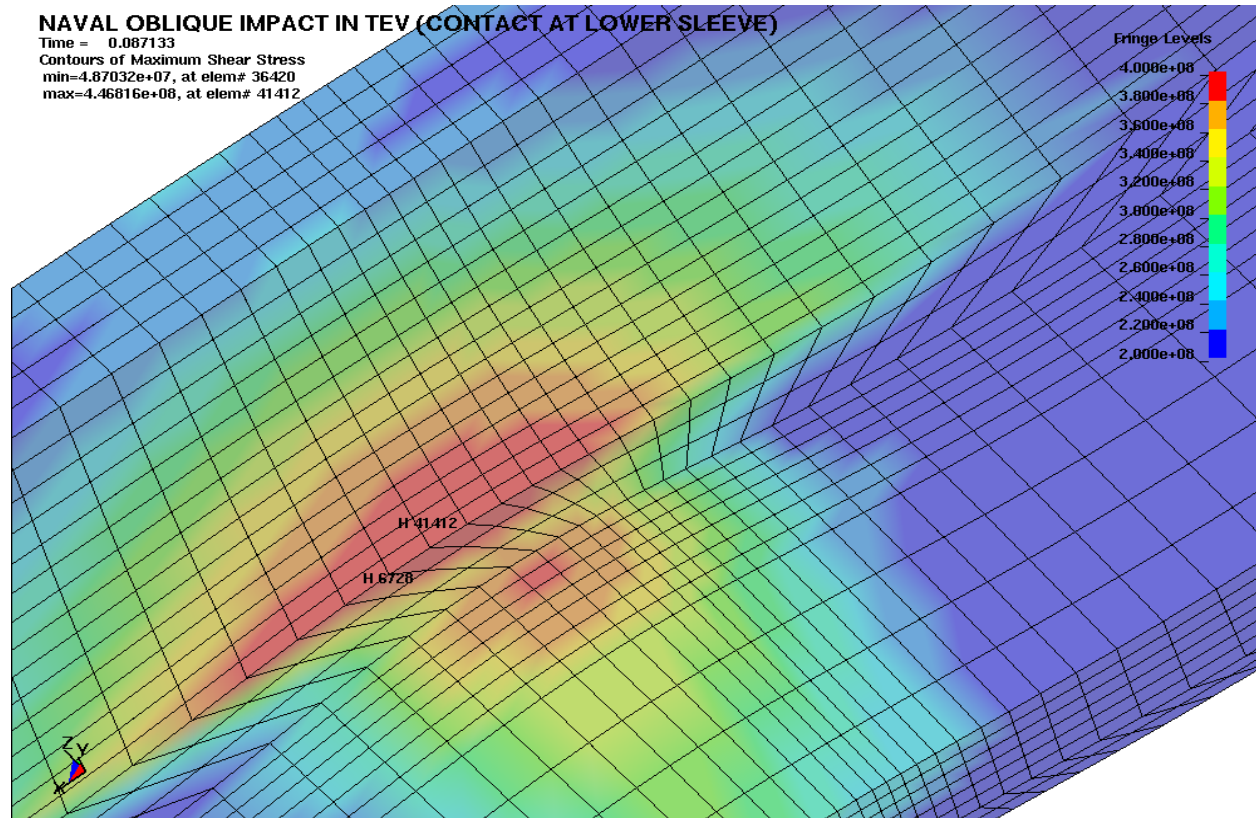


Figure 7-17. OCB Shell-Upper Lid Interface MSS (Pa) Location for Fine Mesh (run 4)

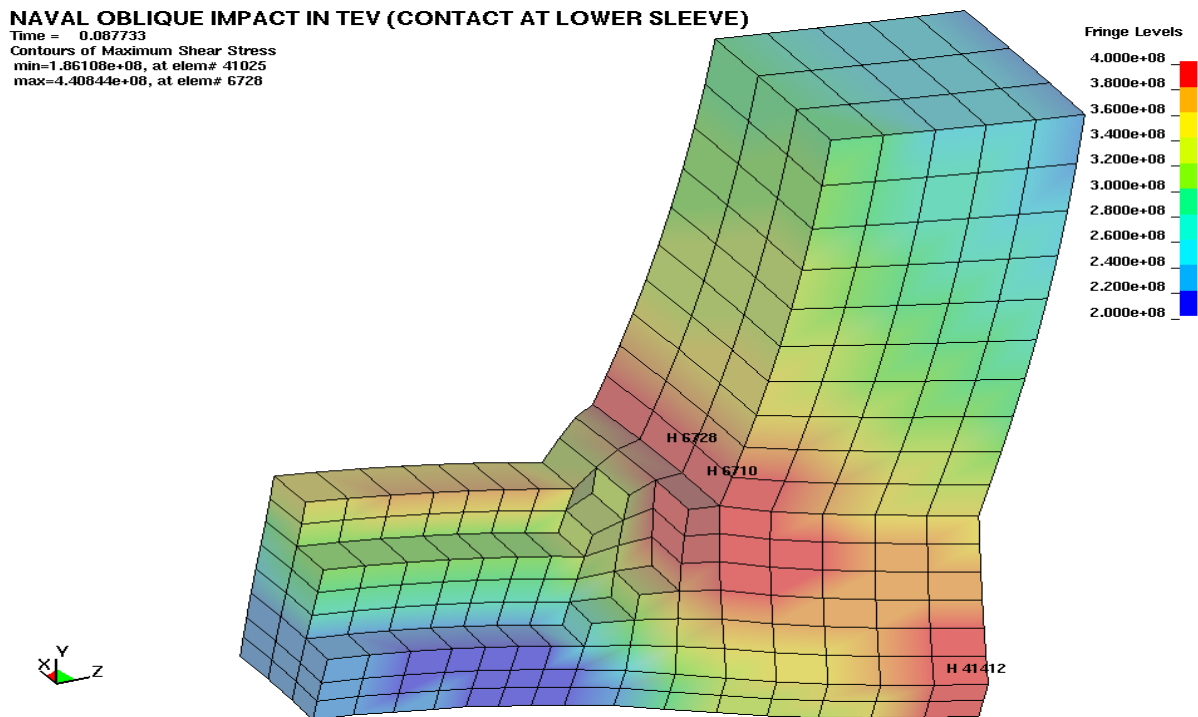


Figure 7-18. OCB Shell-Upper Lid Interface MSS (Pa) Location for Fine Mesh (run 4)

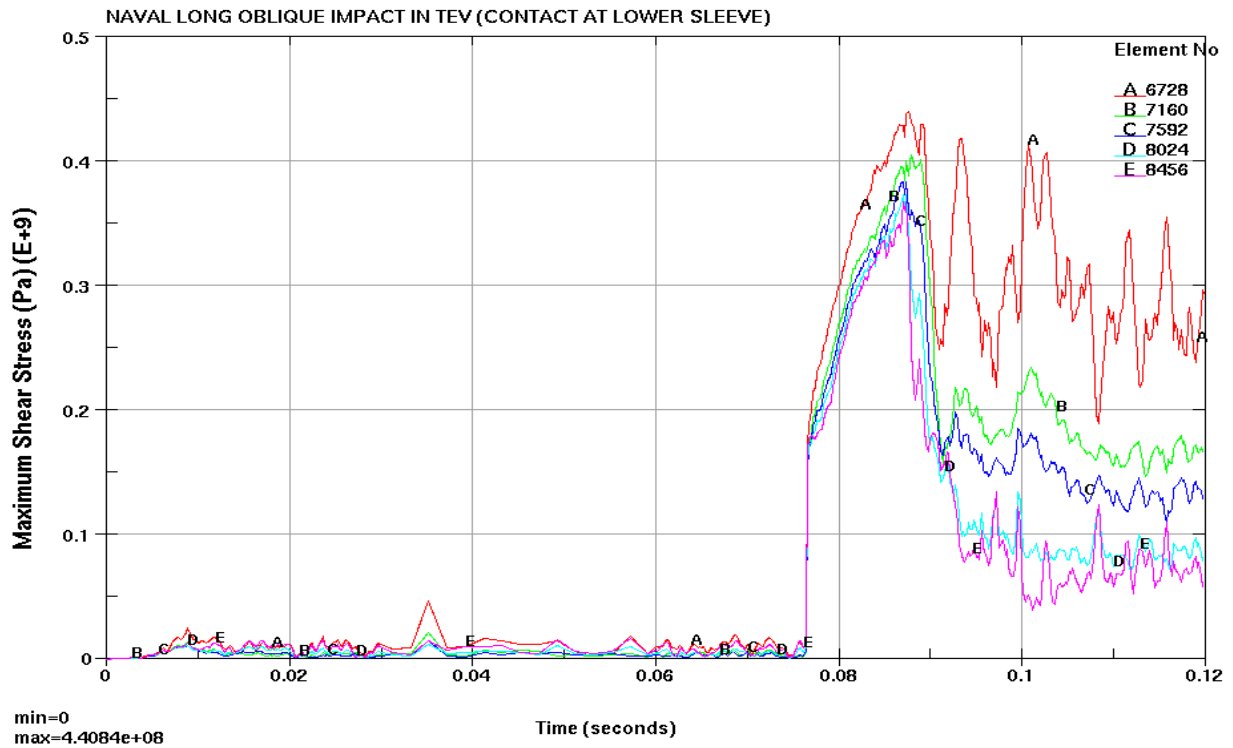


Figure 7-19. OCB Through-Wall Maximum Shear Stress for Fine Mesh (run 4)

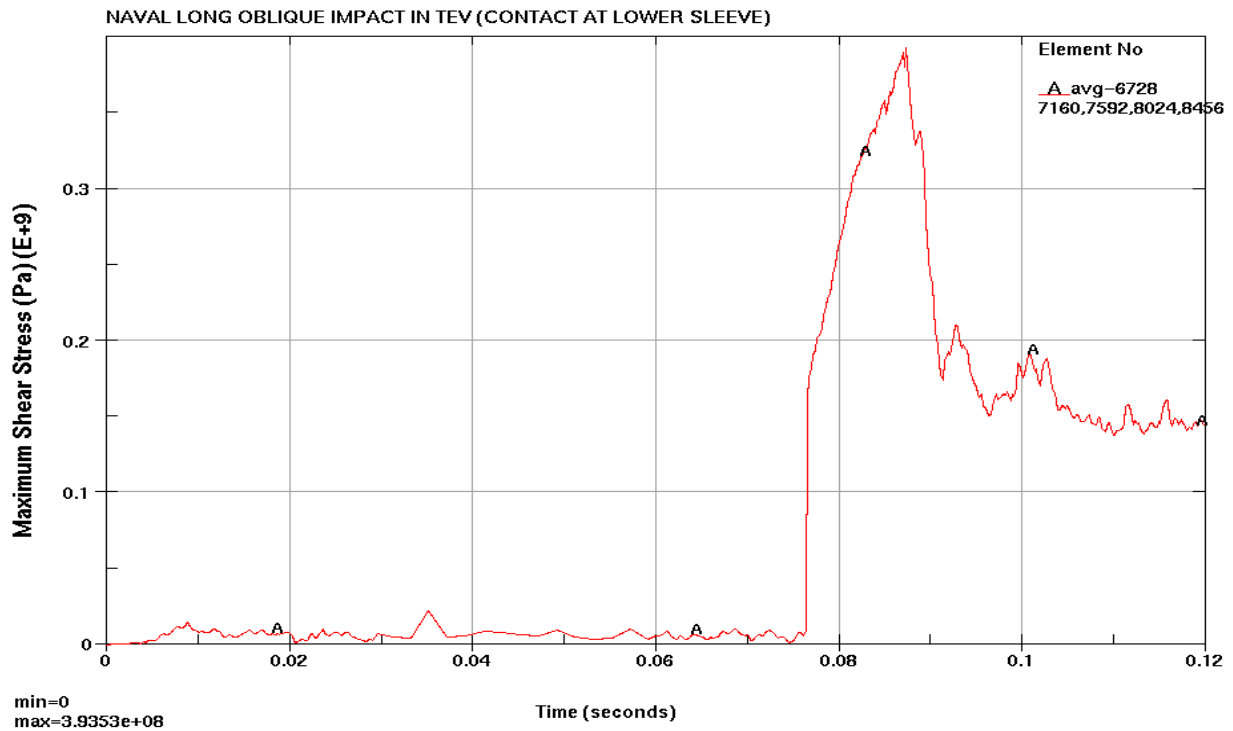


Figure 7-20. OCB Through-Wall Averaged Maximum Shear Stress for Fine Mesh (run 4)

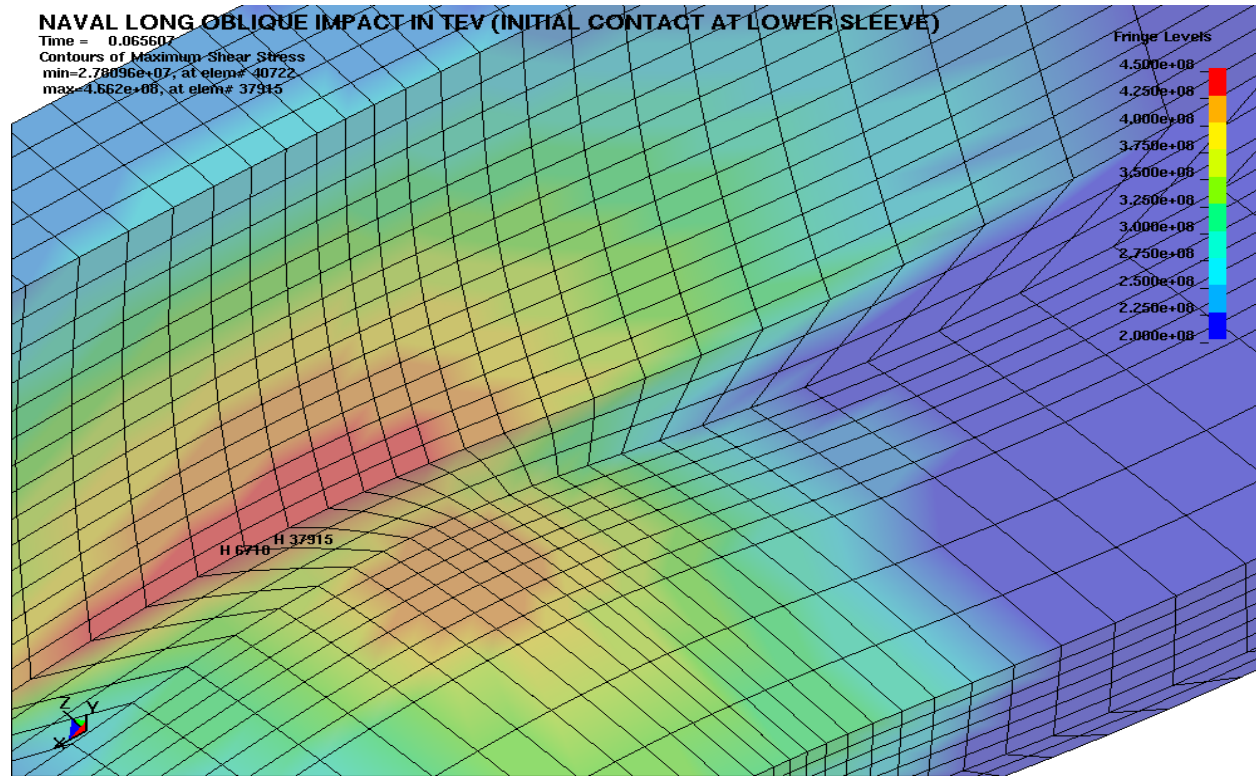


Figure 7-21. OCB Shell-Upper Lid Interface MSS (Pa) Location for Fine Mesh (run 5)

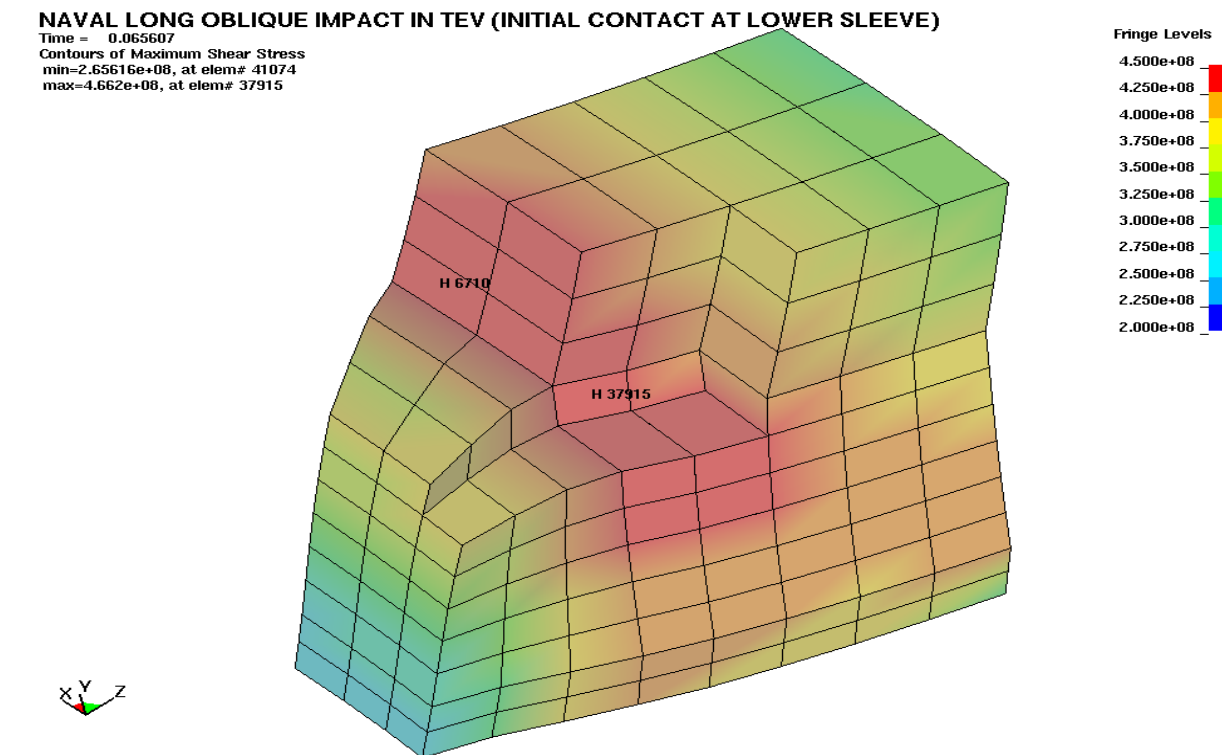


Figure 7-22. OCB Shell-Upper Lid Interface MSS (Pa) Location for Fine Mesh (run 5)

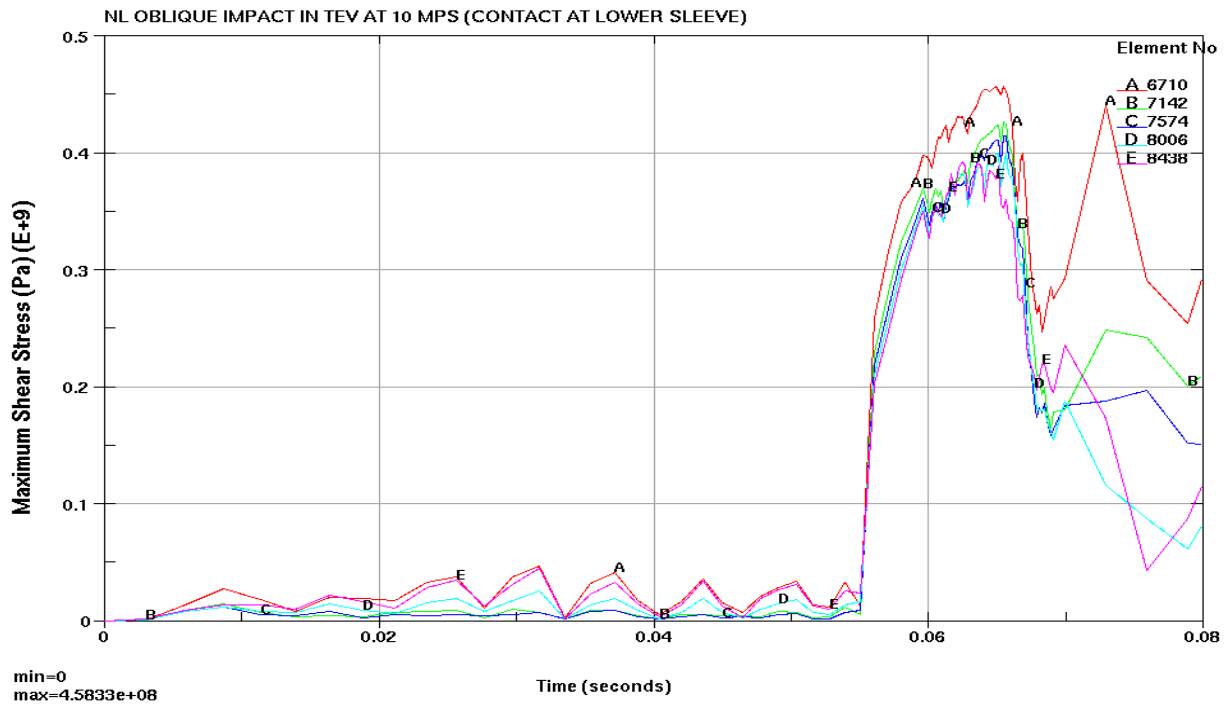


Figure 7-23. OCB Through-Wall Maximum Shear Stress for Fine Mesh (run 5)

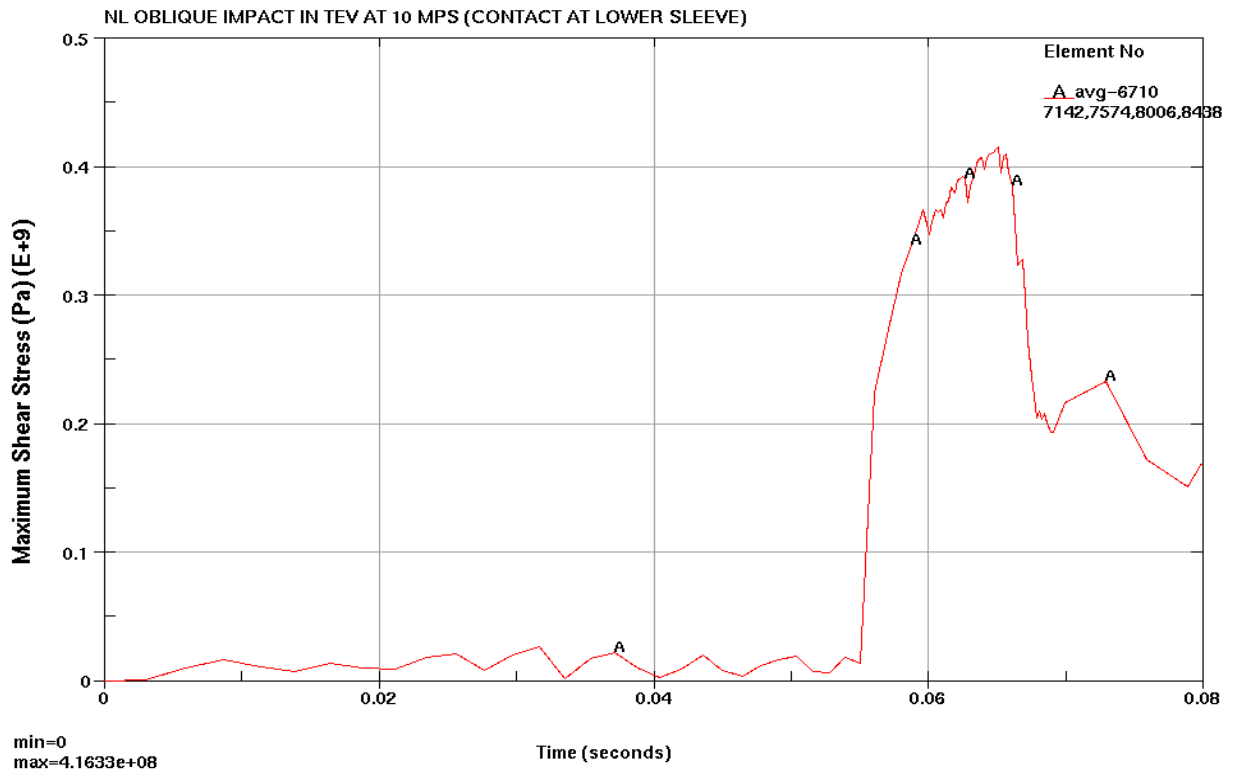


Figure 7-24. OCB Through-Wall Averaged Maximum Shear Stress for Fine Mesh (run 5)

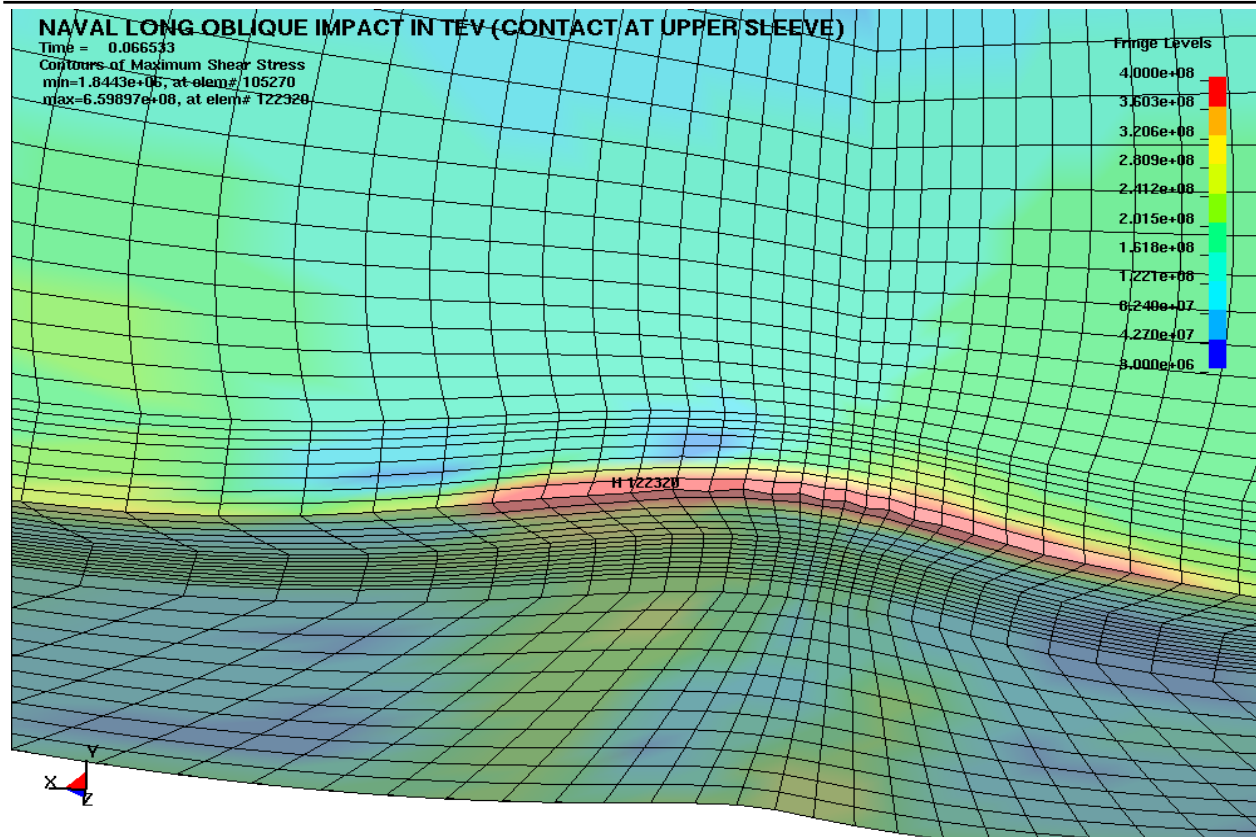


Figure 7-25. Maximum Shear Stress (Pa) Location for Fine Mesh (run 6)

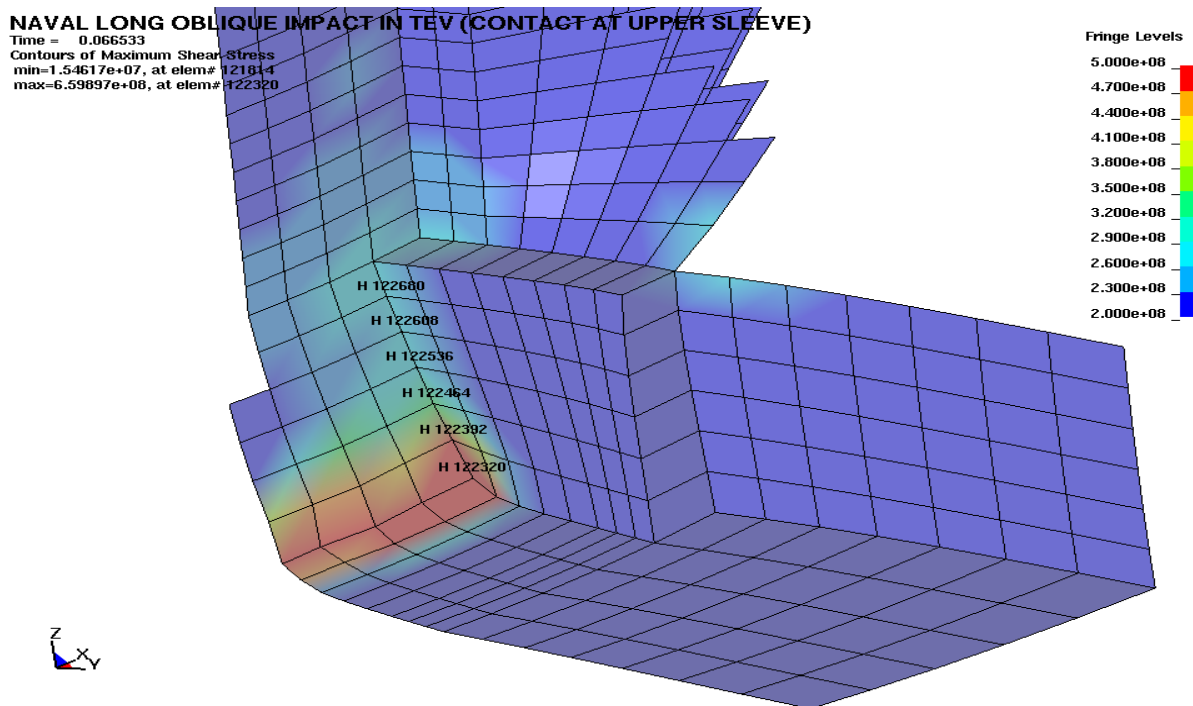


Figure 7-26. Max. Shear Stress (Pa) Location (vertically along OCB Lid) for Fine Mesh (run 6)

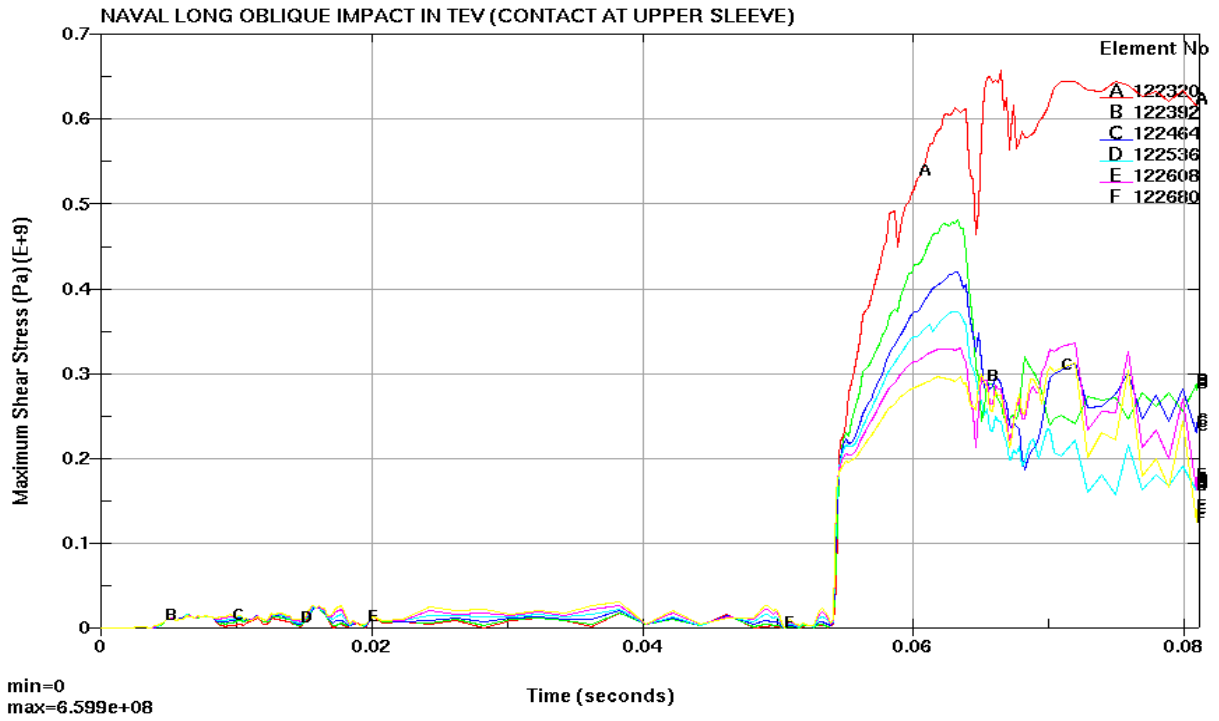


Figure 7-27. OCB (Vertical) Maximum Shear Stress for Fine Mesh (run 6)

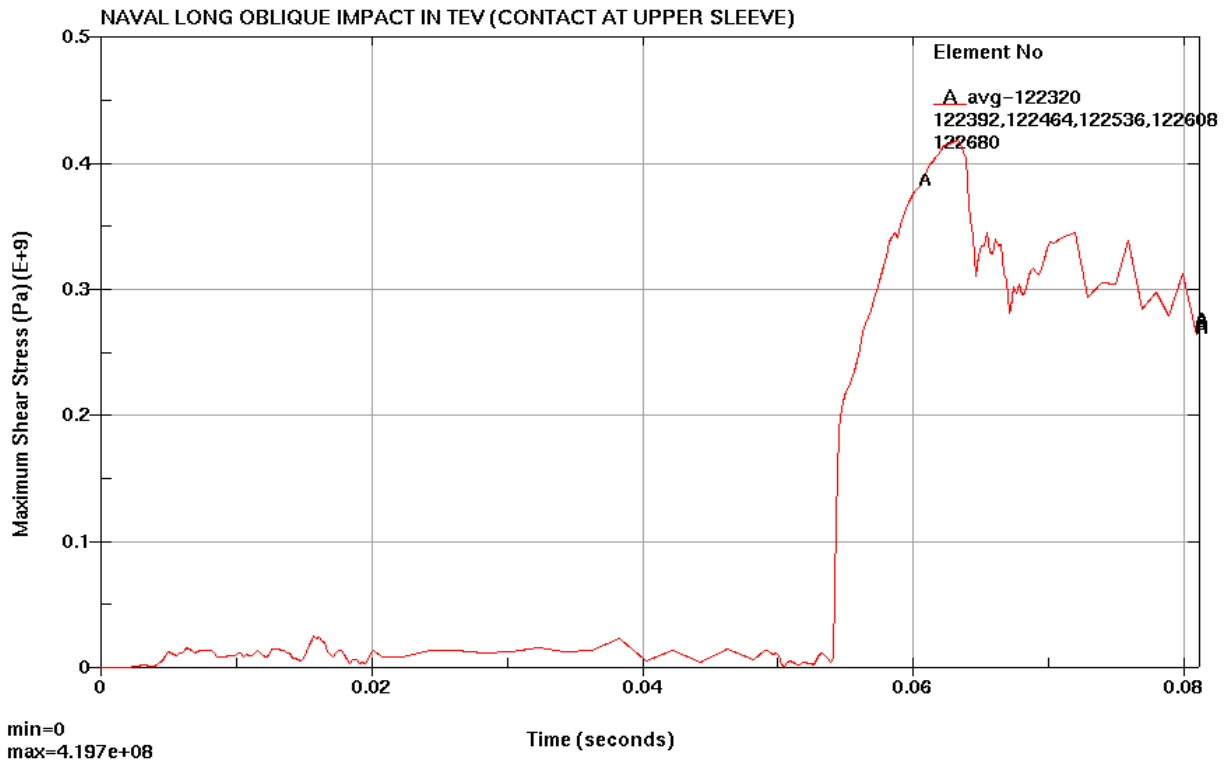


Figure 7-28. OCB (Vertical-Averaged) Maximum Shear Stress for Fine Mesh (run 6)

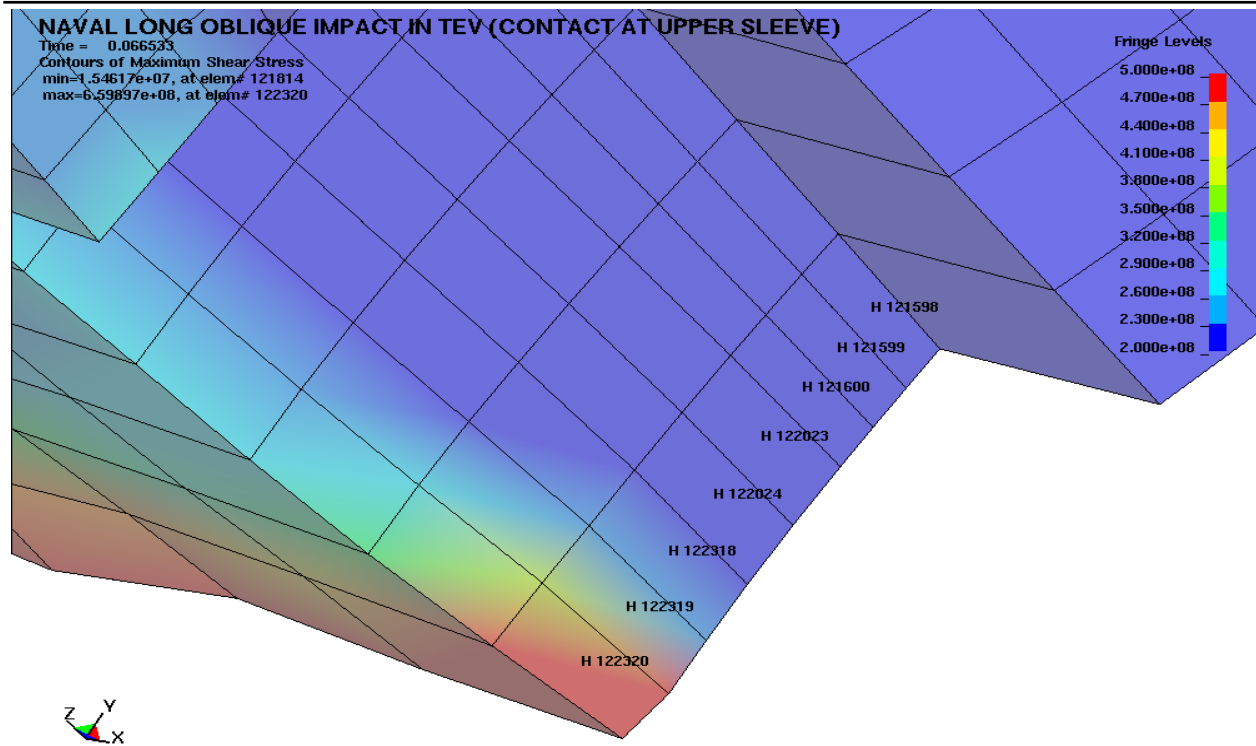


Figure 7-29. MSS (Pa) Location (horizontally along OCB Lid) for Fine Mesh (run 6)

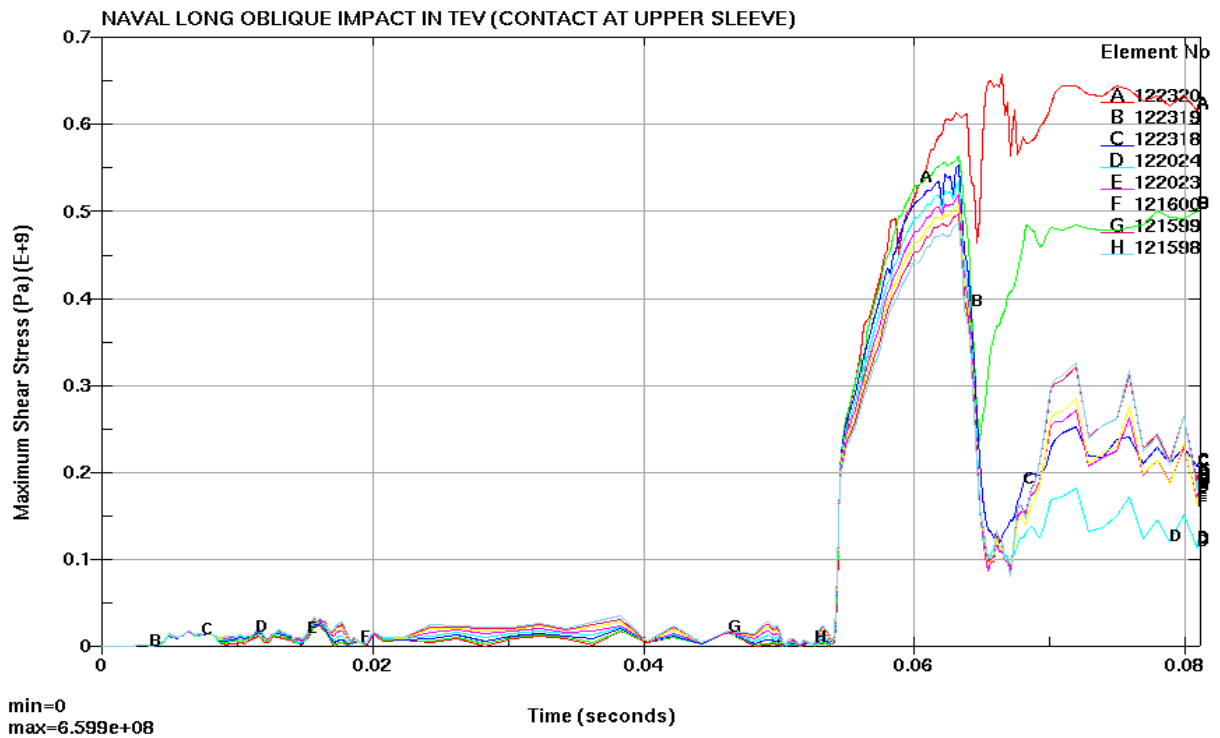


Figure 7-30. OCB (Horizontal) Maximum Shear Stress for Fine Mesh (run 6)

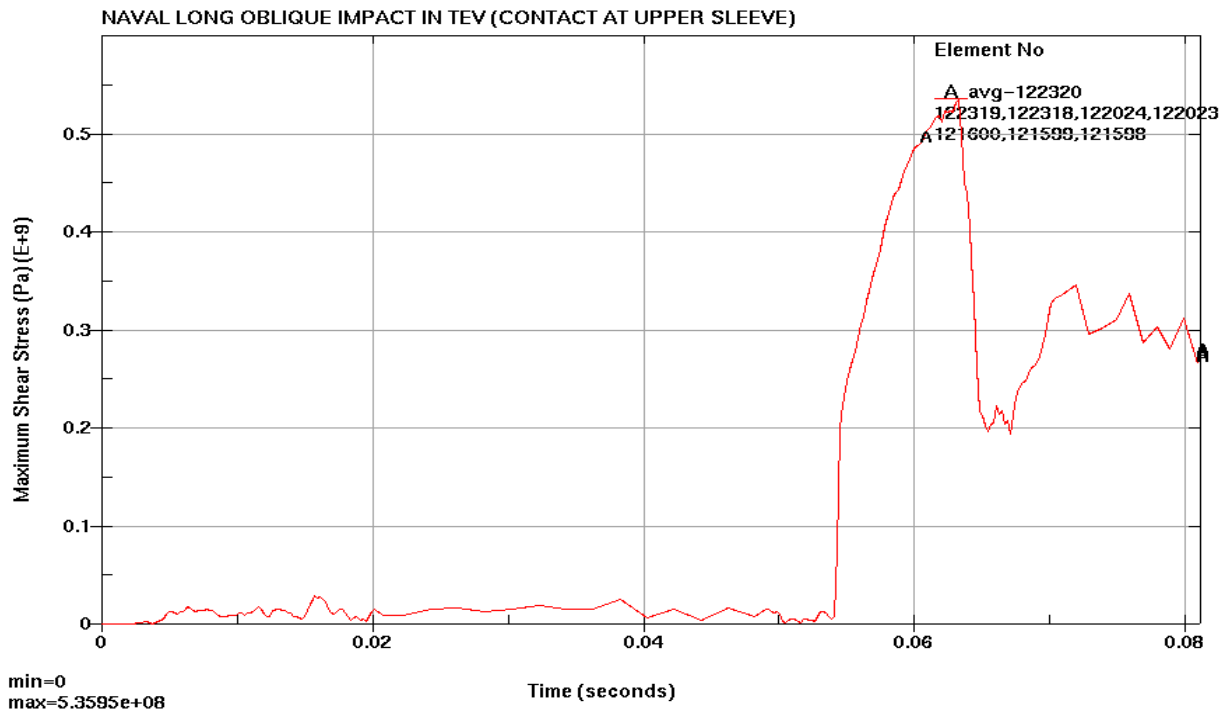


Figure 7-31. OCB (Horizontal-Averaged) Maximum Shear Stress for Fine Mesh (run 6)

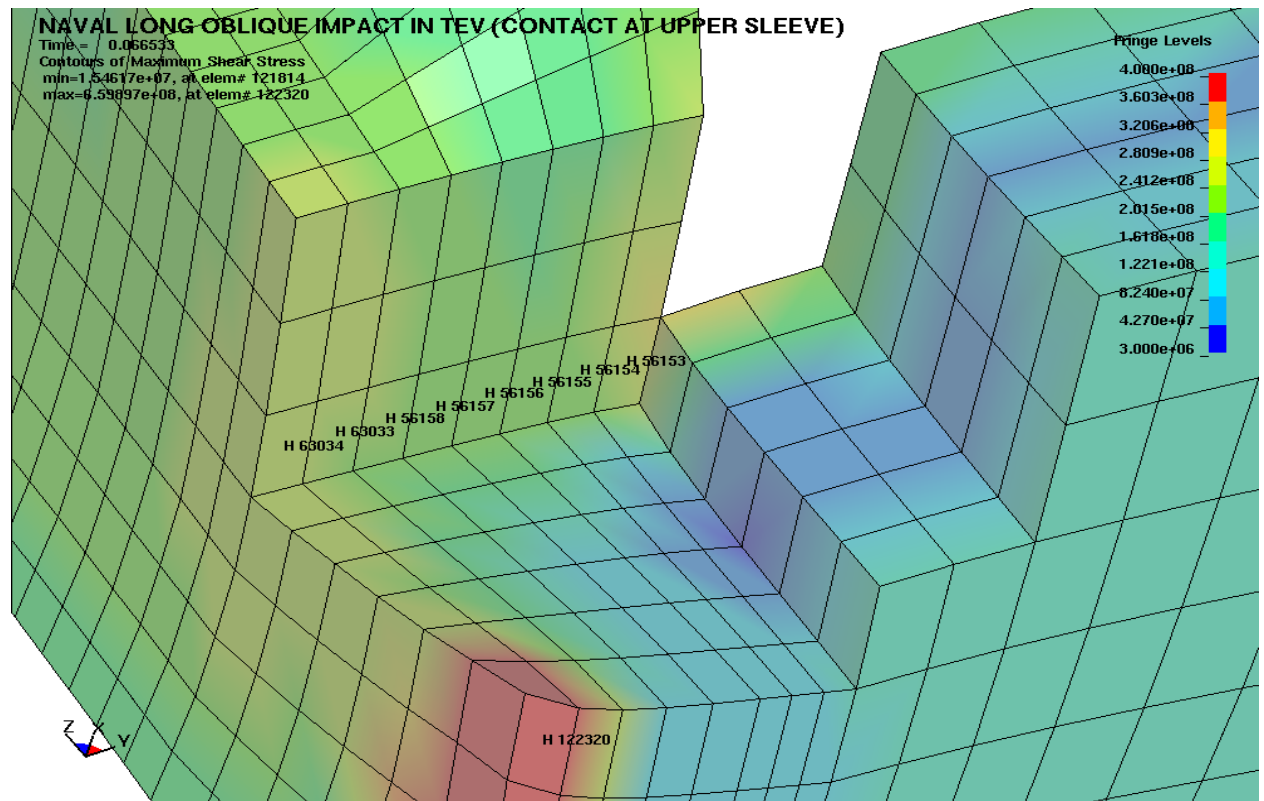


Figure 7-32. OCB Shell-Lower Lid Interface MSS (Pa) Location for Fine Mesh (run 6)

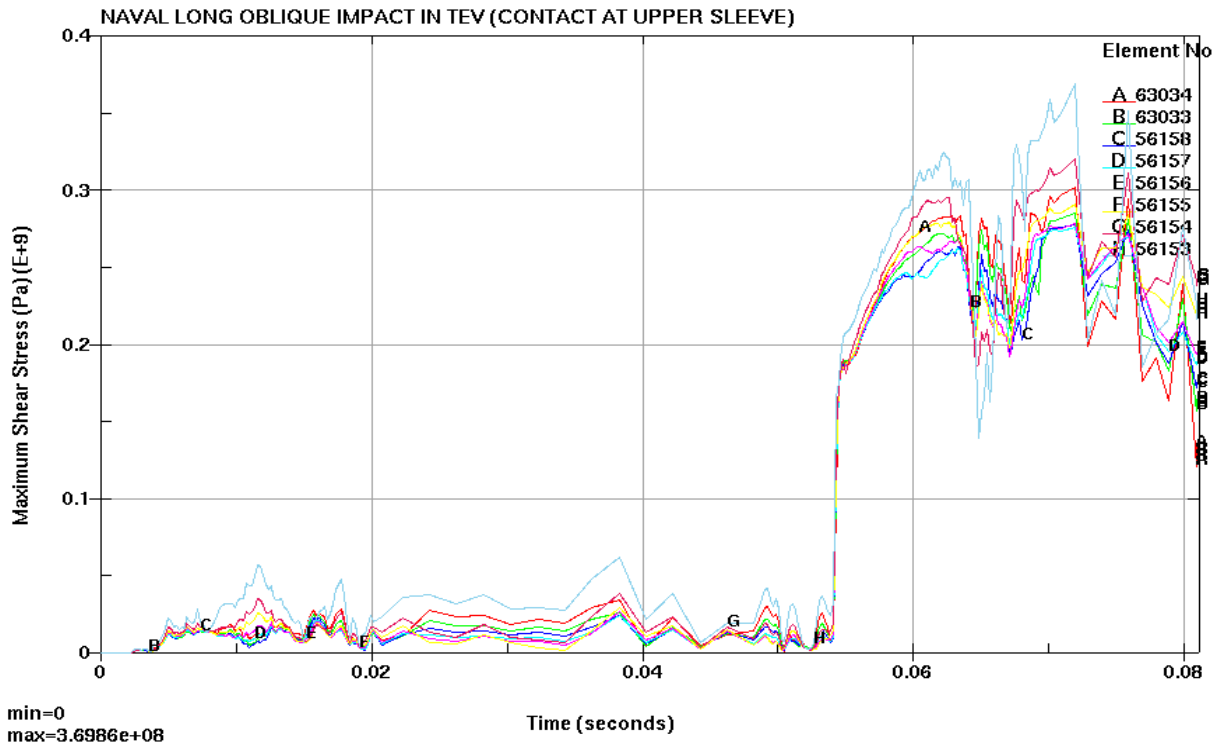


Figure 7-33. OCB Through-Wall Maximum Shear Stress for Fine Mesh (run 6)

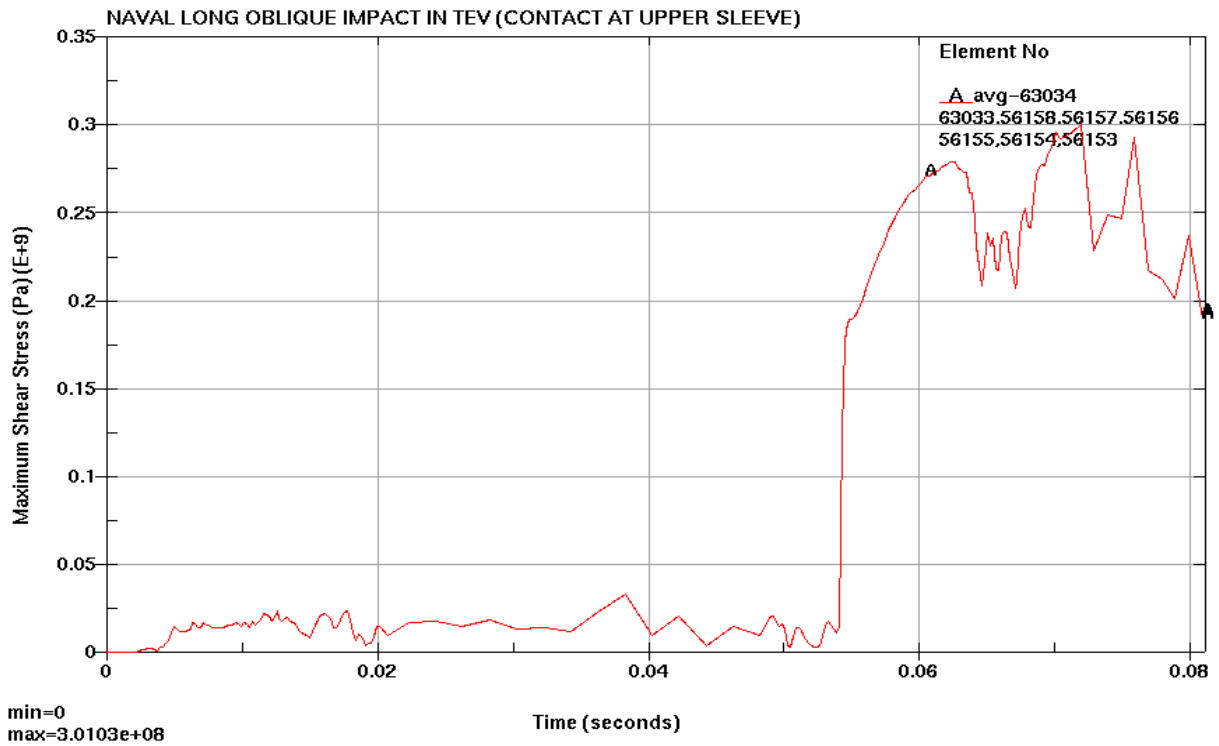


Figure 7-34. OCB Through-Wall Averaged Maximum Shear Stress for Fine Mesh (run 6)

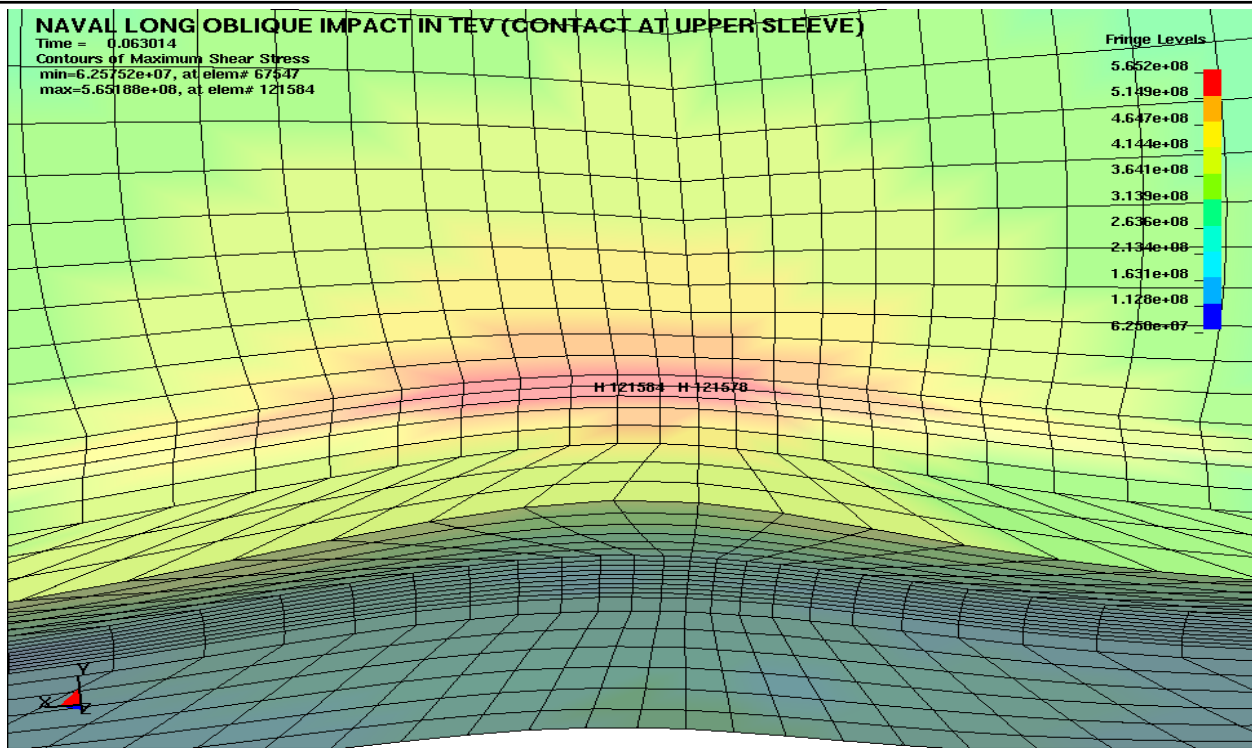


Figure 7-35. OCB Shell-Lower Lid Interface MSS (Pa) Location for Fine Mesh (run 7)

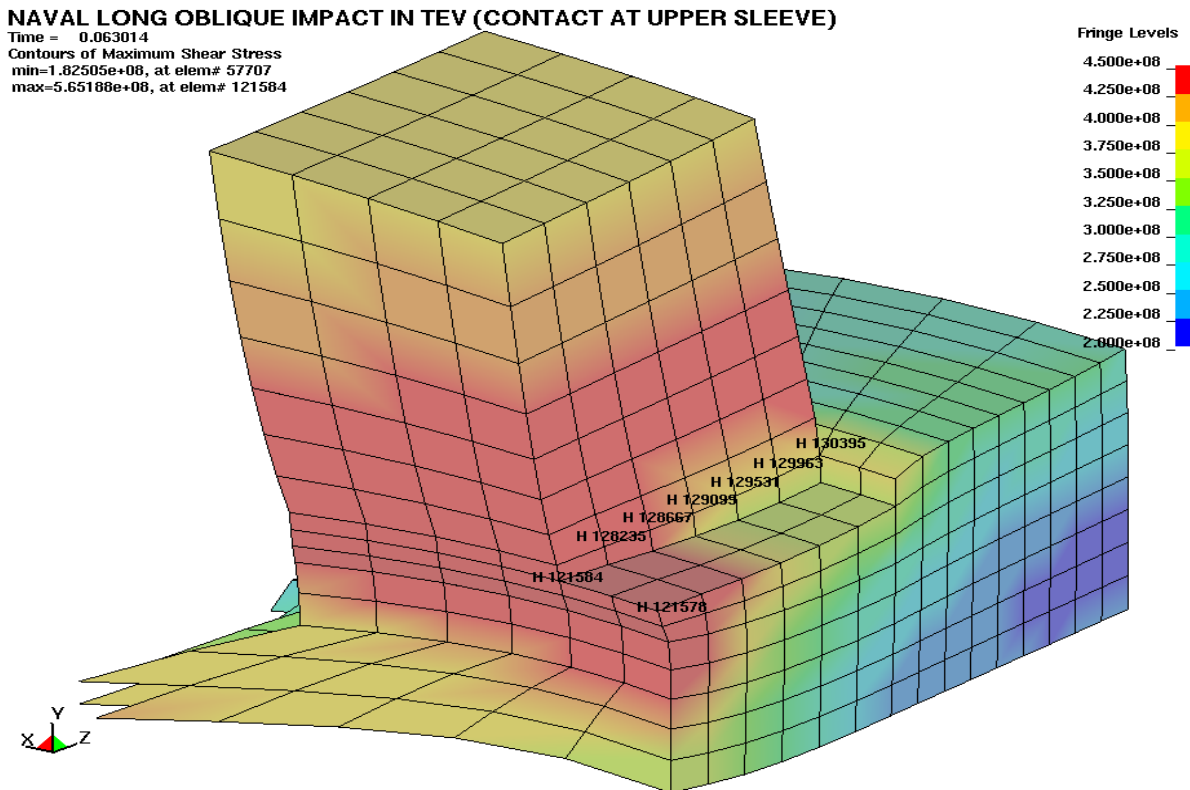


Figure 7-36. OCB Shell-Lower Lid Interface MSS (Pa) Location for Fine Mesh (run 7)

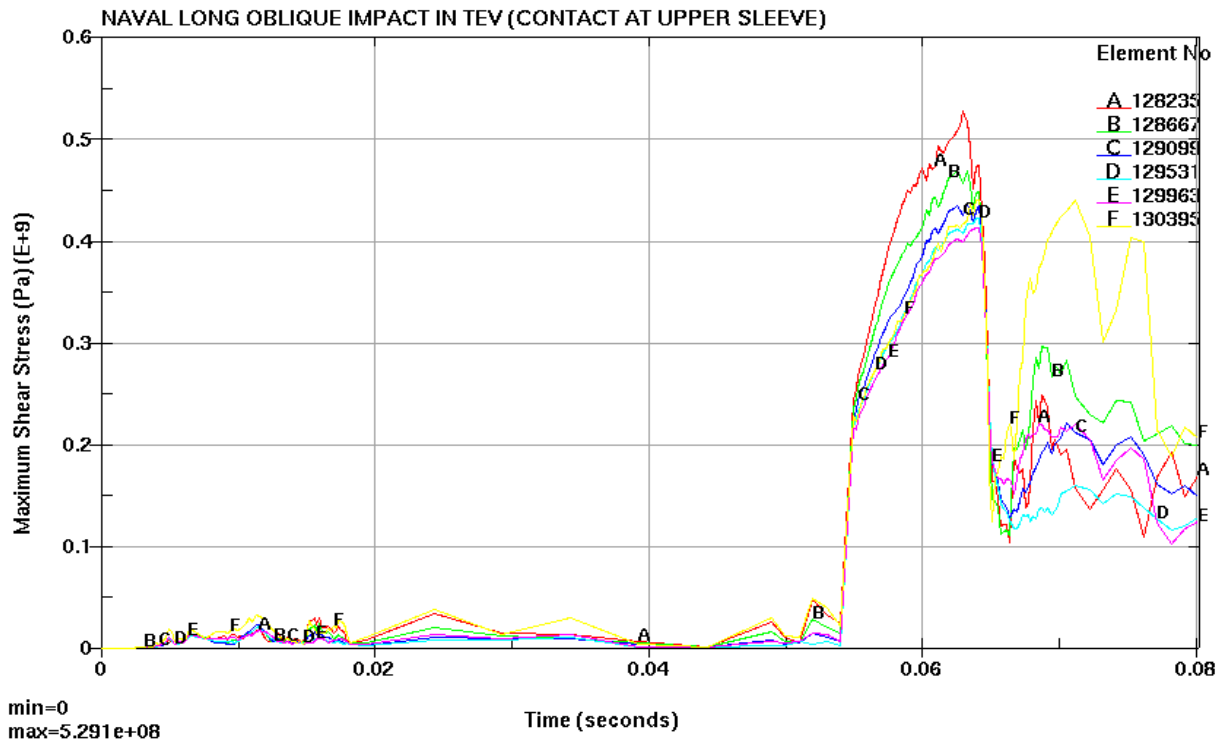


Figure 7-37. OCB Through-Wall Maximum Shear Stress for Fine Mesh (run 7)

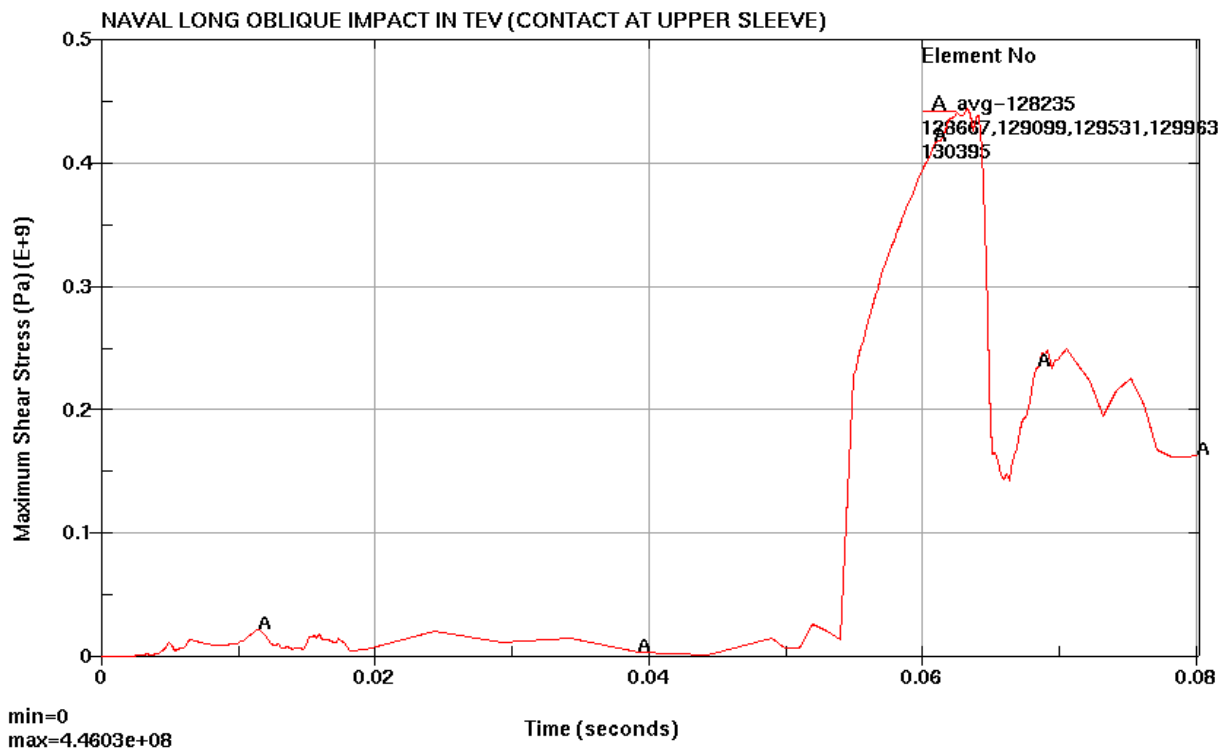


Figure 7-38. OCB Through-Wall Averaged Maximum Shear Stress for Fine Mesh (run 7)

BSC

Calculation/Analysis Change Notice

1. QA: QA
2. Page 1 of 1

000-00C-DNF0-01200-000-00A-CACN001

Complete only applicable items.

3. Document Identifier: 000-00C-DNF0-01200-000-00A	4. Rev.: 00A	5. CACN: 001
6. Title: Naval Long Oblique Impact inside TEV		
7. Reason for Change: Editorial change to a reference.		

8. Supersedes Change Notice:	<input type="checkbox"/> Yes	If, Yes, CACN No.: <u>N/A</u>	<input checked="" type="checkbox"/> No
9. Change Impact:			
Inputs Changed:	<input type="checkbox"/> Yes	<input checked="" type="checkbox"/> No	Results Impacted:
Assumptions Changed:	<input type="checkbox"/> Yes	<input checked="" type="checkbox"/> No	Design Impacted:
	<input type="checkbox"/> Yes	<input checked="" type="checkbox"/> No	<input type="checkbox"/> Yes
	<input type="checkbox"/> Yes	<input checked="" type="checkbox"/> No	<input checked="" type="checkbox"/> No

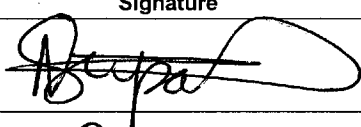
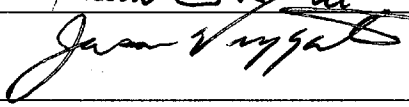
10. Description of Change:

First two lines under bullet point #6 of Section 6.1 on Page 20 of 58 which read:

- (From Reference 2.2.11, p. 14, Table "Average Dynamic Modulus of Elasticity")
(This is the best available data and suitable for use in the calculation)

is now replaced by the following:

- (From Reference 2.2.5, Section II, Part D, Table TM-4)

11. REVIEWS AND APPROVAL		
Printed Name	Signature	Date
11a. Originator: Sripathi Nilkar		10-22-2007
11b. Checker: Mohan Durani		October 22, 2007
11c. EGS: J. Viggato		10/22/07
11d. DEM: M.J. Anderson		10/23/07
11e. Design Authority:		